Investigation into the behaviour of a wash-coated PGM-based catalyst layer in micro-channel reactors for the steam reforming of methane.

by Wesley van Niekerk

In partial fulfilment of the requirements for a
Master of Science in Engineering

University of Cape Town

Plagiarism Declaration

I know the meaning of plagiarism and declare that all the work in the document, save for that which is properly acknowledged, is my own

Signed by candidate Signature Removed 17 - 06 - 2017

Wesley van Niekerk Date

Synopsis

The purpose of this study was primarily to test the behaviour and robustness of a wash-coated PGM based catalyst layer in a micro-channel reactor configuration. The catalyst and micro-channel reactors were designed for steam methane reforming. The wash-coating procedure adopted in this study was designed by Zapf et al. (2006). Originally the adopted wash-coating procedure had been used for the reforming of propane catalyst, a reaction under far less harsh operating conditions, but Zapf et al. (2006) also made use of stainless steel micro-channels and a rhodium/alumina catalyst. Thus, a secondary objective was to test the applicability of using the wash-coating procedure of Zapf et al. (2006) specifically for the harsher conditions of steam methane reforming. The catalyst powder used for the wash-coating suspension was an in-house prepared 1.0 wt% Rh/Al_2O_3 catalyst. The main testing was conducted using a 3 µm alumina.

Prior work by Zhou (2014), which also used the same coating procedure for steam methane reforming, yielded an unstable catalyst layer and, despite numerous tests, the causes of the instability were never clarified.

A benchmark test was conducted in a fixed bed configuration and was used as a proof of concept test to show the in-house prepared catalyst was stable in the conventional industry standard reactor configuration. The results proved this with a stable catalyst at numerous space velocities. This benchmark test would be used to compare the operating space velocities between the fixed bed and micro-channel reactor at a given methane conversion.

Initial tests for wash-coat adhesion were done using the 'drop test' which was performed by Zapf et al. (2006). The results indicated the wash-coated catalyst had sufficient adhesion.

Subsequently in the testing of the stability of the catalyst layer coated onto the micro-channels, a mixture of results was attained. In the first batch of wash-coating suspensions and coated reactors (Experiments 2 and 3), a stable, robust catalyst layer was attained. SEM and EDS characterisation proved that the catalyst was still intact despite coming away from the micro-channel wall in a complete tubular catalyst layer.

In the next 4 subsequent micro-channel tests (Experiments 4-7) unstable catalyst layers were seen with rapid declines in catalyst activity over time. The post run characterisation (SEM imaging and EDS analyses) showed that the wash-coated catalyst layer was no longer attached to the micro-channel reactor wall.

A second more vigorous adhesion test was performed on coated reactor plates from each of the different batches of coating suspensions made including spare unused plates from the successful first batch. The test used was a chemical adherence patented by Yasaki et al. (1993). The results showed that the first batch had a 'stable' wash-coated catalyst layer according to Boix et al. (2003), however the results were on the borderline of the stated 10 % catalyst loss with a loss of 9.4 %. The results of the chemical adherence testing for

experiments 4-7 showed over a 30 % loss in the catalyst layer's mass, illustrating that the adhesion quality of the wash-coated catalyst in these tests were inadequate.

In experiment 8, a new reduction procedure was used to see if the calcination and reduction procedure had an influence on the quality of the wash-coat adhesion. The results of this test also yielded a loss of the catalyst shown by the fast decline in catalyst activity at a mass specific space velocity of 1 800 000 $scc \cdot (g_{cat} \cdot h)^{-1}$.

In the final micro-channel test, a replica of the catalyst used by Zhou (2014) was made and wash-coated onto a set of micro-channel reactor plates. Zhou (2014) made use of a milled 50 µm Sasol Puralox NWA-155 alumina in his wash-coating suspension and a 34 µm alumina was used in this test. The post-run characterisation SEM images showed that the catalyst layer was again breaking away from the micro-channel wall in pieces which was consistent with the slow decline in catalyst activity. This shows that again the wash-coated catalyst had insufficient adhesion to the micro-channel wall.

Literature was found for different wash-coating methods and found that the application of an alumina primer layer prior to wash-coating will aid the catalyst layer's adhesion quality by introducing more oxide bonds in closer proximity to one another (Peela et al., 2009 and Penneman et al., 2013).

The methods and procedures used were analysed in order to understand what caused the difference in adhesion quality between the successful experiments (experiments 2 and 3) and the subsequent experiments. The results of the analyses point to the following issues:

- The over-reduction of the wash-coating suspension
- Thermal expansion of the stainless steel micro-channel reactor plate
- Effects of coking on the wash-coated catalyst layer

In experiments 4-9, the original quantities of the Zapf et al. (2006) wash-coating suspension was reduced too much to reduce wastage. This reduction in suspension batch size incorporated small air bubbles into the wash-coated catalyst layer which is believed to have an adverse effect on the quality of the catalyst layer's adhesion.

The original use of the wash-coating procedure created by Zapf et al. (2006) which was for the reforming of propane. The reforming of propane occurs at a lower temperature of approximately 300 °C (Kolb, 2009) and the effect of thermal expansion of the micro-channel reactor is far less pronounced than it would be at the 700 °C required for steam methane reforming (Steele and Heinzel, 2001). The thermal expansion of the micro-channel reactor plate could possibly exacerbate the low adhesion quality of the catalyst layer.

In all the experiments, the catalyst layer had removed itself from the micro-channel wall, but in the case of the successful experiments it broke away in a single complete tubular catalyst layer which would not have been able to pass through the reactor causing a loss of

catalyst. This would have shown a stable performance or activity profile as the catalyst layer was still in the reactor channels. In the case of the latter experiments where air bubbles were present in the wash-coat, these bubbles may have caused the catalyst layer to break apart easier by creating weak points in the wash-coat. This would allow the broken pieces of the catalyst layer to pass through the reactor like that seen in the SEM images of experiment 9. However, further testing is required to confirm the effect of the thermal expansion.

The effect of coking on the catalyst layer was speculated to possibly enhance the brittleness of the wash-coated catalyst layer and when combined with the effect of thermal expansion and incorporation of bubbles into the wash-coated catalyst layer only adds to the insufficient adhesion of the catalyst layer. These factors are believed to have led to the loss of catalyst during the tests.

Its recommended that the coating procedure pioneered by Zapf et al. (2006) be altered in order to improve the adhesion of the alumina supported catalyst layer on the stainless steel micro-channel reactor plates. With the procedure developed by Zapf et al. (2006), the harsher conditions involved with methane steam reforming are unsuited to standard coating methods and minor changes should be made to increase wash-coat adhesion. It is also unknown whether the thermal expansion of the microchannel reactor or coking that takes place during the tests negatively affects the catalyst layer by making the wash-coat more brittle and more susceptible to breaking away from the micro-channel wall.

The following changes are recommended for future projects:

- Place the reactor set up on a UPS if possible, particularly the pump due to the sensitivity of the system to steam concentration

- Introduction of a small air stream to burn off the carbon deposition

- Implementation of a two-step coating procedure. After the heat treatment of micro-channels, a preliminary alumina primer wash-coat should be added before wash-coating the rhodium containing catalyst layer.

- More reactors need to be made and subsequently wash-coated at once (after primer application). This will require making a bigger batch of the rhodium containing wash-coating suspension so as not to allow the formation of bubbles and not transferring the bubbles to the micro-channels during wash-coating.

- The use of a micro-channel reactor with a high heat tolerance that will be less susceptible to the effects of thermal expansion.

Acknowledgements

I like to take this opportunity to express my gratitude to everyone who contributed directly or indirectly in any way possible to the successful completion of this study.

Firstly, I wish to thank my supervisor Prof. Jack Fletcher for letting me work in the fuel processing labs and supporting me in many ways during the last three years. I would also like to thank Mr Niels Lüchters for all the help, guidance and for the enlightening discussions about the work at hand. I would also like to thank Mr Niels Lüchters for acting as the co-supervisor in my project.

I am also grateful to Mr Yi Zhou for his help and support in the laboratory, interesting insights into problems experienced in the labs and for providing a pleasant friendly atmosphere.

I would like to mention my follow MSc students Ms Zaheera Ahmed, Riddhi Maharaj and Sibongile Muziki for helping me wherever they could.

Without the support of the administrative and technical staff at the Centre for Catalysis Research and HySA/Catalysis Research Centre, it would not have been possible to complete this research. I would like to express my respect for their excellent support: Marc Wüst, Mr Gideon Kaufmann, Mr Waldo Koorts, Mr Nabeel Hussain, Roald Brosius and Mr Dirk Reyskens.

Furthermore, I am grateful to HySA/Catalysis for funding this study.

Most importantly, I am indebted to thank my caring parents, Charlotte and Clive, for their constant love and invaluable support during the last three years and my life thus far.

Lastly I must thank my loyal and patient girlfriend, Sasha, for her unwavering support and patience making sure I don’t falter and keep focused with the tasks at hand.

Table of Contents

List of figures

List of tables

Nomenclature

Symbol	Description
PEM Fuel Cell	Proton Exchange Membrane Fuel Cell
PGM	Platinum Group Metals
S/C	Steam to carbon ratio (molar basis)
PVA	Polyvinyl alcohol
Tylose	Methylhydroxyethyl cellulose
PEG	Polyethylene glycol
ICP-OES	Inductively coupled plasma optical emission spectroscopy
BET	Brunauer – Emmett - Teller
TGA	Thermogravimetric Analysis
SEM	Scanning electron microscopy
TEM	Transmission electron microscopy
EDS	Energy dispersive microscopy
rpm	revolutions per minute
MFC	Mass flow controller
scc	standard cubic centimetre
sccm	standard cubic centimetres per minute
SGHSV	Standard gas hourly space velocity (h^{-1}) at 0 °C and 1 atm
SSV	Specific space velocity at at 0 °C and 1 atm ($scc \cdot (g_{cat} \cdot h)^{-1}$)
PPQ	Pora Plot Q chromatography column
MS5	Molsieve 5Å chromatography column
FeCrAlloy	Ferrous chromium alloy

PrOX	Preferential oxidation of CO
WGS	Water-gas shift reaction
HTS	WGS reaction at high temperature (High temperature shift)
LTS	WGS reaction at low temperature (Low temperature shift)
TPR	Temperature programmed reduction

1 Introduction

In the 21st century, the increased drive to develop energy sources that have a minimal carbon foot print has led to the subsequent booming development of the hydrogen economy for portable and smaller power generation applications. Besides the issues associated with the inner workings of the PEM fuel cell, such as catalyst and membrane lifespan, another large issue is the process by which we obtain the hydrogen fuel for the PEM fuel cells (Taylor et al., 2016). Currently steam methane reforming is done on an extremely large scale, however with a number of inefficiencies. In industry, the main limiting factor is the heat transfer limitations experienced by the conventional reactor set up and designs (Kolb et al., 2009).

Again, current industrial fuel processing practices if taken to a smaller portable power generation level needed to power households, such methods are very inefficient, as the reaction is limited to the rate at which heat is transferred to the catalyst. To answer such inefficiency problems, novel developments such as micro-channel reactors with walls coated with catalysts have shown to eliminate the dependency the reaction has on the heat flux by eliminating nearly all temperature profiles. Industrial catalysts due to their chemical properties are not well suited and PGM catalysts have been suggested the best replacement, with rhodium leading the way.

The availability of natural gas networks in North America and Europe have made the steam reforming of methane a possible viable fuel processing option to produce hydrogen in one's household and then utilise the PEM (proton exchange membrane) fuel cells in the household to generate power for the household and other smaller applications (Taylor et al., 2016).

The use of methane as a source of hydrogen is the best in terms of hydrogen density, however the procurement of methane outside North America and Europe is not as easy. In the case of other areas, the easiest and most widely available source of hydrogen to be attained is LPG (liquefied petroleum gas).

At the HySA/Catalysis research centre, this opportunity has been realised and plans to develop stable steam methane reforming catalysts to be used in micro-channel reactors to produce a compact, miniaturised way of producing hydrogen for the PEM fuel cell. This miniaturisation makes the prospect of a complete power generation unit possible. This unit will integrate the methane steam reforming step, subsequent CO clean up steps and the PEM fuel cell (power generation step) together.

However, the reforming step will eventually need to generate and serve as its own heat source through a modification of the micro-channel system. Reuse et al. (2004) explains that this modification is possible using the auto-thermal reformer concept, novel reactor design and the heat transfer advantages that the micro-channel reactor offers. In the auto-thermal reforming process whereby a portion of the methane or another hydrocarbon is burnt in a

certain ratio in the presence of steam to generate sufficient heat. By doing this co-currently in the same pipeline you create a synthesis gas ('syngas' – a mixture of carbon dioxide, carbon monoxide and hydrogen) lower in hydrogen and far richer in carbon dioxide and carbon monoxide than in normal steam reforming (Reuse et al., 2004). This lower concentration of hydrogen from a partial oxidation step is not the desired result when wanting to utilise the hydrogen for fuel cells.

Novel micro-channel designs have come about that can separate the oxidation reaction and steam reforming reaction while still being able to transfer sufficient heat to drive the endothermic steam reforming reaction. This micro-channel reactor is essentially three plates, with two separate compartments and two tailored catalysts to suit the combustion reaction and reforming reaction while still transferring the heat from the exothermic combustion reaction to the endothermic reforming reaction. This will then help generate a syngas far richer in hydrogen (Rostrup-Nielsen, 1993).

The use of methane as a fuel is the primary step in the development of household or portable power generation as the reaction mechanism is the least likely to form carbonaceous compounds through side reactions (Aartun et al., 2005). There are plans in the pipeline to produce a catalyst that can reform LPG and provide the hydrogen in the same manner of steam methane reforming for the PEM fuel cells.

This study will involve the investigation into the behaviour of a PGM based wash-coated catalyst layer for the use in steam reforming. The wash-coating method to be used is the procedure developed by Zapf et al. (2006) which makes use of a rhodium metal supported on alumina and is coated onto sets of stainless steel micro-channel reactors for the reforming of propane. The aim is to test the robustness and see the resulting behaviour of the wash-coated catalyst layer using Zapf et al.'s (2006) coating procedure in the harsher methane steam reforming environment.

2 Review of Literature and Theory

2.1 Fuel cell technology

A fuel cell is an electrochemical device capable of converting the chemical energy of a fuel directly into electricity (Barbir, 2005). The fuel cell combines a fuel such as hydrogen with oxygen in a series of redox reactions to produce electricity, with the only by-products being water and heat. Depending on the kind of fuel cell used, carbon dioxide may also be produced. Hydrogen as fuel is very attractive as it is very reactive when an appropriate catalyst is used, and has a high-energy density and efficiency in comparison to other fuels (Viswanathan & Aulice Scibioh, 2006).

Fuel cells are usually categorised by the electrolyte used in the cell. They can then be further classified based on the operating temperature or fuel consumed (Carrette et al., 2000). A summary of the major fuel cell types is shown in Table 2.1.

Table 2.1 – Types of Fuel Cells and Their Electrolytes, Operating Temperatures and Common Electro-catalyst (Adapted from Carette et al.,2000)

Type of Fuel Cell	Electrolyte	Operating Temperature	Common Electrocatalyst
Alkaline	Concentrated Potassium Hydroxide	80 °C	Pt/Au, PtAu alloy or Ni, Ag
Proton Exchange Membrane	Proton conductive polymer membrane	60-80 °C	Pt-alloy/C
Phosphoric Acid	Concentrated phosphoric acid	200 °C	Pt-alloy/C
Molten Carbon	Alkalicarbonate	650-700 °C	Ni/Cr, NiO
Solid Oxide	Solid, nonporous metal oxide	800-1000 °C	Ni/YSZ $(La,Sr,Ca)MnO_3$

Structure and operation of the PEM fuel cell

The hydrogen for the Proton Exchange Membrane (PEM) fuel cell can be produced using several methods such as the steam reforming of methane or methanol and by water electrolysis (Carrette et al., 2000).

Although fuel cells differ in the electrolyte used, they all operate in the same way. A fuel cell consists of two electrodes (an anode and a cathode) which are separated by an electrolyte. The oxidation and reduction reactions occur on the surface of the electrodes. Each electrode contains a catalyst layer which increases the rate of the electrochemical reactions. In the case of conventional PEM fuel cells these electrodes are made of platinum metal particles (Pt) on a carbon-based support material. Hydrogen gas enters a fuel cell and moves towards the anode via diffusion and/or convection. At the anode, hydrogen is adsorbed

onto the catalyst surface and dissociates to form hydrogen ions and electrons (Barbir, 2005). Oxidation of hydrogen occurs via the following reaction:

$$H_2 \Leftrightarrow 2H^+ + 2e^- \quad (1)$$

The resulting protons are allowed to pass through the selectively permeable membrane (electrolyte) to the cathode. The electrons pass through an external electrical circuit. At the cathode, oxygen enters the system. The electrons, protons and oxygen combine in a reduction reaction on the cathode to form water (Barbir, 2005). This is achieved via the following reaction:

$$\tfrac{1}{2} O_2 + 2H^+ + 2e^- \Leftrightarrow H_2O \quad (2)$$

The overall reaction can be represented by the following equation (Barbir, 2005):

$$H_2 + \tfrac{1}{2} O_2 \Longrightarrow H_2O \quad (3)$$

In a hydrogen fuel cell, a theoretical cell voltage of 1.23 V can be achieved. In practical applications, this voltage drops to less than 1 V. In order to obtain a useful voltage and subsequently a higher power output, single cells can be connected in series to produce a fuel cell stack. The voltage output depends on the number of unit cells in the stack. The cells are connected in series with bipolar plates. In a stack, the cathode of one cell is electrically connected to the anode of the adjacent cell (Barbir, 2005).

However, for fuel cells running on reformate, a typical hydrogen utilisation is around 80% (Kolb, 2009). Yet when decreasing the power withdrawal from the fuel cell the hydrogen utilisation may drop further even when keeping the reformate flow rate constant (Kolb, 2009).

The platinum catalyst used in conventional PEM fuel cells is very easily poisoned by the carbon monoxide (CO) due to the preferential adsorption of CO over hydrogen to the platinum particles' surface. This preferential adsorption essentially blocks the catalytically active sites available such that the hydrogen can no longer oxidise and dissociate (Kolb, 2009). This poisoning of the platinum material can be supressed through the introduction of certain platinum based metal alloys. Typically, these alloys will incorporate metals such as ruthenium (Ru), cobalt (Co), iron (Fe) and tungsten (W) along with the platinum. In these systems, the platinum still adsorbs the CO; however, water is then adsorbed to the secondary metal which then promotes the in-situ oxidation of carbon monoxide to carbon dioxide (CO_2) and thus allowing the CO_2 to desorb easier than the CO. Such alloy systems can thereby increase the tolerance of PEM fuel cells to CO poisoning up to 50-100 ppm (Wang et al, 2011). Mehta and Cooper (2003) describes the poisoning effects of methane up to 5 volume % to be minimal and have no detrimental effects on PEM fuel cell performance.

2.2 Fuel Processing

Now hydrogen can be produced through two different types of technology, fuel processing and non-reforming technologies such as electrolysis etc. Fuel processing refers to the technology and systems involved in the reforming of an energy carrier, generally a hydrocarbon or alcohol based feedstock, with steam over a heterogeneous catalyst to yield hydrogen or a hydrogen rich gas mixture, also known as a reformate.

The generic way in which fuel processing is undertaken on an industrial scale to produce a feed for use in PEM fuel cells is first by reforming the original fuel source to synthesis gas (a mixture of CO and H_2 with a minor fraction CO_2 also known as syngas). After the reforming step, most of the CO present in the syngas is converted to CO_2 through the water-gas shift reaction (WGS) leaving a mixture that is rich in hydrogen and carbon dioxide with a minor portion of carbon monoxide. Due to the susceptibility of the platinum to poisoning from CO, a final purification step involving the preferential oxidation (PrOx) or selective methanation of the remaining CO needs to be implemented.

2.2.1 Reforming

The two main ways in which hydrogen is extracted from a carbonaceous feedstock is through steam reforming or auto-thermal reforming/partial oxidation (ATR).

Steam reforming

Steam reforming began as the demand for hydrogen grew exponentially due to the commercialisation of Haber-Bosch ammonia process. Thus, through the endothermic reaction between coal and steam (see reaction 4 below) and water-gas shift side reaction, hydrogen was able to be produced.

$$C + H_2O \Leftrightarrow CO + H_2 \quad (4)$$

$$CO + H_2O \Leftrightarrow CO_2 + H_2 \quad (5)$$

This then led to the realisation that any hydrocarbon based feedstock ($C_XH_YO_Z$) can be used to extract hydrogen through a form of syngas production (Kolb, 2009). The composition of the reformate product can be expressed using reaction 6 (Kolb, 2009) below.

$$C_xH_yO_z + (x - z)\,H_2O \Leftrightarrow x\,CO + \left(x - z + \frac{y}{2}\right)H_2 \quad (6)$$

The most common modern-day fuels utilised for the process of steam reforming is methane (CH_4) and methanol (CH_3OH) due to their availability and high hydrogen content. Other fuels such as liquefied petroleum gas (LPG) and heavier alcohols (ethanol etc.) have also started being used.

Partial oxidation

Kolb (2013) explains partial oxidation as the conversion of fuels at oxygen deficient feed composition and proceeds to explain the concept further with equation 7 below:

$$C_xH_yO_z + \frac{(x-z)}{2}(O_2 + 3.76\,N_2) \Longrightarrow x\,CO + \frac{y}{2}H_2 + 3.76\frac{(x-z)}{2}N_2 \quad (7)$$

The reaction kinetics of the partial oxidation reaction are far faster and kinetically favoured over the steam reforming reactions (Aartun et al., 2005). Partial oxidation only requires the fuel and air in the feed as water evaporation is not required (Kolb, 2013). However, as a result of the lack of water in the system the carbon monoxide (CO) concentrations are far higher compared to steam reforming and subsequently adds a far higher demand on CO clean up devices if fuel cells are connected to the fuel processor (Kolb, 2013).

Auto-thermal reforming

Auto-thermal or oxidative steam reforming is a process similar to that of steam reforming, the difference comes in when air or oxygen is co-fed with the steam into the reactor. The addition of air into the system allows the hydrocarbon feedstock to be reformed to a certain degree while the rest is oxidised.

$$CH_4 + \frac{3}{2}O_2 \Leftrightarrow CO + 2H_2O \qquad \Delta H°_{rxn}{}^{298K} = -519\ kJ/mol \quad (8)$$

The air is fed in such a ratio to the steam in order for the exothermic oxidation of the hydrocarbon, to provide the exact theoretical heat required to drive the endothermic reforming reaction, and as a result forms a theoretical self-sustaining reaction (Kolb, 2013). The net reaction was described by Kolb (2013) and is shown below by equation 9.

$$C_xH_yO_z + n(O_2 + 3.76\,N_2) + (x - 2n - z)\,H_2O \Longrightarrow x\,CO + \left(x - 2n - z + \frac{y}{2}\right)H_2 + 3.76n\,N_2 \quad (9)$$

The auto-thermal reforming process produces a reformate product with a lower H_2: C ratio than that of steam reforming making steam reforming the more ideal choice for hydrogen production for use by PEM fuel cells. However, Kolb (2013) mentions that the drawbacks making use of the auto-thermal reforming is the formation of 'hotspots' at the reactor inlet due to the favouring of the faster, more kinetically favoured, oxidation reaction compared that of the steam reforming reaction.

The addition of small amounts of air into the steam reforming system, where a low oxygen to carbon (O/C) ratio is held, prevents the formation of coke at the catalyst (Kolb, 2013). Table 2.2 compares the advantages and challenges of each the reforming technologies.

Table 2.2 – Comparison of the different reforming technologies (adapted from Holladay et al., 2009)

Technology	Advantages	Disadvantages
Steam reforming	Most extensive industrial experience	Highest air emissions
	Oxygen not required	
	Lowest process temperature	
	Best H_2/CO ratio for H_2 production	
Auto-thermal reforming	Lower process temperature than partial oxidation	Limited commercial experience
	Low methane slip	Requires air or oxygen
Partial oxidation	Decreased desulfurization requirement	Low H_2/CO ratio
	No catalyst required	Very high processing temperatures
	Low methane slip	Soot formation/handling adds process complexity

2.2.2 Water-Gas Shift

As mentioned in the PEM fuel literature, the PEM fuel cell's (PEMFC) platinum based catalyst and Nafion® based membrane are highly sensitive to the concentration of carbon monoxide. The carbon monoxide bonds irreversibly to the platinum in the case of the low temperature PEMFC and drastically reduces the operating efficiency of the fuel cell. The threshold concentration is mentioned by Barbir (2005) is around 50 ppm. Ideally the concentration of CO in the feed coming from the fuel processor train should be less than 10 ppm (Kolb, 2009).

As a result, CO clean up steps are required to reduce the CO concentrations to the desired ppm levels. These steps include a WGS step followed by either a selective methanation or preferential oxidation step.

The reformate product stream is generally made up of up to 12 % CO in the case of steam reforming and 8 % in the case of auto-thermal reforming (Farrauto et al., 2003). The WGS reaction allows this CO to produce more hydrogen via the reaction below:

$$CO + H_2O \Leftrightarrow CO_2 + H_2 \qquad \Delta H^{\circ}{}_{rxn}{}^{298K} = -44\ kJ/\ mol \qquad (9)$$

Due to the lower temperatures being favoured thermodynamically (slightly exothermic reaction), the kinetic rate is very slow at these temperatures making low space velocities being required (Farrauto et al., 2003). The use of conventional base metal catalysts (Fe for high temperature shift and Cu-Zn for low temperature shift) also thermodynamically favour lower temperatures and again the low temperatures result in low reaction rates. However, Farrauto et al. (2003) explains that in the case of fuel cell applications, the pyrophoricity of these base metal catalysts make in impractical and dangerous.

This pyrophoricity of the base metal catalysts point again to PGM based catalysts and despite the excessive cost, the PGM catalysts are non-pyrophoric, stable at high temperature and more tolerant to catalyst poisons like hydrogen sulphide (Farrauto et al., 2003).

Koryabkina et al. (2002) showed tests of the initial activity of Pt/Ceria (CeO_2) catalysts compared to commercial Cu-Zn-Al show that the Pt/CeO_2 catalyst have a performance advantage at high-space velocities. The base metal catalyst showed that the rate of reaction is governed by the rate of mass transfer, the Pt/CeO_2 catalyst does not and therefore can be operated at elevated temperatures (where the reaction kinetics are sufficiently fast) using a small catalyst volume. These facts then point again to the use of micro-channel reactors for the WGS reaction with a Pt/CeO_2 catalyst layer. However, the low-temperature activity is insufficient to achieve cost-effective low CO outlet concentrations. The exit concentration of CO from the WGS reactors can range from 0.1-1.0 % depending on operating conditions (Holladay et al., 2009).

2.2.3 Preferential oxidation and selective methanation

To further reduce the CO content to the 10 ppm requirement for PEM fuel cells, an additional CO clean-up step is needed. There a number methods available, namely preferential oxidation (PrOX), selective methanation, pressure swing adsorption and the use of a palladium-based membrane (Dagle et al., 2007). However, only PrOX and selective methanation are currently developed enough to be applicable to small scale reformate clean-up for use in PEM fuel cells (Kolb, 2009). The added complexity to this final clean-up step is the temperature restriction, whereby the PEM fuel cell operates at 80 °C and the WGS at around 200 °C (LTS) -350 °C (HTS), so these operating temperatures should operate between 80 °C – 300 °C.

The PrOX and methanation reactors both have their advantages and disadvantages. For PrOX small calculated amounts of air need to be incorporated into the reformate stream which in turn complicates the system by diluting the stream. Holladay et al (2009) gives the preferential oxidation equation below:

$$CO + \frac{1}{2}O_2 \Rightarrow CO_2 \qquad \Delta H°_{rxn}{}^{298K} = -283kJ/\,mol \qquad (10)$$

Another aspect is that if excess air is incorporated, hydrogen will be burned. Holladay et al. (2009) explains that the catalyst needs to be highly selective in only oxidising the minute quantity of CO remaining and not the hydrogen. The unwanted side reaction that occurs is shown below (Holladay et al., 2009):

$$H_2 + \frac{1}{2}O_2 \Rightarrow H_2O_{(l)} \qquad \Delta H°_{rxn}{}^{298K} = -286kJ/\,mol \qquad (11)$$

The selective methanation is simpler by virtue of the fact no air is introduced into the system (Holladay et al.,2009); however, three hydrogen molecules are used up to form one methane molecule (see equation 12). Additionally, CO_2 can react with the H_2 to form CH_4 and water (equation 13) and a reverse WGS reaction can also take place, so maintaining the correct reaction conditions is crucial for this step to be successful in reducing the CO content while minimising the excessive consumption of H_2.

$$3H_2 + CO \Leftrightarrow H_2O + CH_4 \qquad \Delta H°_{rxn}{}^{298K} = -206kJ/mol \qquad (12)$$

$$4H_2 + CO_2 \Leftrightarrow 2H_2O + CH_4 \qquad \Delta H°_{rxn}{}^{298K} = -165kJ/mol \qquad (13)$$

As a result of the decrease in fuel efficiency from methanation, most work has been focused on PrOX.

2.3 Methane steam reforming

The steam reforming of methane is a combination of 2 reactions. It involves the actual reforming of the methane and the oxidation of carbon monoxide product through the water-gas shift side reaction. The reforming reaction is a very endothermic reaction, while the water gas shift reaction is mildly exothermic which results in a net endothermic reaction and is shown below by equations 8 and 9 (Kolb, 2013).

$$CH_4 + H_2O \Leftrightarrow CO + 3H_2 \qquad \Delta H°_{rxn}{}^{298K} = 206\ kJ/mol \qquad (14)$$

$$CO + H_2O \Leftrightarrow CO_2 + H_2 \qquad \Delta H°_{rxn}{}^{298K} = -44\ kJ/mol \qquad (15)$$

$$CH_4 + 2H_2O \Leftrightarrow CO_2 + 4H_2 \qquad \Delta H°_{rxn}{}^{298K} = 165\ kJ/mol \qquad (16)$$

The net stoichiometric reaction (equation 10) is not equimolar, but has a larger number of moles on the right side, which according to Le Chatelier's principle will favour a low operating pressure but high temperature. The stoichiometric ratio of steam to methane (S/C) in the reforming reaction is 1:1, however this is not practical in industrial applications. The reasoning for this is with all base metal catalysts due to the carbon deposition (coking) occurs, rendering the catalyst inactive. So to counteract this coking effect excess steam is used to supress the rate at which coking occurs. Additionally, the use of excess steam favours the forward reforming reaction which is desired, the only negative aspect is the additional energy consumption associated with it. Typical steam-to-carbon ratios used in practical application are between 2.5 and 4.0 (Grasso et al., 2011).

The effect of temperature, pressure and steam-to-carbon ratio on the equilibrium conversion of methane is shown by Joensen and Rostrup-Nielsen (2002) in Figure 2.1 below.

The way in which the catalysed methane steam reforming reaction mechanism proceeds is very dependent on the type of catalyst used. The type of catalyst is characterised by the

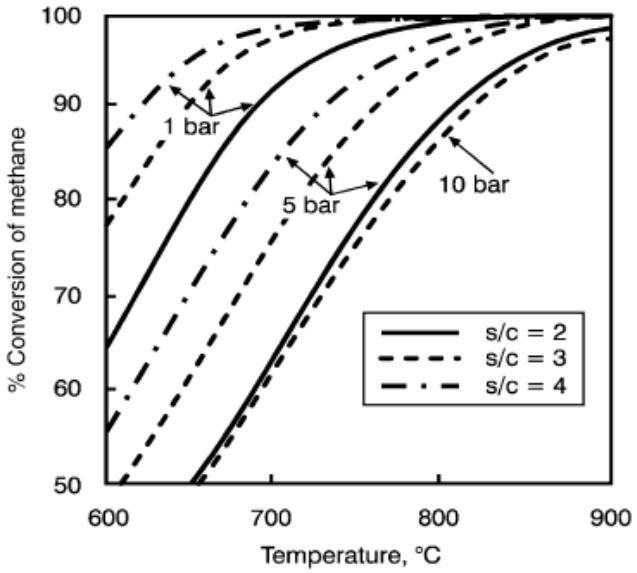

Figure 2.1 – Steam reforming of methane. Equilibrium conversion as a function of temperature, pressure and steam-to-carbon ratio (Taken from Joensen and Rostrup-Nielsen [2002])

catalytically active metal and the support material upon which the metal is deposited.

2.3.1 Catalysts for methane steam reforming

The most widely used catalysts for industrial steam reforming of methane is nickel or cobalt based and used as an egg shell catalyst. The catalysts are generally prepared by precipitating the active metal as an insoluble compound from a soluble salt form while in the presence of various refractory support materials, which are generally aluminates, silicates and other metal oxide promoters (Twigg, 1989). Another method of catalyst synthesis is the impregnation of a preformed support, generally alumina, with a metal salt solution which is subsequently heated to bring the metal to its oxide form. Alumina is the preferred catalyst as a result of the acidic nature of the alumina which aids the reforming reaction, the larger BET surface area and the lower cost. The added metal oxide promoters are normally alkaline-earth metals such as magnesium oxide, potassium oxide and calcium oxide. These metal oxides aid in accelerating carbon removal and improving the mechanical strength of the support.

As with most catalysts, the calcination and reduction procedures affect the nature and effectiveness of the catalysts. Wang and Lu (1998) and Matsumura and Nakamori (2004) both found that the Ni/γ-Al_2O_3 catalysts when reforming methane, are not as active when calcined at 500 °C than when calcined at 700 °C. The reduction of a catalyst allows the catalyst to be in its most active and usable form. In the case of the Ni reforming catalyst, when exposed to air, the presence of oxygen oxidises the Ni which then requires a reactivation step. Furthermore, the exposure of the active nickel metal to air can cause the

spontaneous ignition of the catalyst due to the pyrophoric nature of nickel (Provendier et al., 1999). The heat produced during the oxidation of the nickel metal is sufficient to cause the sintering and thus deactivation of the metal crystallites (Farrauto et al., 2003).

These things pose problems in the start stop operation in smaller scale fuel processors with the fuel having to be replaced relatively often. The low effectiveness factor (η) and utilisation per mass catalyst on an industrial scale, is normally counteracted with very high loadings of the catalytically active phase. Yet for small scale applications the quality of the catalyst proves to outweigh the quantity. Farrauto et al. (2007) explains how wash-coats with precious metals have proven to have excellent mechanical and chemical durability, a low-pressure differential across monolithic reactors and rapid responses to transient operation. Wang et al., 2004 then shows how PGMs have more great advantages with the higher resistance to coking The larger cost of the PGM catalysts may be offset by the improved utilisation of the catalyst through novel techniques and applications like micro-channel reactors and the wash-coating of catalysts to the micro-channel walls (see Sections 2.5 and 2.6).

Many experiments have been conducted to try find the optimum PGM and support to aid in producing the most stable and active catalyst. The testing done by Trimm and Önsan (2001) with PGM metals on an alumina support suggested that rhodium was the most active catalyst given the following turnover frequency numbers:

$$\text{Rh (13)} > \text{Ru (9.5)} > \text{Pd (1.0)} \sim \text{Ni (1.0)} > \text{Pt (0.9)}$$

In recent times testing of the Rh based catalysts have been performed by a number of groups. Wang et al. (2004) evaluated the effect of catalyst loading by preparing a 1, 5 and 10 wt % $Rh/MgO\text{-}Al_2O_3$ catalyst and testing them as wall catalysts within a micro-channel reactor set-up (see Figure 2.2). The different loadings resulted in different rhodium crystallite sizes as a result of the agglomeration and sintering of the particles during preparation. Hydrogen to carbon monoxide ratios of around 3.5 were achieved at a temperature of 830 °C and with a contact time of 1.9 ms. Testing of steam-to-carbon ratios of 1.0 was also conducted for 14 hours. The testing at low S/C ratios shows the higher resistance rhodium has to coking, and thus stability, by showing no loss in activity over the testing period (Wang et al., 2004). Similarly, Johnson et al. (2007) investigated methane steam reforming over Rh based catalysts in integrated micro-channels. They studied the reaction at high temperatures (900 °C) with S/C ratios of 1.0 and at a contact time of 27 ms. The 100-hour test carried out by Johnson et al. (2007) gave a stable catalyst performance; the test was done at 900 °C with a 3.7 wt % Rh catalyst.

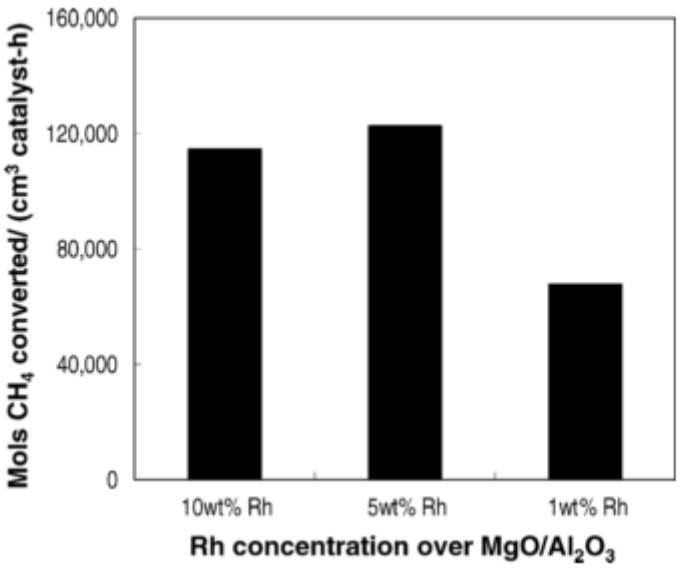

Figure 2.2 – The effect of rhodium catalyst on volumetric activity for methane steam reforming on a Rh/MgO-Al_2O_3 catalyst (830 °C, 12 atm, steam/carbon ratio = 2, contact time = 1.9 ms) (taken from Wang et al., 2004)

2.3.2 Kinetics of methane steam reforming catalysts

The earliest proposed steam reforming mechanisms were based on a non-porous nickel (Ni) foil based catalyst and was proposed by Fujimoto in 1933. Fujimoto (1933) had reported on methane steam reforming and methane decay over a reduced nickel foil and a 90 % nickel-alumina catalyst at atmospheric pressure. This was reported over an extensive temperature range of 400 - 1000 °C. For methane steam reforming a steam-carbon ratio of approximately 2.5 and constant feed conditions, constant methane conversions were achieved. The pure nickel foil catalyst showed severe deactivation over 593 °C, with a low methane conversion rate of a few percent being achieved between 704 – 899 °C. The nickel-alumina catalyst illustrated far higher stability at 700 °C by maintaining equilibrium conversion over a 250-hour testing period.

The mechanistic scheme based on Fujimoto's nonporous nickel foil (A) and a high activity porous nickel-alumina catalysts with diffusion limitations proposed by Van Hook (1980) is as follows:

A – Methane steam reforming/degradation over a nonporous nickel foil

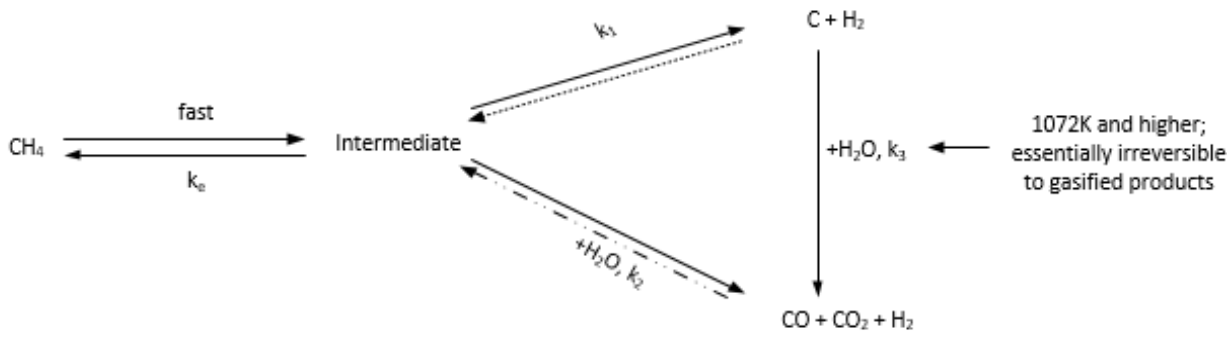

B – Methane/steam reaction on porous nickel-alumina catalyst with diffusion limitations

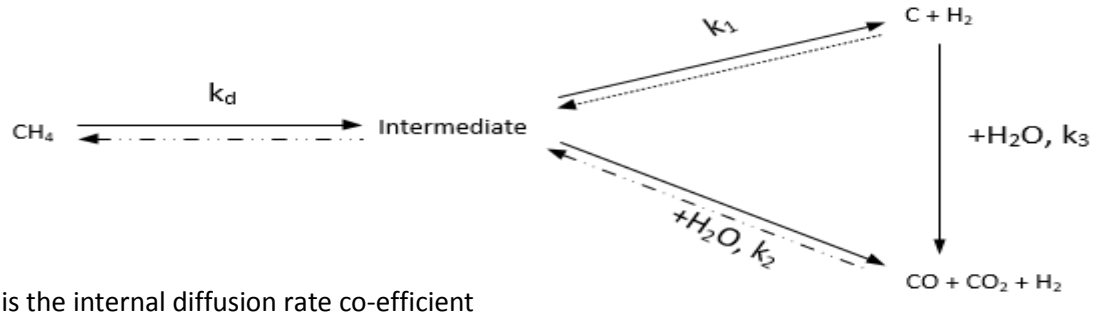

k_d is the internal diffusion rate co-efficient

Figure 2.3 – Methane steam reforming reaction pathway kinetics over a nonporous nickel foil catalyst (A) and a porous nickel-alumina catalyst with diffusion limitations (B)

After Fujimoto (1933) and Van Hook (1980), Xu and Froment (1989) proposed a far more detailed kinetic rate expression methane steam reforming with the nickel catalyst was supported on a magnesium oxide (MgO) promoted alumina (Al_2O_3). The reaction mechanism that Xu and Froment (1989) proposed for steam reforming of methane reaction kinetics is shown below. The reaction mechanism integrates the water-gas shift (WGS) reaction with the main methane steam reforming reaction.

In the mechanism steps below S represents the catalytically active site and the X in $X \cdot S$ is a surface bound complex. There are three steps in the proposed mechanism that are rate determining steps.

$Step\ 1$: $CH_4 + S \Leftrightarrow CH_4 \cdot S$ (17)

$Step\ 2$: $H_2O + S \Leftrightarrow O \cdot S + H_2$ (18)

$Step\ 3$: $CO \cdot S \Leftrightarrow S + CO$ (19)

$Step\ 4$: $CO_2 \cdot S \Leftrightarrow S + CO_2$ (20)

$Step\ 5$: $H \cdot S + H \cdot S \Leftrightarrow S + H_2 \cdot S$ (21)

$Step\ 6$: $H_2 \cdot S \Leftrightarrow S + H_2$ (22)

$Step\ 7$: $CH_4 \cdot S + S \Leftrightarrow CH_3 \cdot S + H \cdot S$ (23)

$Step\ 8$: $CH_3 \cdot S + S \Leftrightarrow CH_2 \cdot S + H \cdot S$ (24)

$Step\ 9$: $CH_4 \cdot S + O \cdot S \Leftrightarrow CH_2O \cdot S + S$ (25)

$Step\ 10$: $CH_2O \cdot S + S \Leftrightarrow CHO \cdot S + H \cdot S$ (26)

$Step\ 11$: $CHO \cdot S + S \Leftrightarrow CO \cdot S + H \cdot S$ $-$ $Rate\ determining\ step$ (27)

$Step\ 12$: $CHO \cdot S + O \cdot S \Leftrightarrow CO_2 \cdot S + H \cdot S$ $-$ $Rate\ determining\ step$ (28)

$Step\ 13$: $CO \cdot S + O \cdot S \Leftrightarrow CO_2 \cdot S + S$ $-$ $Rate\ determining\ step$ (29)

Xu and Froment (1989) found the rate equations based on the rate determining steps as the following:

For the steam reforming reaction $CH_4 + H_2O \Leftrightarrow CO + 3H_2$:

$$r_1 = \frac{k_1}{{P_{H_2}}^{2.5}}\left(P_{CH_4}P_{H_2O} - \frac{{P_{H_2}}^3 P_{CO}}{K_1}\right)/(\theta)^2 \quad (30)$$

And for the water-gas shift reaction $CO + H_2O \Leftrightarrow CO_2 + H_2$:

$$r_2 = \frac{k_2}{P_{H_2}}\left(P_{CO}P_{H_2O} - \frac{P_{H_2}P_{CO_2}}{K_2}\right)/(\theta)^2 \quad (31)$$

Where $\theta = 1 + K_{CO}P_{CO} + K_{H_2}P_{H_2} + K_{CH_4}P_{CH_4} + K_{H_2O}P_{H_2O}/P_{H_2}$

2.3.3 Industrial steam methane reforming

Industrial steam reforming is carried out fixed bed tubular reactors within a fired furnace to provide the heat necessary to drive the endothermic reaction. Typical reactors consist of 40-400 tubes with a diameter between 80-160 mm and lengths between 6-12 m (Grasso et al., 2011). The inlet temperatures for these reactors, depending on the application, can vary from 450 °C – 650 °C and exit temperatures between 700 °C – 950 °C (Rostrup-Nielsen, 1993).

There are some inherent problems with the length of the tubes required for this process. The main problem is that the reaction is mainly limited by the amount of heat that can be transferred across the packed bed which as a result can lead to accentuated axial and radial temperature gradients (Grasso et al., 2011). Another problem with the length of tubes and packed bed reactors is the large pressure drop across the reactor due to the catalyst packing. Thus for fuel cell application, a more compact and more efficient method of reforming would be required to make the fuel cell a transportable fixture.

2.4 Micro-channel reforming technology

In recent times the need or demand for lower capital and operating costs of chemical processes have led to novel approaches in reactor and process design. The chief way in which these costs are reduced is through process intensification. Process intensification refers to the strategy of making dramatic reductions in physical size while still achieving a given production objective (Dautzenberg and Murkherjee, 2001). The way in which these novel techniques have led to the intensification of reaction processes is through the miniaturisation of flow pathways into set geometric patterns (Simsek et al., 2011) and by integrating momentum, heat and mass transfer into a single vessel (Dautzenberg and Murkherjee, 2001).

2.4.1 Advantages and disadvantages of micro structured reactors

These micro-channel reactors are made of a number of parallel tubular reactors that have diameters ranging from 10 micrometres to several hundred micrometres. The small diameters relative to their length improve the reactors contact surface area) to reactor channel volume ratio to give values between 10 000 – 50 000 m^2/m^3 as opposed to 100 – 1000 m^2/m^3 attained in conventional fixed bed reactors (Kiwi-Minsker and Renken, 2005). The increased surface area to volume ratio can then enhance the speed at which thermodynamic processes occur by providing more catalytically active reaction sites.

The reduced diameter of the reactor channels ensures short radial diffusion paths leading to a narrow residence time distribution (RTD), which allows for high selectivity of the desired intermediate to be attained (Kiwi-Minsker and Renken, 2005). Due to heat transfer coefficients being inversely proportional to reactor diameter, the smaller reactor diameter results in the heat transfer coefficient to be vastly improved. Ehrfeld et al. (2012) measured heat transfer coefficients of approximately 10 $kW/m^2 \cdot K$ in micro-channel reactors, which is around an order of magnitude higher than the conventional fixed bed. This improved heat transfer then eliminates the problem of hot and cold spots that result in the reforming reaction being limited by the amount of heat that can be transferred for the endothermic reaction to proceed; thereby allowing the complete utilisation of the catalyst.

The negative aspects of the micro-channel reactors are the development of concentration gradients that form due to the lack of mixing as result of the laminar flow regime within the channel. These gradients then govern the external mass transfer rate and the extent at which molecular diffusion can occur. During the scale-up from the individual reactors to a stack multiple reactors in a parallel configuration, the ability to uniformly distribute the inlet gas across the channels has proved to pose some problems (Quiram et al., 2007). Furthermore, the generic way in which micro-channel reactors are created, is the laser welding of two plates together. This seal then makes it almost impossible to clean the inside of the reactors.

2.5 Catalyst preparation and application onto micro-channels

There are many ways in which the catalyst can be coated onto the walls of the micro-channels. These methods depend on the catalyst and on the properties of the surface onto which the catalyst is to be coated. The techniques utilised includes wash-coating, chemical vapour deposition, sol-gel deposition and impregnation (Meille, 2006). The most commonly practiced form of catalyst coating is wash-coating which will be discussed in further detail in Section 2.5.1 below.

2.5.1 Wash-coating of catalysts

The wash-coating method is the most common technique for catalyst preparation (Meille, 2006). The method described by Zapf et al. (2006) has been frequently referred to in order to get successful adhesion of various metal catalyst wash-coats onto the walls of micro-channel reactors.

The technique described by Zapf et al. (2006) involved the preparation of a γ-alumina supported catalyst wash-coat. The wash-coat suspension involved γ-alumina powder with an average particle size of 3 μm, de-ionised water, a polyvinyl alcohol (PVA) binder and acetic acid. Once the stainless steel micro-channel plates had been made, they were cleaned with isopropyl alcohol and dried. Thereafter the plates are calcined at 800 °C in order to create an oxide layer on the plate surface to aid in the adhesion of the alumina based wash-coat. The channels were then filled with the suspension and the excess scraped off with a blade. Two reactor platelets, each prepared with a Rh/Al_2O_3 catalyst, are then sealed by laser welding and tested for 100 hours by reforming propane. The catalyst showed great stability and activity over the entire testing period (Zapf et al., 2006).

Zhai et al. (2011) developed a technique for the steam reforming of methane whereby they created a metal-ceramic complex substrate onto which they impregnated the active metal. The ferrous chromium alloy (FeCrAlloy) substrate was first preheated to 1200 °C before spraying nanoparticles of α-alumina at high temperature onto the metallic substrate to achieve the required strength of the metal-ceramic complex. Thereafter a higher surface area boehmite sol made of aluminium hydroxide (γ-AlOOH) is applied which is converted to γ-alumina during the calcination process at 600 °C. Once the calcination was completed the metal-ceramic complex substrate was further impregnated with the prepared metal salt solution. The results attained from the study show that the Ni catalyst is stable for 500 hours at a steam-to-carbon ratio of 3.0 and for 12 hours at a steam-to-carbon ratio of 1.0 thereafter we can assume activity drops as a result of the catalyst deactivation (Zhai et al., 2011).

2.6 Factors affecting the properties of the wash-coat suspension

The properties of the wash-coat suspension are responsible for the quality of adhesion and properties that wash-coated layer within the micro-channel exhibits. The rheological properties of the suspension in combination with the general suspension composition would influence how the solids in a suspension will be dispersed and hence the suspension stability (Vallar et al., 1999).

The basic components to the suspension are the catalytically active metal deposited onto the support material and a solvent. However, there are a number of additives which are added to try alter the rheological properties of the suspension like binders, deflocculants and peptising agents like acids which affect the uniformity and reproducibility of the wash-coat.

2.6.1 Solids concentration

The solids concentration has a strong influence on the viscosity of the suspension. Studies performed by a number of groups (Agrafiotis and Tsetsekou [2000a]; Barbero et al. [2008]; Zamaro et al. [2005]; Mitra and Kunzru [2007]) have all seen the viscosity of the suspension increase logarithmically with increasing solids concentration until the solids content reaches 50 %.

2.6.2 Particle size

The particle size of the support is a large contributor to the overall stability of the suspension due to the effect it has on the viscosity of the suspension and the adhesion attained to the metal substrate which ultimately affects the nature of the wash-coat layer.

Agrafiotis and Tsetsekou (2000a) investigated the effect of the size of the support particle (2 µm and 6 µm) on the wash-coat suspension properties for the wash-coating of γ-alumina onto a cordierite monolith. The 2 µm particle exhibited an exponential effect on the suspension viscosity as the solids content increased while the 6 µm particle exhibited a far less pronounced exponential curve (see Figure 2.4 for the trends). These results indicated that the smaller particles had a higher suspension viscosity for the same solids content. The higher viscosity at a lower solids content increases the catalyst loading which would require less immersions/coating procedures and allows the result to be more reproducible in comparison to that of the larger particles.

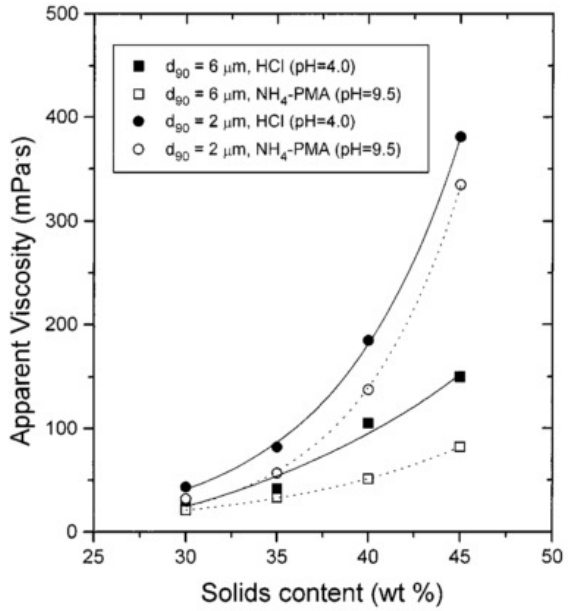

Figure 2.4 – The effect of particle size, solids content and deflocculants on the apparent viscosity of the wash-coat suspension (taken from Agrafiotis and Tsetsekou, 2000a)

In a previous study also conducted by Agrafiotis and Tsetsekou (2000b), the drop test to test adhesion quality indicated that the 2 μm particle had a better quality adhesion to the metal substrate than the 17 μm or 52 μm particle.

2.6.3 Solvent

The most common solvent of choice for studies preparing wash-coat suspensions is water. The solvent influences the slurry's properties by altering the viscosity and surface tension of the suspension which affects the final wash-coat. Water is the most ideal as solvent as it's relatively cheap, unreactive and the pH can be altered easily through addition of acids or bases. There have been minimal investigations into the use of other solvents as a result of these reasons.

2.6.4 Binder

A binder is always added to a wash-coat suspension not only to improve the stability of the suspension but also to improve the quality of the adhesion to the metal substrate and the amount of catalyst that can be loaded onto the support (Mitra and Kunzra, 2007).

A binder's particle size is the reason for the increased quality of adhesion and suspension stability. A binder is generally made up molecules that are smaller than the size of the catalyst particles in use. This enables the smaller binder molecules to pack themselves between the bigger catalyst/support particles. In practice, there are organic and inorganic binders, the choice between them is very catalyst and process specific as is the choice of metal salt from which you attain your active metal phase. Organic binders are seen to improve the contact between the larger catalyst particles, however are removed during the

calcination step by thermal decomposition due to the high temperature. Agrafiotis and Tsetsekou (2000a) explain that during the drying and calcination step the contact between larger catalyst particles is increased through the movement of the smaller binder molecules to the point of contact between the larger catalyst particles. This movement is achieved by capillary forces and aids in improving the quality of adhesion.

A frequently used organic binder is polyvinyl alcohol (PVA). The study conducted by Zapf et al. (2006) utilised 5 % PVA in their suspension to coat γ-alumina onto micro-channels, however no reasoning was given as to why this binder was chosen or this concentration of PVA. Hwang et al. (2007) indicated when coating alumina, that the use of a solution containing 1.5 % PVA produced a slower evaporation rate, but the slower evaporation reduced the rate of shrinkage and degree of cracking the wash-coat experiences. Zapf et al. (2006) recommends a calcination temperature of 600 °C to remove the PVA from the wash-coat. However, Germani et al. (2007), found small amounts of PVA remained on the deposited layer through their temperature programmed desorption (TPD) studies conducted under vacuum at 600 °C, which make sense as the PVA would not oxidise under vacuum.

Germani et al. (2007) also showed that the type of binder used influences the size and structure of the pores (particle packing) attained during the wash-coating after drying and calcination (see Figure 2.5).

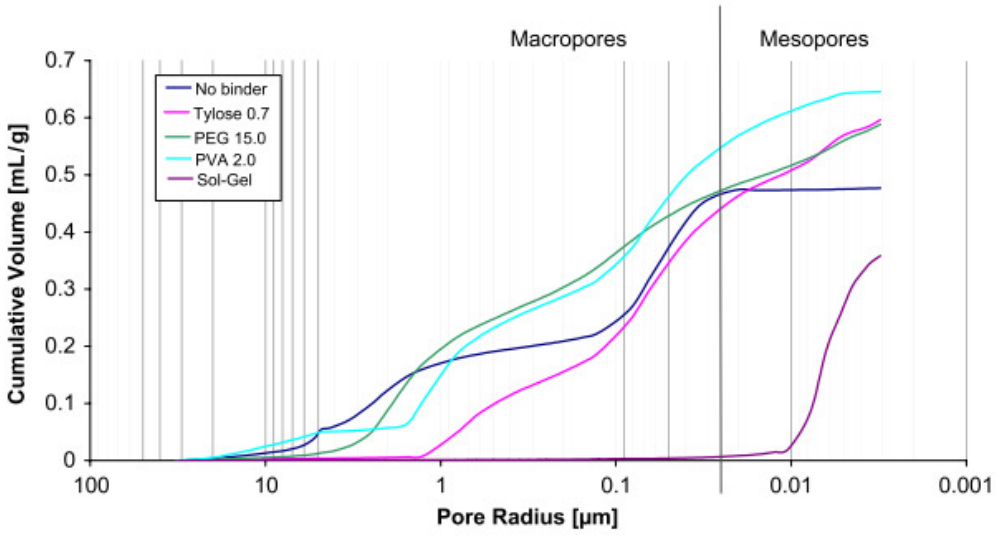

Figure 2.5 – Mercury porosimetry plot to illustrate the effect of the type of binder on the type of pores formed (type of particle packing) during the wash-coating process (taken from Germani et al. [2007])

Polyvinyl alcohol (PVA), methylhydroxylethyl cellulose (Tylose®) and polyethylene glycol (PEG) were compared by Germani et al. (2007) as organic binders for the deposition of an

alumina wash-coat on micro-channel surfaces. The binder's molecular weight influenced the suspension's viscosity, so for the equivalent amount of binder, the trend for the increase in suspension viscosity was as follows: Tylose® > PVA > PEG (Germani et al., 2007). Tylose® was found to provide the best compromise between particle packing and shrinking behaviour. The shrinking behaviour of the wash-coat is proportional to the bulk density of the suspension. A very low bulk density of the suspension results in a low shrinking of the wash-coat and insufficient cohesion of the catalyst particles. Alternatively, a very high bulk density of the suspension results in the cracking of the wash-coat as there is a large degree of shrinkage (Germani et al., 2007).

2.7 Properties of the wash-coated catalyst layer

The properties of the catalyst wash-coat layer that will influence the performance is the catalyst loading and in the sense that all micro-channel systems are generally made of several parallel reactors, the uniformity and reproducibility of the wash-coated layer will also influence performance. Moreover, the quality of wash-coat adhesion will also affect the performance. The uniformity of the wash coat is how evenly the suspension had taken to the curvature of the micro-channel and the reproducibility is how well the uniformity can be reproduced.

2.7.1 Uniformity and reproducibility

The uniformity and reproducibility of the catalyst wash-coat layer need to be high to have a minimal effect on other properties like catalyst loading and quality of adhesion. These factors ultimately influence mass transfer resistances, overall reaction conversion and reaction selectivity.

Both groups, Agrafiotis and Tsetsekou (2000b) and Mitra and Kunzru (2008), concluded that to be able to achieve high levels of coating reproducibility a lower solids concentration is required. Germani et al. (2007) and Mitra and Kunzru (2008) showed how the viscosity of the suspension affects the uniformity and reproducibility respectively. A lower viscosity suspension improved the uniformity and reproducibility, however a suspension with a viscosity that's too low affects the shape of the final wash-coated layer. A high viscosity solution was found by Germani et al (2007) to leave a thicker wash-coat layer on the walls of the micro-channel while the low viscosity solution left a thickened layer in the centre of the channel (see Figure 2.6).

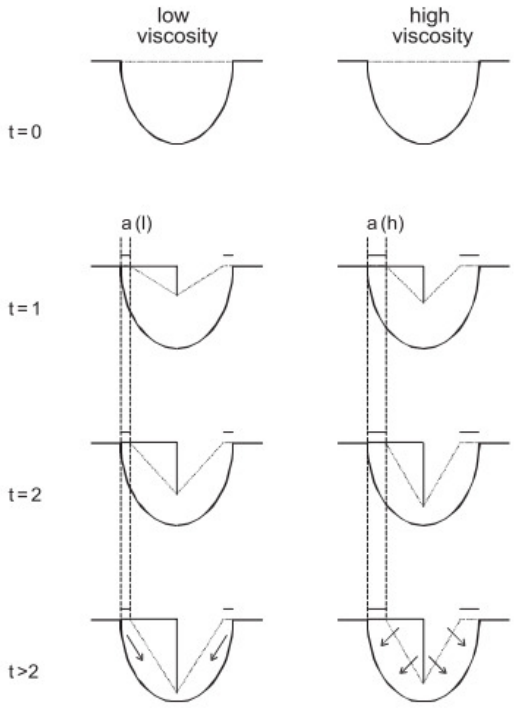

Figure 2.6 – Illustration of the drying process of a high and low viscosity suspension inside a micro-channel reactor as a function of time

2.7.2 Adhesion Testing

A few different tests have been developed to test the adhesion quality of the catalyst to the metal substrate. An early patented method by Yasaki et al. (1993) involved the catalyst coated layer being exposed to an ultra-sonication treatment for an hour in petroleum ether and dried thereafter for 2 hours at 110 °C. Once dried the loss in catalyst can then be determined. Stefanescu et al. (2007) utilised the ultrasonic adhesion testing and quotes results from Valentini et al. (2001) and Boix et al. (2003) saying that a stable wash-coat is a wash-coat that loses 10 % or less of its mass during the test

A more recently developed method by Zapf et al. (2006) is known as the 'drop test'. In this test the reactor platelet is drop from a fixed height and the loss of catalyst is recorded.

2.8 Previous micro-channel work at HySA/Catalysis

The purpose of this project is to further the work done by Zhou in 2014. In this study, Zhou (2014) tested two commercial catalysts, named catalyst YR and XR, and a single in-house synthesised Rh/Al_2O_3 catalyst in both packed bed and microchannel configurations.

These catalysts were proven to be stable in the packed bed configuration (Zhou, 2014). Catalyst YR was sent to a commercial partner to be wash-coated onto a set of micro-channel plates using their own undisclosed coating procedure. This catalyst was tested at 700 °C and 1 bar_g for a range of space velocities and steam to carbon ratios (2, 3 and 5). The catalyst on the walls of the micro-channel reactor was proved by Zhou (2014) to be stable for up to 100 hours on stream at space velocities 10 times that of the fixed bed when considering the activity per mass catalyst.

Zhou (2014) then proceeded to use the catalyst wash-coating procedure described by Zapf et al. (2006) to coat all three catalysts in-house. In all three cases, the in-house coated micro-channel reactors 'exhibited an immediate and continuous decline in activity with time on stream' as quoted by Zhou (2014), see Figure 2.7 below.

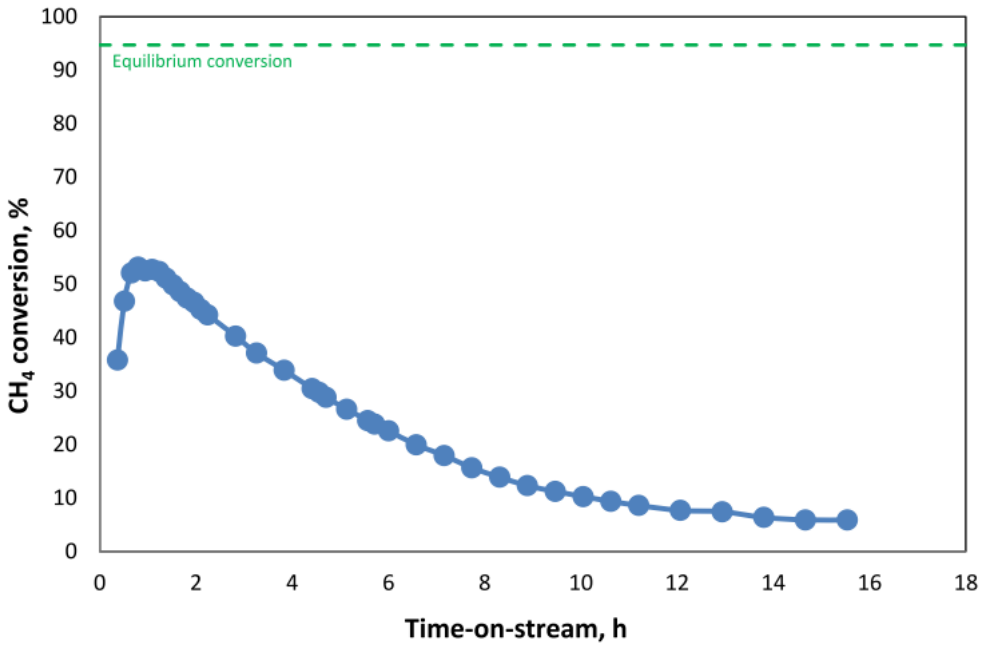

Figure 2.7 – A plot from Zhou (2014) showing the deactivation of the catalyst layer in a micro-channel test over a 16-hour period

Zhou (2014) carried out tests to ascertain the cause of the rapid deactivation of the in-house coated catalysts while the reactor plates coated with in-house catalyst but wash-coated by the commercial partner yielded a stable catalyst. Zhou showed experimentally that neither high temperature, nor steam induced sintering, nor carbon deposition were the cause of the deactivation. Zhou (2014) showed too that neither the coating process, alumina addition to

the catalyst coating nor reduction in particle size effected the reforming stability. No reason for the deactivation was ultimately determined.

Zhou (2014) proposed that alternative coating binders and a two-step coating/metallisation technique be evaluated.

Possible flaws

It must be noted that Zhou (2014) utilised a 150 µm alumina particle initially in his studies and used a reduced size (10-50 µm) particle at a later stage. In a study carried out by Truter (2011), she states that for sufficient adhesion of a wash-coat to a micro-channel reactor the particles should not exceed that of 5 µm, however this study involved the wash-coating of zeolites. This can be reinforced by the procedure described by Zapf et al. (2006) where a 3 µm alumina particle was used in the suspension preparation.

Zhou (2014) recommended the installation of an external water vapouriser to ensure that all the water entering the micro-channel is in the vapour phase as Zhou (2014) proposed the old set-up with a short, fixed bed did not allow for sufficient heat transfer rates.

3 Objectives of the Study

The aims of this study are to investigate the stability of an in-house manufactured and wash-coated catalyst layer in steam methane reforming micro-channel reactors. More specifically the objectives of this study are therefore to:

- Determine a bench mark methane conversions for different specific space velocity set points for a fixed bed reactor using an in-house prepared catalyst to compare with the micro-channel reactor. This is to compare the space velocities between reactor types at similar methane conversions

- To study the behaviour of an in-house produced and wash-coated catalyst layer used for methane steam reforming in micro-channel reactors

- Test the robustness of the coating procedure adopted in this study, produced by Zapf et al. (2006), under the conditions used in the steam reforming of methane
    - Determine possible causes of a non-robust system if instability is seen

- Understand catalyst instabilities in the work carried out by Zhou (2014)

3.1 Key Questions

- Will the micro-channel reactor outperform the conventional fixed bed reactor by an order of magnitude as stated by Kiwi-Minsker and Renken (2005)?

- Zapf et al. (2006) used 3 µm for the steam reforming of propane with a rhodium catalyst. Will the 3 µm alumina used by Zapf et al. (2006) provide sufficient adhesion at the harsher steam methane reforming conditions?

- Will coke formation play a role in catalyst instability?

- Is it possible to attain similar quality wash-coated catalyst layers across different wash-coating suspension batch sizes?

4 Experimental Procedures

The experimental procedures in this project involve the testing of in-house prepared catalysts in both fixed bed and micro-channel reactor configurations.

4.1 Catalyst synthesis

4.1.1 In-house catalyst preparation

The in-house prepared, alumina supported, rhodium catalysts were prepared using incipient wetness impregnation. A few different catalysts were prepared with varying types of alumina. The standardised catalyst was a 1.0 wt% Rh/Al_2O_3 catalyst using 3 µm alumina powder from Alpha Aesar. However, to draw a comparison a 1.0 wt% Rh/Al_2O_3 catalyst using the 150 µm NWA-155 Puralox alumina powder from Sasol was also prepared to see if the particle size of the support affects the catalyst stability.

The metal precursor used for the synthesis of catalysts was a Sigma-Aldrich rhodium nitrate salt [$Rh(NO_3)_3$], containing 36 wt% rhodium. Depending on the amount of catalyst and metal content required the amounts of salt water and alumina will vary accordingly. The salt is dissolved in the de-ionised water at room temperature before being added drop wise to the alumina powder until the point at which all the pores of the support are filled (point of incipient wetness).

Once the incipient wetness impregnation step is complete, the resulting catalyst is subsequently dried in air at 60 °C for 2 hours and calcined at 450 °C for 2 hours (ramp rate 1°C/min). The calcined catalyst with 150 µm support is then manually micronized with a mortar and pestle to give a particle size distribution (PSD) shown in Table 4.1 below. For the PSD a Malvern Mastersizer 2000 was used.

Table 4.1 - Particle size distribution results of the milled Sasol Puralox catalyst

d (0.1)	d (0.5)	d (0.9)
2.835	33.843	155.099

4.2 Chemical and physical catalyst characterisation

4.2.1 Brunauer-Emmett-Teller surface area and hydrogen chemisorption

The Brunauer-Emmett-Teller surface area analysis for all samples was conducted using the standard adsorption procedures in a micromeritics apparatus (ASAP 2000) equipped with two vacuum pumps (E2M-0.7)

4.2.2 Inductively coupled plasma optical emission spectroscopy (ICP-OES)

Inductively coupled plasma optical emission spectroscopy was used for the determination of rhodium of content in all catalyst samples. The apparatus used was a Varian 730 ICP-OES spectrometer. The catalyst sample was first added to a mixture of highly corrosive acids, predominantly made up of hydrofluoric acid, to be digested in a MARS-5 microwave digester before being neutralised with boric acid prior to the sample analysis.

4.2.3 Scanning electron microscopy coupled with energy dispersive X-ray spectroscopy (SEM-EDS)

A FEI Nova Nano-SEM instrument was used with a 200 V to 30 kV electron beam using a tungsten or LaB6 filament. The samples were placed on the sample plate in the temperature controlled chamber before being closed and evacuated. The samples were photographed up to a magnification of 100 000 times. The EDS utilises an Oxford X-Max silicon drift EDS detector which produces high resolution EDS spectra with productive count rates at low beam currents.

4.3 Micro-channel reactor preparation

4.3.1 Micro-channel plates

The microchannel plates utilised in this project are identical those used by Zhou (2014) and are made from stainless steel and the micro-channels were acid etched by Ätzetechnik Herz GmbH in Germany.

Figure 4.1 below gives an illustration of a single micro-channel plate showing the relevant dimensions. Each microchannel plate has 15 semi-circular channels and as Figure 4.1 shows, each channel has a 300 µm depth and a width of 500 µm. Two $\frac{1}{8}$ inch holes were drilled at the inlet and outlet of the plate to accommodate an $\frac{1}{8}$ inch tube for the feed delivery and product removal during the process. A complete micro-channel reactor is formed when two plates are laser-welded together after being thermally treated, wash-coated with a catalyst and subsequently calcined.

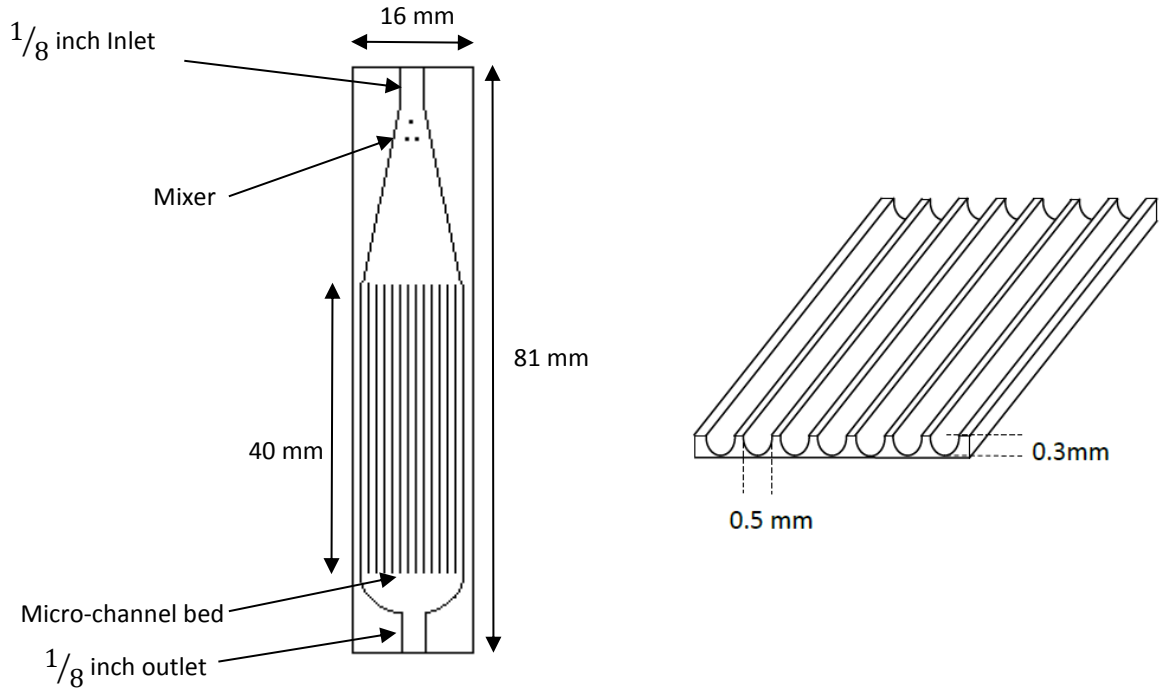

Figure 4.1 – A) A schematic of a typical micro-channel with relevant dimensions B) micro-channel cross-sectional view (adapted from Zhou (2014))

Zhou (2014) had an elemental analysis conducted on the plates and the results of this analysis are shown below in Table 4.2.

Table 4.2 – Results of the elemental analysis conducted on the stainless steel micro-channel plates by Zhou (2014)

Element	wt%
Carbon	≤ 0.08
Silicon	≤ 1.0
Manganese	≤ 2.0
Phosphorus	≤ 0.045
Sulphur	≤ 0.015
Chromium	16.5 – 18.5
Molybdenum	2.0 – 2.5
Nickel	10.5 – 13.5
Titanium	5 C ≤ 0.7

4.3.2 Wash coating methodology

The wash-coating procedure developed by Zapf et al. (2006) for alumina based catalyst wash-coating onto micro-channel reactors was followed. The process involves the following smaller procedural steps:

- Thermally pre-treating the micro-channel plates
- Preparing a suspension for catalyst wash-coating
- Wash-coating the catalyst suspension onto the prepared plates
- Post wash-coating plate treatment

Micro-channel plate pre-treatment

The pre-treatment process begins with the drilling of $\frac{1}{8}$ inch holes at the inlet and outlet of the reactor plate to allow the fitting of an $\frac{1}{8}$ inch tube for feed delivery and product removal. Thereafter the plates are submerged in isopropanol and cleaned in the ultrasonic bath for 15 minutes to remove all residual impurities on the plate and channel surfaces. The plates are then left to dry at room temperature.

The plates are then thermally treated in air at 800 °C for two hours. The purpose of this is to form a thin oxide layer on the surface of the micro-channel plates to aid in the proper adhesion of the wash-coated catalyst layer and the metal substrate. The plates were thermally treated using the following temperature program:

- Heat to 120 °C at a rate of 1 °C/min, and hold for 2 hours
- Heat to 800 °C at a rate of 1 °C/min, and hold for 2 hours
- Allow to cool to room temperature

Once heat treated the plates are now a dark brown colour and not the metallic colour as before; also, the plates are now always handled with gloves. The plates are weighed after this thermal treatment and again after the final plate calcination once wash-coated.

Catalyst wash-coating suspension preparation

Zapf et al. (2006) used the following components to prepare the catalyst suspension:

- 5 g of Polvinyl alcohol (PVA)
- 75 ml de-ionised water
- 20 g of prepared catalyst powder
- 1 g of acetic acid

To prepare the suspension, 5 g of PVA was added to 75 ml of de-ionised water in a vial and placed in a water bath with a magnetic stirrer and was stirred at 160 rpm and 65 °C for 3 hours or until all the PVA had dissolved. Thereafter the solution was left overnight to allow get rid of the air in the now viscous solution.

The 20 g of catalyst powder is then added to the solution along with 1 g of the peptising agent, acetic acid. The suspension is then stirred at 160 rpm at 65 °C for two hours, followed by stirring for another 3 days or until the suspension has homogenised. The test to see if the suspension has sufficiently homogenised is to visually see if the suspension has 'smooth' edges on the vial walls when swirled. If the suspension had not homogenised sufficiently it is then stirred until such time it passes the visual inspection test.

Micro-channel wash-coating

The micro-channel plate wash-coating process begins with taping the area around the channels and taking care not to cover the channels themselves. Figure 4.2 below illustrates how the taped area is marked, where the taped area is shown in grey.

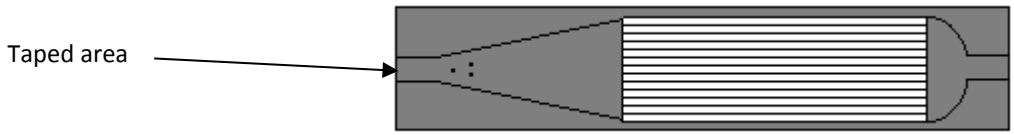

Figure 4.2 – Illustration of how the micro-channel plate is taped off prior to catalyst wash-coating. The grey area indicates the taped off area while the white area shows the free channels.

Truter (2011) advised that the coating procedure happens in three stages. Firstly a couple of drops of the suspension are added to the centre of the plate (See Figure 4.3 below for step-wise coating procedure) then with the help of a sharp edged scraper, the suspension is scraped from the middle of the plate toward the one edge (stage 1 in Figure 4.3) and is repeated scraping the suspension from the middle to the other side of the plate (stage 2 in Figure 4.3). Lastly the suspension is scraped across the entire plate from the stage 2 edge right across to the edge used in stage 1 (see stage 3 in Figure 4.3), taking care that each of the channels are filled. Truter (2011) also says that the amount of suspension is critical and subsequent additions of suspension will unfavourably effect the wash-coated catalyst layer.

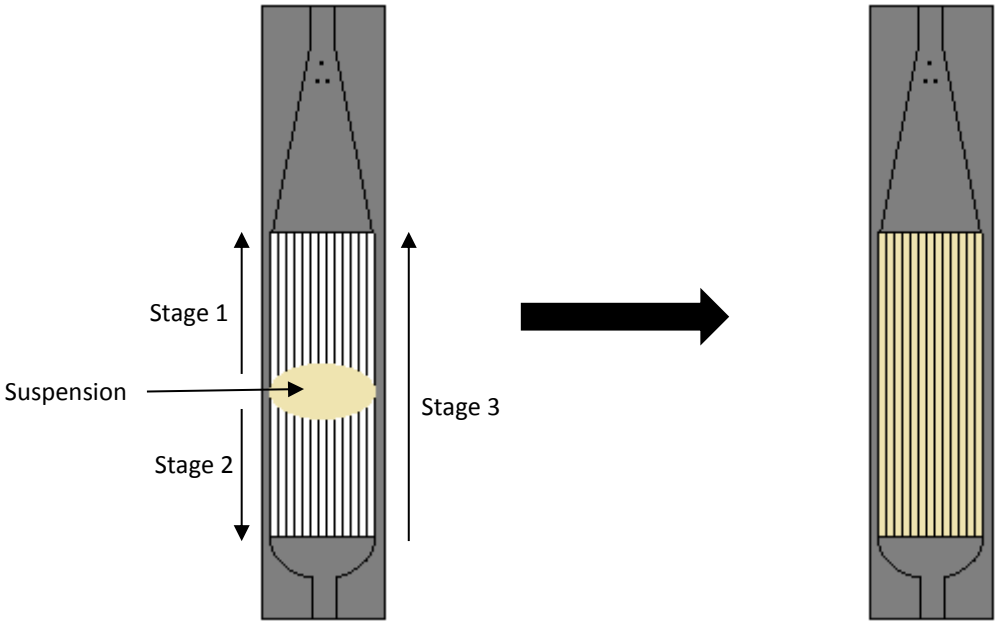

Figure 4.3 – Stage wise micro-channel wash-coating procedure

Post wash-coating plate treatment

Once the wash-coating procedure is complete the plates are then dried in ambient conditions for 3 hours and care is taken to make sure the suspension has sufficiently dried before removing the tape. Once the tape was removed, the plates were then dried further and thermally heated treated to remove the PVA binder, peptising agent and residual water. Thermogravimetric analyses (TGA) were carried out to help ascertain the correct heating rate for the temperature program used in the calcination. The temperature program used was identical to that of Zhou (2014), and is as follows:

- Heat to 120 °C at a rate of 1 °C/min, and hold for 2 hours
- Heat to 600 °C at a rate of 1 °C/min, and hold for 2 hours
- Allow to cool to room temperature

Once the plates were cooled the excess catalyst outside the micro-channels was removed and thereafter the plate were weighed again to ascertain the exact mass of catalyst on each plate to establish accurate flow rates to maintain a constant space velocity numbers.

Once establishing the final catalyst weight on the reactor plates, the micro-channel plates are laser-welded together face to face along with a corresponding $\frac{1}{8}$ inch tube at the inlet and outlet. These components form the reactor and can be seen in Figure 4.4 below. Due to the temperature sensitivity of the coated catalyst, Pulsco laser-welding was used in the welding process due to its high accuracy and concentrated heat source.

4.4 Steam methane reforming test unit

The steam methane reforming apparatus used in this project consists of two different set-ups, one for the microchannel reactor and one for that of a fixed bed reactor. Besides the physical difference in reactors, the variance in set-up is only the way in which steam is introduced into the system.

Apart from the different steam (water) delivery systems the unit consists of a segment for feed gas delivery, the reactor assembly itself (micro-channel or fixed bed) and a water knockout system after the reactor prior to the online gas chromatography product analysis.

A piping and instrumentation diagram is given in Figure 4.4 below.

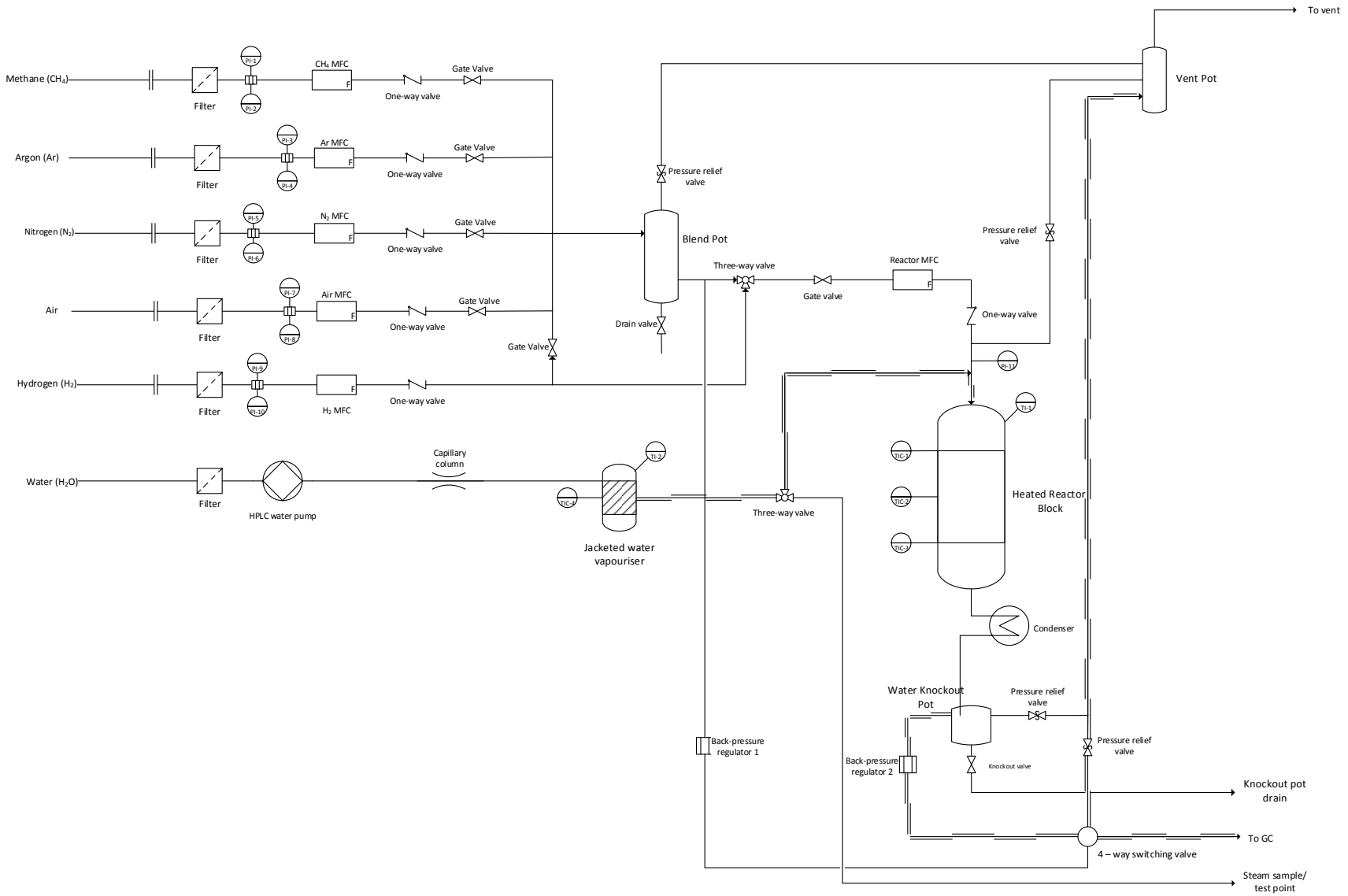

Figure 4.4 – Piping and instrumentation diagram of the micro-channel reactor configuration

4.4.1 Feed gas delivery

All the dry gases used in this project are from gas cylinders supplied by Air Liquide South Africa or Air Products South Africa. The flow rates of each gas into the system are regulated using individual Brooks instruments mass flow controllers (MFCs, T97692 series) that are calibrated for standard temperature and pressure conditions (STP). After each individual gas MFC, the dry gases are then fed into a blend pot, whereby a large fraction of the gas is fed to the reactor via a further reactor specific MFC and the excess gas is sent to a bypass stream. The bypass stream is then analysed using the online gas chromatography (GC) to determine the composition of the dry feed.

Deionised water was introduced into the system using an HPLC pump (Lab Alliance – series 1500) and a 50 cm long capillary column. The HPLC pump feeds the water through the capillary column (internal diameter of 50 µm) and into the vaporiser section for each of the reactor assemblies. The purpose of the capillary is to provide a pressure difference between the pump head and that of the vaporiser and results in a more constant feed of water.

4.4.2 Water vaporiser

In the case of the fixed bed reactor, water is fed into the reactor through the capillary and into the top of the reactor vessel. Special care was taken to ensure the capillary was in physical contact with the silicon carbide packing inside the reactor tube to avoid any flash vaporisation of water droplets but rather a smoother vaporisation as the water passing over the packing before reaching the catalyst particles.

The micro-channel reactor set-up contains an external vaporiser that is fed by the HPLC pump and capillary column to feed the system with steam instantly as opposed to the fixed bed where the water evaporates over the packing inside the reactor vessel. The vaporiser has a three-way valve with a ‘vent’ position that allows one to check for the presence of steam prior to feeding the reactor. This ensures no water but only steam encounters the catalyst.

4.4.3 Reactor Assembly

There were different reactor assemblies used in this study, namely the packed bed and micro-channel reactor configurations. Each reactor was placed within the cylindrical core of a furnace containing three heating bands. These bands could be controlled individually to aid in the establishment of the biggest isothermal zone possible during reaction proceedings (see Reactor temperature profile plot in the appendix).

Packed bed reactor

The packed bed reactor used in this study has a length of approximately 70 cm and an inner diameter of 16 mm. The reactor was subdivided into 3 zones, firstly the vaporiser zone, the catalyst zone and then the lower heating zone. The reactor wall has been fitted axially with a 3 mm thermowell in order to incorporate a thermocouple and in the case of this study, a high temperature K-type thermocouple. These sectors are illustrated in Figure 4.6.

To assemble the three different reactor sectors, the reactor is first to be put into a vice on a work bench. Once the reactor is secure, a small piece of quartz wool is placed down at the very bottom of the reactor to prevent any silicon carbide (SiC) blowout at the end of the reactor. Thereafter the lower heating band is filled with 1 mm silicon carbide packing. Once the lower sector had been completed, 0.3 g of catalyst was diluted with finer packing (300 µm silicon carbide) to take a total volume of 2 cm^3. The remaining volume is filled with 1 mm SiC packing in such a way that the capillary column is able to feed water into the reactor bed. This is to allow the drop-wise vaporisation of water.

Micro-channel reactor

Due to the shaping of the microchannel reactor and the need for an even distribution of heat to ensure a constant temperature profile, the micro-channel reactors are fitted inside a special metal sleeve made of an Inconel® alloy. The metal sleeves are made up of 4 segments (S1-S4) and are shown in Figure 4.5. Segments 1 and 4 have a circular opening to accommodate the $\frac{1}{8}$ inch inlet and outlet pipes while segments 2 and 3 have a rectangular opening large enough to fit and encapsulate the microchannel itself. In addition to these openings, there are two more circular openings, one is the thermowell to house the K-type thermocouple and the other is to accommodate the tie-bolt to hold all four segments together.

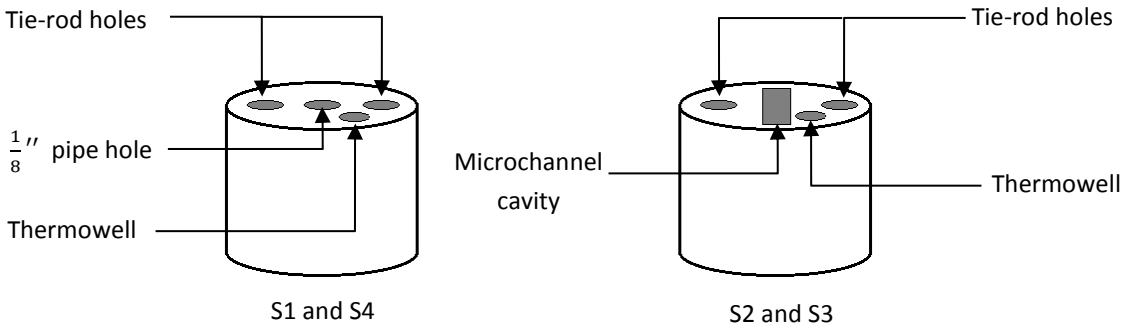

Figure 4.5 – Micro-channel sleeve segment illustration

Once the micro-channel reactors are fitted into the metal sleeves, the inlet is connected to the external vaporiser, which provides the steam, and the feed gas from the blend pot.

Figure 4.6 and 4.7 give an illustration of the completely assembled micro-channel and fixed bed reactor configurations.

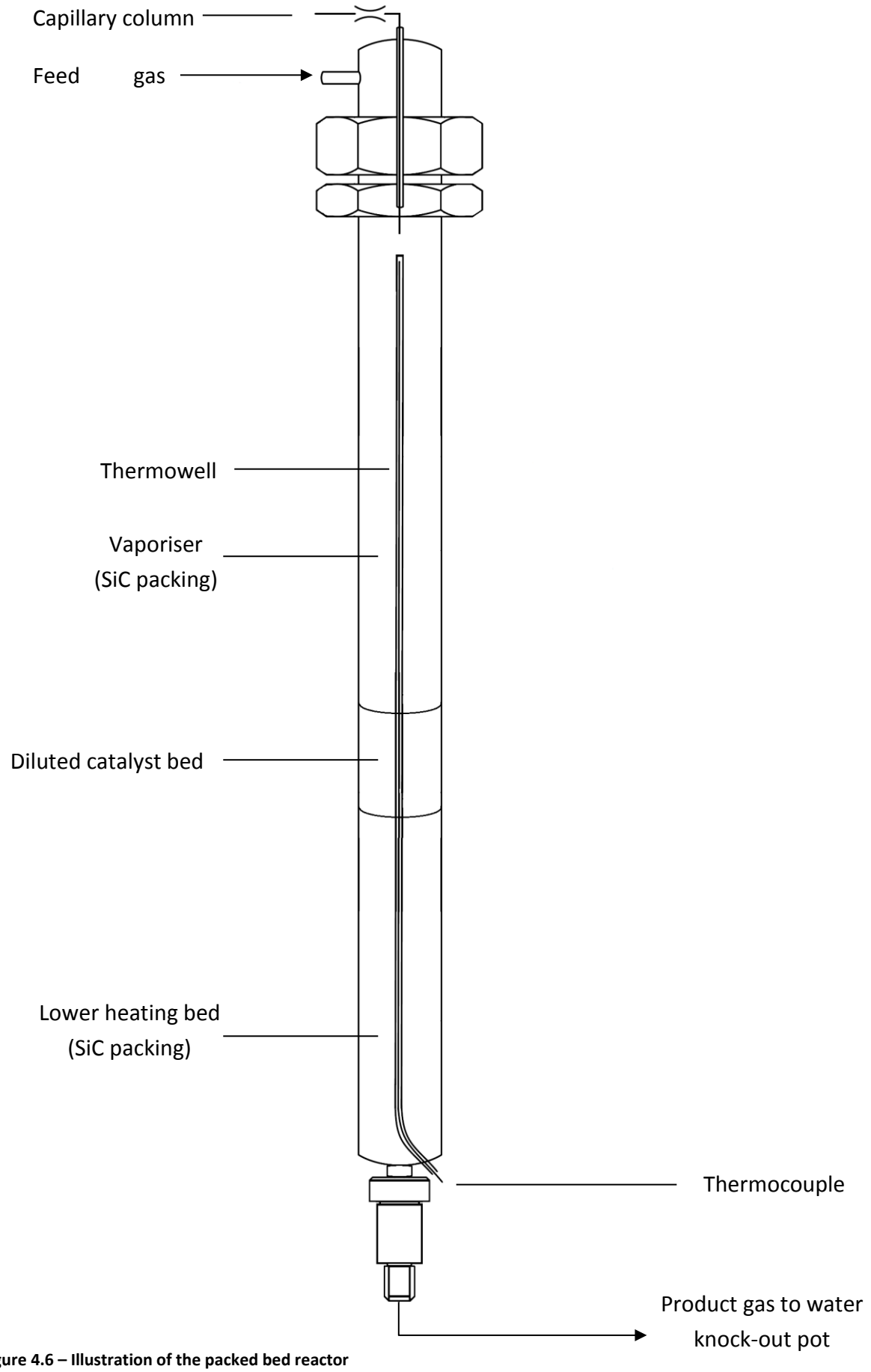

Figure 4.6 – Illustration of the packed bed reactor

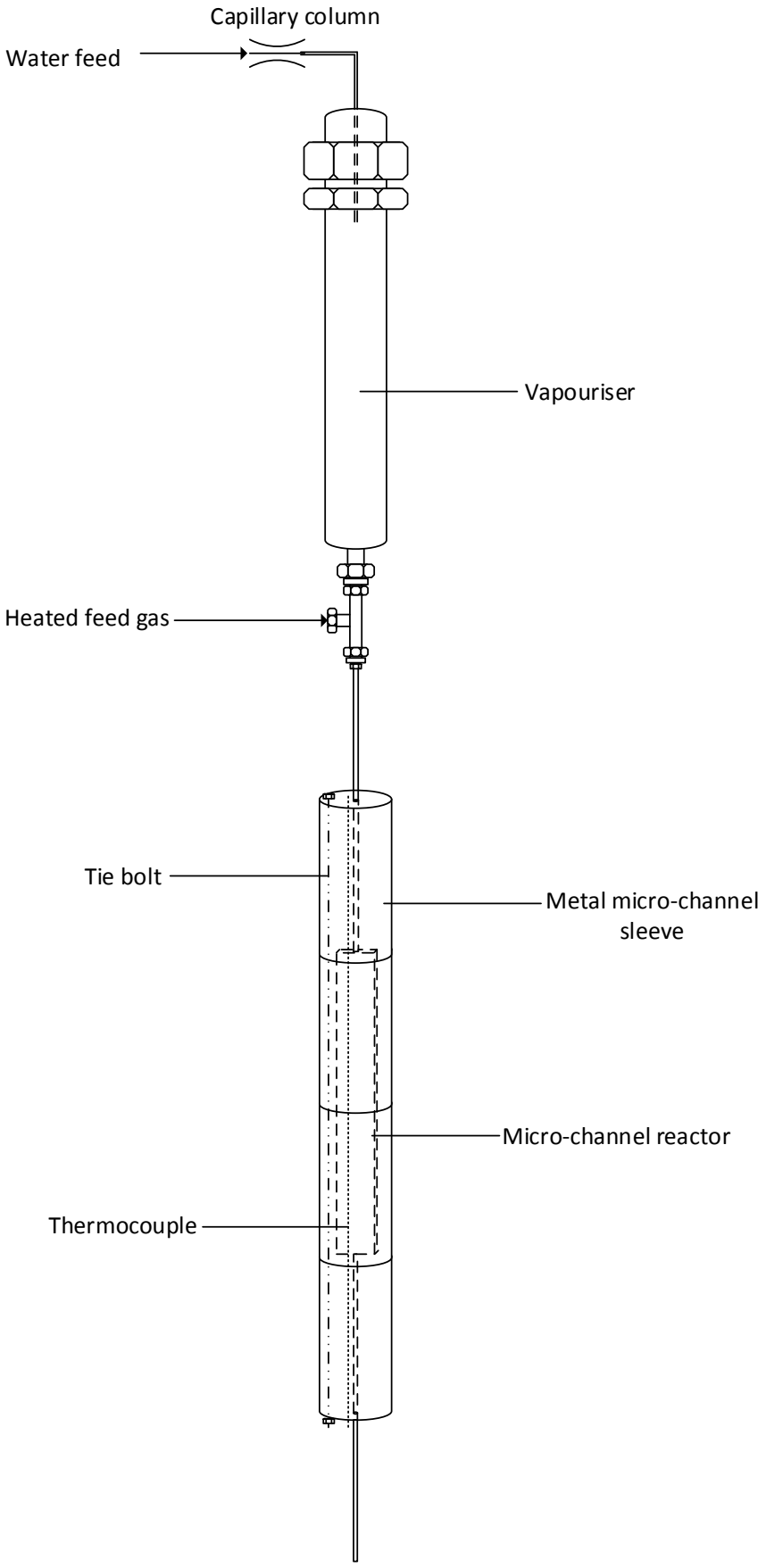

Figure 4.7 – Illustration of the experimental set-up for the micro-channel configuration

4.5 Steam methane reforming testing procedures

4.5.1 Reactor assembly and pressure testing

The welded micro-channel (Figure 4.7) and packed bed reactor (Figure 4.6) assembly is placed inside the furnace opening, followed by the connection of the feed and product lines and the insertion of the thermocouple into the reactor's thermowell. A pressure or leak test is then performed before an experiment and is conducted at 4 bar_g for approximately 5 hours. An acceptable pressure drop for the 5-hour duration of the test was deemed to be 0.1 bar.

4.5.2 Catalyst reduction procedure

Once a satisfactory pressure drop was achieved, the catalyst is then reduced in 40 sccm of pure H_2. The reactor temperature is then ramped up to 750 °C at 1 °C per minute from ambient temperature and then held at 750 °C for 2 hours before dropping the temperature back down to 700 °C.

4.5.3 Reactor operation

Start-up procedure

The heated lines and vessels were heated to the following temperatures and allowed to reach steady state before the run commences.

Table 4.3 – Temperature set points of heated lines and vessels

Heated lines or vessels	Temperature set point
Water vapouriser	300 °C
Feed gas and steam line to reactor	135 °C
GC lines	60 °C

- The dry methane and argon reactor feed was fed in excess to the blend pot using the respective mass flow controller settings. The excess dry feed gas was then released via a bypass stream through a back-pressure regulator.
- The water pump is started to begin steam production with the steam sampling valve open. Once the vapouriser and pump flow have reached steady state at the desired set point the three-way valve is switched from sampling to the reactor.
- After approximately 20 minutes the H_2 is switched off and the dry feed gas is introduced into the system.

On-line procedure

The on-line procedures used are procedures specific to changing a reaction condition. A minimum time of 6 hours was given for the system to reach a steady state.

During a run, temperature increases were done at a rate of 1 °C/min and for cooling a temperature set point is set and allowed to cool naturally.

When changes to the space velocity are made, the changes are done incrementally to both the dry feed and steam in order to maintain a constant steam to carbon ratio throughout. When the space velocity is increased, the water flow is first manipulated and allowed to stabilise before the dry feed gas flow is also changed; when the space velocity is decreased the dry feed gas flow is reduced before decreasing the steam flow.

Shut-down procedure

In shutting down an experiment the following procedure is put into effect:

- Methane and argon mass flow controllers are switched off and supply valves closed
- Immediately nitrogen is introduced to flush the system of the 'dry' reactants
- The steam flow is then switched off after 30 minutes
- Heating to all vessels is then shut down and allowed to cool naturally

Sampling procedure

During an experiment both the feed and product gas streams were sampled using a four-way switching valve prior to the online micro GC. The product gas is sent to the online micro GC after passing through a water catch pot and the 4-way valve, the excess dry feed is then diverted to the vent vessel during this time. This is then similar to the dry feed sampling and analysis, where the feed is sent to the online micro GC via the 4-way valve and the product gas is sent to the vent.

4.6 Steam methane reforming product analysis

4.6.1 Product analysis

The feed and product streams were analysed online by a Varian CP-4900 micro GC. This micro GC is fitted with 3 different columns:

- 10 m Molsieve 5 A column (MS5-10 m)
- 20 m Molsieve 5 A column (MS5-20 m)
- 10 m Pora Plot Q column (PPQ)

Each column could be operated independently at a different set of conditions and different carrier gases. These conditions at which each column operates can be seen in Table 4.4.

Each sample analysis takes approximately 7 minutes. In the data analyses, the H_2 peak was taken from the MS5-10m column and the CO_2 peak area from the PPQ column. However, the Ar, CH_4 and CO peaks were taken from the MS5-20m column for data analysis.

Table 4.4 – Operating conditions and carrier gases for the respective columns within the micro GC

	Column		
	MS5-10m	**MS5-20m**	**PPQ**
Carrier gas	Argon	Hydrogen	Hydrogen
Oven Temperature (°C)	50	50	50
Injector Temperature (°C)	40	43	42
Pressure (kPa)	150	150	80

The peak areas obtained from the GC chromatograms were related to the volumetric flow rate of each component using their respective relative response factors (RRF) and by the use of an internal standard of known volume. In this study argon (Ar) was used as the internal standard.

The relative response factors were determined through equation 28 during the GC calibration. The RRF of each component can be seen in Appendix 9.2. Using a reworked version of equation 28, the molar flow rates of reactants and products could then be determined when used in combination of the relative integrated peak areas (relative to the internal standard) under the chromatogram for each component.

$$\left(\frac{Moles_i}{Moles_{Ar}}\right) RRF_i = \left(\frac{Peak\ Area_i}{Peak\ Area_{Ar}}\right) \tag{32}$$

$$Moles_i = \left(\frac{Moles_{Ar}}{RRF_i}\right)\left(\frac{Peak\ Area_i}{Peak\ Area_{Ar}}\right) \tag{33}$$

5 Results

In this project, a number of tests were carried out to test the behaviour and robustness of an in-house made and wash-coated PGM catalyst layer using a procedure developed by Zapf et al. (2006). These tests also looked at the applicability of the coating procedure developed by Zapf et al. (2006) to wash-coat stainless steel micro-channel substrates for steam methane reforming. The catalyst selected for methane steam reforming was an alumina supported rhodium catalyst. The metal loading of rhodium in each catalyst was 1.0 wt%.

Two different forms of γ-alumina support were tested whereby they had two different manufacturers and two different particle sizes. The description and particle sizes can be seen in the table below:

Table 5.1 – The different forms of γ-alumina used in the study with their particle sizes as provided by their manufacturers

Manufacturer	Mean Particle Size
Sasol NWA-155 Puralox	150 µm
Alfa Aesar (K27Y013)	3 µm

The reported size of the alumina support used by Zapf et al. (2006) in their wash-coating procedure was 3 µm and thus the alumina used to make the benchmark catalyst was the 3 µm Alfa Aesar alumina. This standard catalyst was tested in both microchannel and fixed bed configurations.

The Sasol NWA-155 Puralox was used to replicate the experiments carried out by Zhou (2014), where the support was impregnated with the rhodium before being milled down to a mean particle size of 34 µm and once dried and calcined it was wash-coated onto the micro-channel reactor plates. Zhou (2014) tried to determine whether the catalysts and coating procedures that he employed yielded a stable performance at the conditions relevant to steam methane reforming.

The objective of replicating Zhou's experiments was to determine the cause of the instability in his wash-coated catalyst. Initial thoughts pointed towards particle size as the cause of the instability, as this was the only discrepancy in method used by Zhou (2014) and the method designed and carried out successfully by Zapf et al. (2006).

All experiments were carried out at 700 °C, 1 bar_g and with a steam/carbon ratio of 3. A list of catalysts, suspensions and experiments can be seen in Section 5.1 below.

5.1 Catalyst Preparation Summary

In this study 4 separate batches of catalyst were made, with 3 batches containing alumina supported rhodium catalysts and one 'blank' catalyst made with only alumina support. Table 5.2 summarises the 4 batches and includes the ICP results with the planned and actual respective metal content, alumina support used and the calcination procedure followed after incipient wetness impregnation.

Table 5.2 – Summary of the catalysts prepared for the wash-coating procedure

Name	Metal content	Type	Support Manufacturer	Size of support	Heat Treatment Method	Quantity	ICP Results
A	1 wt %	Rh/Al_2O_3	Alpha Aesar	3 µm	60 °C, 2 hours 450 °C, 2 hours	2.5 g	0.87 wt %
B	1 wt %	Rh/Al_2O_3	Alpha Aesar	3 µm	60 °C, 2 hours 450 °C, 2 hours	3.0 g	0.74 wt %
C	1 wt %	Rh/Al_2O_3	Sasol Puralox	30 µm	60 °C, 2 hours 450 °C, 2 hours	1.5 g	0.99 wt %
D	0 wt %	Al_2O_3	Alpha Aesar	3 µm		2.0 g	0.00 wt %

5.2 Summary of catalyst wash-coating suspensions

From the 4 batches of catalyst, a further 5 wash-coating suspension batches were made. The first batch of wash-coating suspension (I) was made with 2.0 g of catalyst A and 8 plates were wash-coated. Thereafter two batches of suspension (II and III) were made with 0.75 g of catalyst B per batch coating 4 and 12 reactor plates respectively. The last batch of suspension (IV) containing metal was with 1.5 g of catalyst C, the Sasol Puralox supported catalyst. The solids quantity refers to the wash-coating suspension batch size, where 2.0 g indicates a 10-fold reduction in batch size from the original batch size used by Zapf et al. (2006).

Table 5.3 – Summary of the catalyst wash-coating suspensions with the catalyst batch, solids concentration, treatment procedure

Name	Number of plates (reactors) coated	Catalyst	Solids Concentration	Solids quantity in Suspension	Reactor Plate Heat Treatment	Mass Distribution
I	8 plates (4 reactors)	**A**	20 wt %	2.0 g	120 °C, 2 hours 600 °C, 2 hours	[21 - 25] mg
II	4 plates (2 reactors)	**B**	20 wt %	0.75 g	120 °C, 2 hours 600 °C, 2 hours	[15, 23 - 19, 18] mg
III	12 plates (6 reactors)	**B**	20 wt %	0.75 g	120 °C, 2 hours 600 °C, 2 hours	[19 - 22] mg
IV	4 plates (2 reactors)	**C**	20 wt %	1.5 g	120 °C, 2 hours 600 °C, 2 hours	[18, 19 - 21, 23] mg
V	16 plates (8 reactors)	**D**	20 wt %	2.0 g	120 °C, 2 hours 600 °C, 2 hours	[19 - 21] mg

5.3 Summary of experiments

There were total of 9 experiments carried out in this study, only one of which was a fixed bed test using an un-coated, powdered 1 wt % Rh/Al_2O_3 catalyst, while the remainder of the experiments were micro-channel reactor runs at several conditions. Table 5.4 summarises the experiments and includes the catalyst batch and suspension batch codes which can be traced back to Table 5.2 and Table 5.3 to find out more details about the catalyst used and size of the suspension.

Table 5.4 – Summary of the experiments carried out with a title description, reactor type used and catalyst and suspension batches used in each of the experiments

Experiment number	Experiment Title	Reactor type	Catalyst Batch	Suspension Batch
1	Experiment 1 - Powdered Catalyst Test/Fixed Bed	Fixed Bed Reactor	A	N/A
2	Experiment 2 – Low starting space velocity	Micro-channel Reactor	A	I
3	Experiment 3 – Medium starting space velocity	Micro-channel Reactor	A	I
4	Experiment 4 – Medium starting space velocity repeat 1	Micro-channel Reactor	B	II
5	Experiment 5 – Medium starting space velocity repeat 2	Micro-channel Reactor	B	II
6	Experiment 6 – Low starting space velocity repeat 1	Micro-channel Reactor	B	III
7	Experiment 7 – High starting space velocity	Micro-channel Reactor	B	III
8	Experiment 9 – New reduction procedure with a medium starting space velocity	Micro-channel Reactor	B	III
9	Experiment 8 – Sasol puralox supported catalyst with high starting space velocity	Micro-channel Reactor	C	IV

5.4 Alumina support characterisation

The 3 μm Alfa Aesar alumina support was characterised for BET surface area. The surface area of the support was measured at two different heat exposure conditions, compared to untreated alumina. The heat exposure conditions were performed through exposing untreated alumina to 800 °C for 2 and 24 hours in stagnant air.

The untreated Alfa Aesar alumina was found to have a BET surface area of 80.81 m^2/g (Table 5.5). The alumina sample that was exposed to 800 °C for 2 hours had a reduced BET surface area of 65.18 m^2/g, a 15.63 m^2/g reduction in surface area. The sample, exposed to 800 °C for 24 hours, had a BET surface area of 50.35 m^2/g. This is a further reduction of 14.83 m^2/g. This reduction in surface area with extended heat exposure is consistent with the general trend seen in papers by Maciver et al. (1963) and Schaper et al. (1983). These papers explain that the exposure of the high surface area alumina to heat causes the sintering of the particles, thereby reducing the overall surface area and increasing the pore size.

Table 5.5 – BET surface areas of the 3 μm Alfa Aesar alumina with varying lengths of time exposed to 800 °C

Sample	BET Surface Area
Untreated Alfa Aesar alumina	80.81 m²/g
Heat treated Alfa Aesar alumina (2 h @ 800 °C)	65.18 m²/g
Heat treated Alfa Aesar alumina (24 h @ 800 °C)	50.35 m²/g

Table 5.6 indicates that with the reduction in surface area with increased heat exposure, the pore volume increases slightly while pore size also increases.

Table 5.6 – Effect of heat exposure on the pore volume and pore size of the 3 μm Alfa Aesar alumina

	Pore Volume		Pore Size	
	Adsorption	Desorption	Adsorption	Desorption
Untreated Alfa Aesar alumina	0.113 cm³/g	0.108 cm³/g	66 Å	78 Å
Heat treated Alfa Aesar alumina (2 hrs @ 800 °C)	0.114 cm³/g	0.117 cm³/g	83 Å	101 Å
Heat treated Alfa Aesar alumina (24 hrs @ 800 °C)	0.119 cm³/g	0.122 cm³/g	92 Å	107 Å

5.5 Powdered 1 wt% Rh/Al_2O_3 catalyst characterisation

Along with the characterisation of the support, characterisation of the 1 wt% Rh/Al_2O_3 catalyst was also done. In the case of the catalyst characterisation, physisorption and chemisorption was done.

Physisorption test gave a BET surface area for the calcined rhodium catalyst of 40.25 m^2/g catalyst. Chemisorption test results indicated the catalyst, 1 wt% rhodium on Alfa Aesar alumina, has a rhodium metal dispersion of 68.9 %. The metallic surface was determined to

be 3.28 m^2/g of sample and 303.24 m^2/g of metal. The average metal crystallite size was found to be 59 nm.

5.6 Catalyst coating characterisation

The characterisation performed on the wash-coating of fresh (before experiments) catalyst on the micro-channel plates included energy dispersive spectroscopy (EDS) and scanning electron microscopy (SEM) imaging to determine coated catalyst thickness and its composition.

The SEM imaging (Figure 5.1) of the side of one of the wash-coated micro-channel reactors showed that the thickness of the wash-coated catalyst layer was 19.65 µm thick. These measurements were done at different points along the channel to see if the thickness of the catalyst layer was a uniform one. Results from the SEM image shows very small differences in thickness between the wall and trough measurements, with the trough being only 0.3 µm thicker.

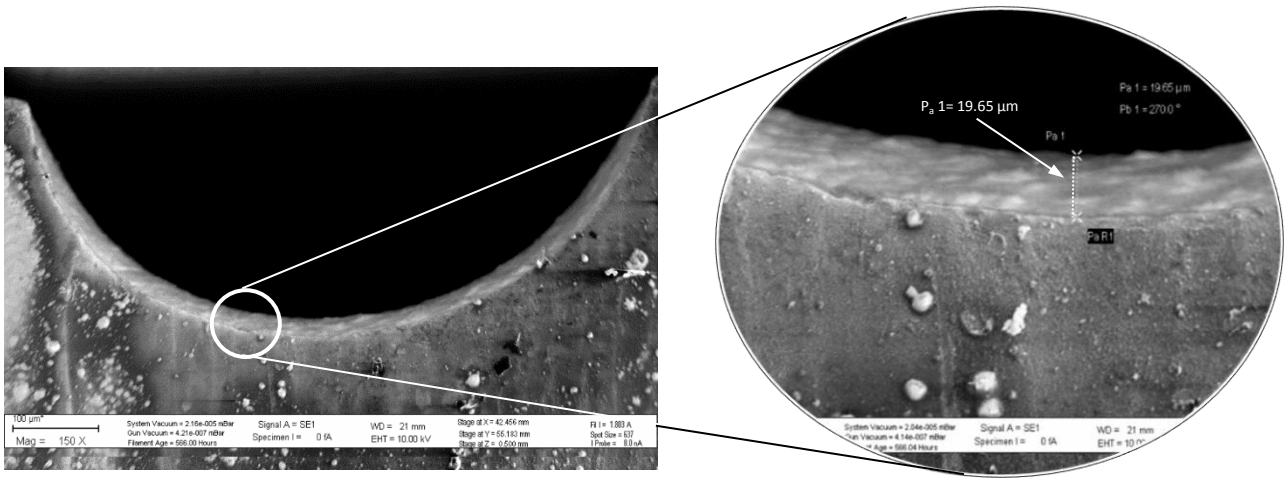

Figure 5.1 – Side view SEM image of the micro-channel reactor plate to determine the wash-coated catalyst thickness

The EDS measurements (Figure 5.2 and Table 5.7) on the wash-coated fresh catalyst layer indicated that there was a presence of rhodium and alumina on all three EDS spectra performed. The three spectra refer to three areas in which the EDS analysis is carried out and the subsequent compositions refers to the distribution of the elements in that area. From the elemental composition in Table 5.7, we can see that there is a presence of the catalytic metal rhodium. There is a variance in the quantity of the rhodium metal, but this is expected due to the limitations of the analysis technique used by the EDS.

Table 5.7 – Tabulated EDS spectral compositions of the wash-coated catalyst layer

Spectrum	O	Al	Rh
Spectrum 1	52.07	47.02	0.91
Spectrum 2	52.02	46.59	1.39
Spectrum 3	54.09	45.37	0.54

The limitation of the EDS analysis technique is the depth with which it can analyse. The depth at which EDS analyses is only up to 1 µm thick, which given the 20 µm thick catalyst layer and its complex pore structure, this leads to variances in analysis compositions**.**

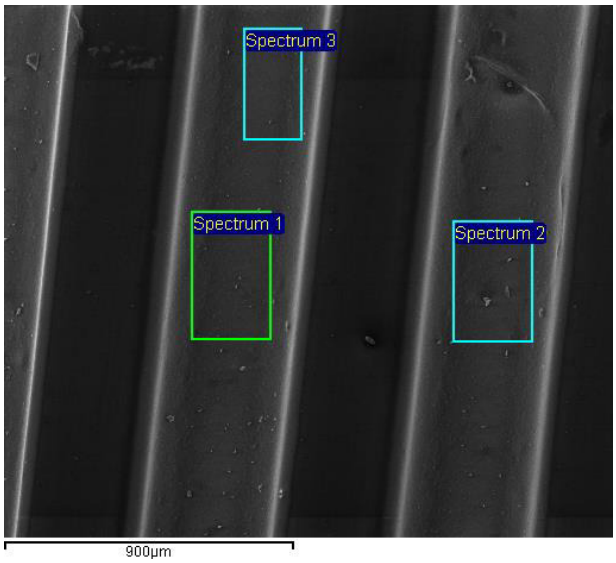

Figure 5.2 - SEM image of the spectral areas whereby EDS was carried out on the fresh coated catalyst layer

Please note that the results of the spent catalyst characterisation is presented with the results of each individual experiment.

5.7 Experiment 1 – Powdered catalyst test/ Fixed Bed

For the first experiment, a fixed bed reactor was loaded with 334 mg of 1.0 wt % Rh/Al_2O_3 catalyst powder. The alumina support used was the 3 µm Alfa Aesar alumina powder. The purpose of this experiment was to determine the stability of the (uncoated) catalyst powder prior to wash-coating the catalyst onto the micro-channel reactor plates. The reaction was started at a specific space velocity (SSV) of 60 000 $scc\cdot(g_{cat}\cdot h)^{-1}$ and subsequent SSV conditions of 120 000, 180 000 and 240 000 $scc\cdot(g_{cat}\cdot h)^{-1}$ were tested. Deactivation was determined by testing the space velocity of 120 000 $scc\cdot(g_{cat}\cdot h)^{-1}$ at the end of the

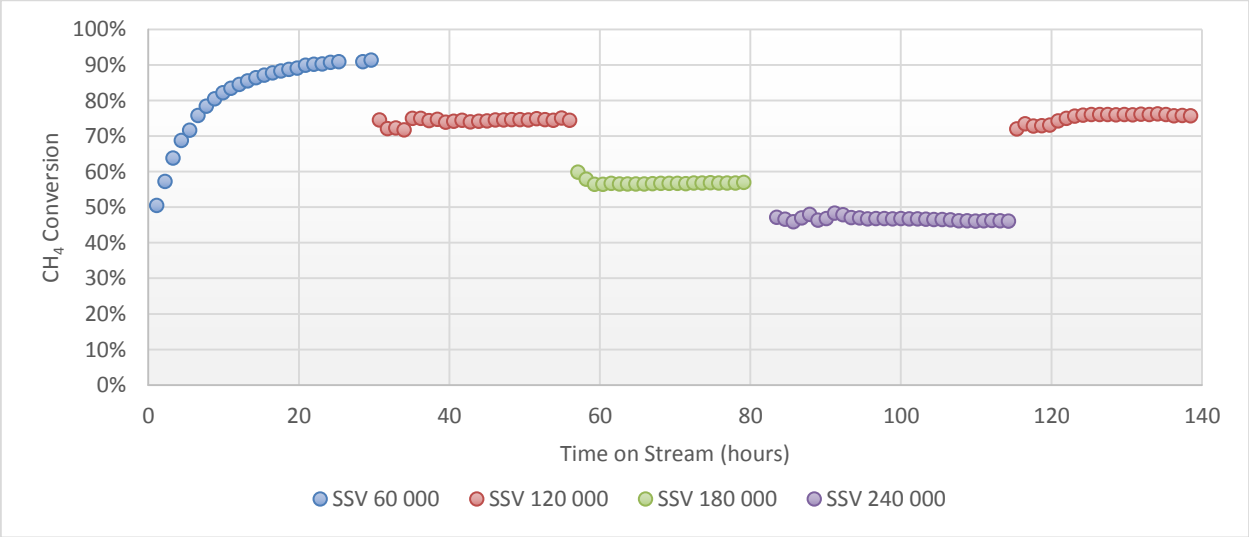

Figure 5.3 – Stability performance plot of the in-house prepared Alfa Aesar supported rhodium catalyst in the fixed bed reactor set up at 700 °C, 1 barg and steam to carbon ratio of 3 for four space velocities (SSV).

experiment.

The powdered catalyst was stable at all space velocity settings. The catalyst showed no signs of deactivation when the specific space velocity set point was brought back to 120 000 $scc\cdot(g_{cat}\cdot h)^{-1}$ at 125 h and remained at a methane conversion of 76 % until the run was shut down at a time on stream of 140 h. The initial 24 hours or 'start-up' period shows the catalyst activity increasing with time as the catalyst reaches steady state.

The initial start-up period whereby the activity of the catalyst increasing from the start of the run until it reaches steady state is not known and further testing is required to confirm whether it's due to a catalytic phenomenon or a rig set-up issue.

The table below gives the stable methane conversions at each space velocity set point.

Table 5.8 – Table of methane conversions at each of the different specific space velocity set points

Time on Stream	Space Velocity [scc·(g_{cat}·h)$^{-1}$]	CH_4 Conversion
0-30 h	60 000	91%
31-55 h	120 000	74%
56-80 h	180 000	57%
81-115 h	240 000	46%
116-140 h	120 000	76%

5.8 Micro-channel stability tests

The experiments in this section will encompass the testing of the wash-coated Rh/Al_2O_3 catalyst onto the stainless steel micro-channel reactors. The following tests will be attempting to reach a stable methane conversion for a substantial time on stream. There were 8 micro-channel experiments conducted, 8 experiments utilising the 3 µm Alfa Aesar and 1 experiment using a milled Sasol Puralox catalyst.

Table 5.9 – Another summary of the micro-channel experiments with the catalyst and suspension batches and the reduction procedure used.

Experiment number	Experiment Title	Catalyst Batch	Suspension Batch	Reduction Procedure
1	Experiment 1 - Powdered Catalyst Test/Fixed Bed	A	N/A	H_2 exposure from 25 °C to 700 °C and held for 2 hours
2	Experiment 2 – Low starting space velocity	A	I	H_2 exposure from 25 °C to 700 °C and held for 2 hours
3	Experiment 3 – Medium starting space velocity	A	I	H_2 exposure from 25 °C to 700 °C and held for 2 hours
4	Experiment 4 – Medium starting space velocity repeat 1	B	II	H_2 exposure from 25 °C to 700 °C and held for 2 hours
5	Experiment 5 – Medium starting space velocity repeat 2	B	II	H_2 exposure from 25 °C to 700 °C and held for 2 hours
6	Experiment 6 – Low starting space velocity repeat 1	B	III	H_2 exposure from 25 °C to 700 °C and held for 2 hours
7	Experiment 7 – High starting space velocity	B	III	H_2 exposure from 25 °C to 700 °C and held for 2 hours
8	Experiment 9 – New reduction procedure with a medium starting space velocity	B	III	H_2 exposure only at 200 °C for 2 hours
9	Experiment 8 – Sasol puralox supported catalyst with high starting space velocity	C	IV	H_2 exposure from 25 °C to 700 °C and held for 2 hours

5.8.1 Experiment 2 – Low starting space velocity

The first micro-channel experiment (experiment 2) was carried out using 44.4 mg of a 1.0 wt% Rh/AA-Al_2O_3 catalyst wash-coated onto a set of heat treated micro-channel reactor plates. The heat treatment process (see experimental section 4.3.1) for all the plates is a standard procedure whereby the plates are heated to 800 °C for 2 hours with a ramp rate of 1 °C per minute. The initial space velocity was set at 200 000 $scc\cdot(g_{cat}\cdot h)^{-1}$ and conditions were varied with space velocities up to 1 200 000 $scc\cdot(g_{cat}\cdot h)^{-1}$.

The experiment was started at a space velocity (SSV) of 200 000 $scc\cdot(g_{cat}\cdot h)^{-1}$ giving a methane conversion of 94%. The space velocity was step wise increased to 300 000 and 400 000 $scc\cdot(g_{cat}\cdot h)^{-1}$ (time on stream 3-6 h and 6-10 h, respectively). The methane conversion at 400 000 $scc\cdot(g_{cat}\cdot h)^{-1}$ remained 92%, however, due to a fault in the pump overnight (air bubble in pump head), the steam to carbon (S/C) ration was incorrect and data was not considered (time on stream 10-20 h). Once the S/C ratio was corrected at 10 h the conversion returned to 92%. Unfortunately, an unplanned power cut at a time on stream of 22 h resulted in the flow of gas without any flow of water as the pump needed to be manually restarted while the gas flow controllers (MFCs) had an automatic reset and restart at their original set points prior to the power cut. This resulted in a S/C ratio of zero for a small period of time.

After restart at 400 000 $scc\cdot(g_{cat}\cdot h)^{-1}$ (ToS – 24 h) the conversion dropped and stabilised at 79 % until 54 h on stream where the space velocity was increased to 600 000 $scc\cdot(g_{cat}\cdot h)^{-1}$. At 600 000 $scc\cdot(g_{cat}\cdot h)^{-1}$ the conversion dropped and stabilised at 66 % for 5 h (ToS 55 – 60 h) before the conversion began increasing to a conversion of 70 % due to what is assumed to be a slow catalyst regeneration after the unplanned power outage. This regeneration continued until the methane conversion levelled off at 73 % after 95 h until the space velocity was increased again to 1 200 000 $scc\cdot(g_{cat}\cdot h)^{-1}$ after 111 h on stream.

The system settled at a conversion of 39 % after 8 hours at a specific space velocity (SSV) of 1 200 000 $scc\cdot(g_{cat}\cdot h)^{-1}$, here the system remained at 1 200 000 $scc\cdot(g_{cat}\cdot h)^{-1}$ for a further 8 hours before the effect of temperature was investigated.

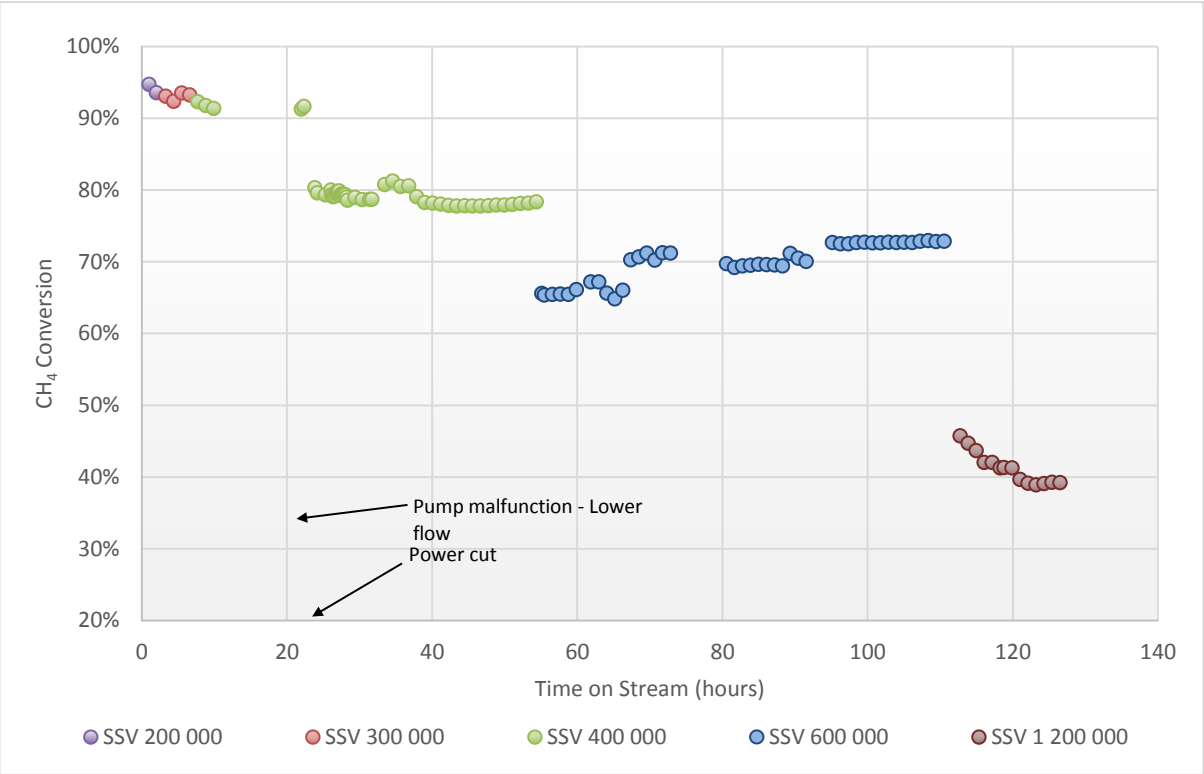

Figure 5.4 – Stability performance of the wash-coated Alfa Aesar supported rhodium catalyst in the micro-channel reactor at 700 °C, 1 bar_g and steam to carbon ratio of 3 for various space velocities.

During the follow[illegible]conditions tested, the effect of temperature on catalyst activity was investigated at a [illegible]velocity of 600 000 scc·$(g_{cat}·h)^{-1}$. Temperature was varied from 700 °C to 750 °C and 80[illegible]before returning to 700 °C. Figure 5.5 shows that the activity increases with increasing [illegible]erature, as expected, and the activity returned to 75% methane conversion simila[illegible]he results around 400 h on stream (both conditions at 700 °C).

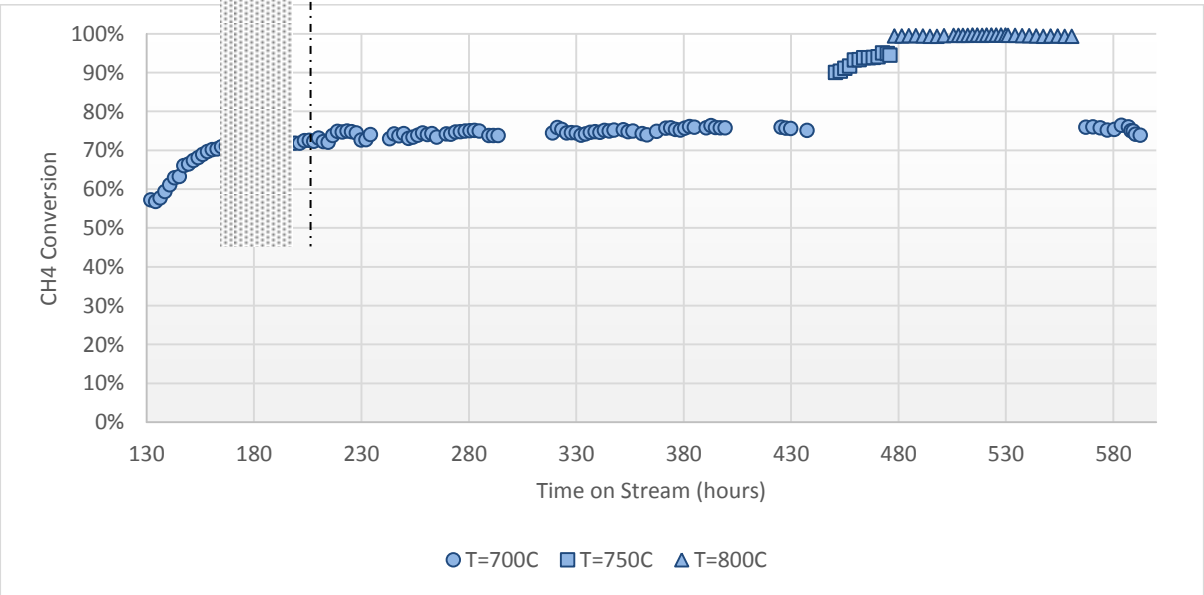

Figure 5.5 – Effect of temperature on the catalyst activity in the microchannel reactor configuration at a SSV of 600 000 scc·$(g_{cat}·h)^{-1}$ in experiment 2.

After completion of the experiment, the micro-channel reactor was opened (using a metal cutter) and post-run characterisation of the spent catalyst was performed. Visual inspection of the spent reactor plates showed grey tubular formations, which was the wash-coated catalyst layer that had separated from the walls of the reactor plate (see Figure 5.6). During operation, the hemi-circular catalyst layers on each micro-channel plate had fused together to form the tubular catalyst layer.

The grey colour of the catalyst layer showed a good resemblance to the colour of the powdered form of the Rh/Al_2O_3 catalyst after the first calcination after the incipient impregnation but prior to the wash-coating procedure. This colour resemblance then lends itself to being assumed that this was not coke, however this was not tested.

Figure 5.6 – Photographic image of the opened reactor for the successful long run (experiment 2)

SEM imaging was performed on a number of different areas of the spent micro-channel plates: along the wall where the catalyst had detached completely, a portion of catalyst inside a broken tubular the inner tube of catalyst and the outer layer of the tubular catalyst layer that were detached from the micro-channel wall.

In SEM Image A in Figure 5.7, EDS spectrum 1 is of the inner portion of a broken tubular catalyst layer while spectra 2 and 3 were analysed on the surface of the reactor plate where the coated catalyst had detached from the wall.

In SEM Image B in Figure 5.7, EDS analyses were performed on of the outside of the tubular catalyst layer that had been in contact with the micro-channel reactor plate.

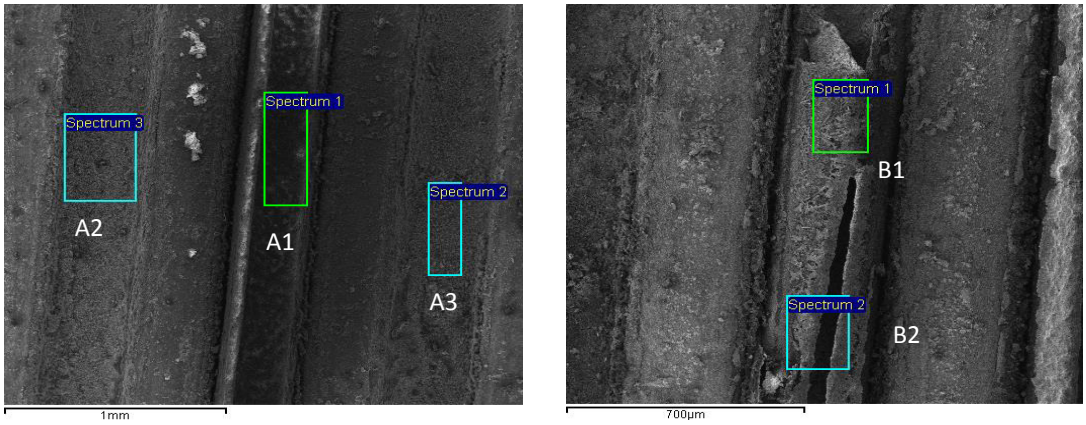

Figure 5.7 - SEM Images of the initial micro-channel experiment with different spectra analysed through EDS

SEM Image A **SEM Image B**

Table 5.10 – EDS results of the three normalised spectra seen in SEM image A shown above in Figure 5.7. The percentages shown are in wt %.

Spectrum	O	Al	Rh	Ni	Fe	Cr
Spectrum A1	27.57	12.73	1.02	5.07	53.6	0.00
Spectrum A2	18.89	1.28	0.00	3.62	75.45	0.76
Spectrum A3	21.01	1.15	0.00	4.1	72.57	1.18
Spectrum B1	31.69	0.99	0.00	11.68	55.65	0.00
Spectrum B2	30.29	0.87	0.00	7.51	61.33	0.00

The results of the A1 EDS analysis of the inner portion of a broken coated catalyst tube still attached the reactor channel wall. The results showed the presence of rhodium metal, aluminium and oxygen indicating the coated, alumina supported rhodium catalyst was still present and aligns with the stable conversion seen throughout the run. There was also a large presence of iron and a smaller percentage of nickel. The presence of the iron and nickel, given the composition of the stainless steel micro-channel reactor plates, indicate these may have leached out from the metal plates. Given the harsh conditions, the presence of steam and steel in the plates, the iron and nickel are most likely to come from the steel oxidising to form ferrous and nickel oxides.

The A2 and A3 EDS spectra were performed on the empty channels without the coated catalyst. The results of the EDS showed the major presence of iron and oxygen with smaller concentrations of aluminium, nickel and chromium. These results are consistent with the composition of the stainless steel reactor plates.

The B1 and B2 spectra were performed on the outer portion of the coated catalyst tube that was attached to the opposing micro-channel reactor plate prior to the plate separation. The results of the EDS analyses showed large concentrations of iron, oxygen and nickel but small concentrations of aluminium.

These results are slightly counter intuitive as one would expect aluminium to be present in the results to account for the alumina support in the coated catalyst tube. The fact the aluminium is not present is a possible verification of the metals within the micro-channels leaching across into the coated catalyst layer. This may explain why in spectrum A1 shows the presence of rhodium as it was inside the coated catalyst tube while the B1 and B2 spectra, were on the outside of the coated catalyst tube which made direct contact with the stainless steel micro-channel plates.

5.8.2 Experiment 3 – Medium starting space velocity

The following micro-channel reactor test (experiment 3) was performed to replicate the results obtained in experiment 2. Identical catalysts (catalyst A) and wash-coating suspensions (suspension I) were used as in experiment 2, however, experiment 3 was started at space velocity of 600 000 scc·$(g_{cat}·h)^{-1}$ instead of 200 000 scc·$(g_{cat}·h)^{-1}$ like in experiment 2. The reasoning behind this starting mass specific space velocity (SSV) was because in experiment 2, 600 000 scc·$(g_{cat}·h)^{-1}$ was the lowest SSV that yielded a conversion far away enough from equilibrium to see the catalyst deactivation.

The same trend which was seen in the uncoated catalyst test was seen again in this test. This trend was whereby the methane conversion increased until 'steady' state was reached instead of the typical reduction in methane conversion.

After 8 hours on stream, a power cut briefly interrupted the feed composition and the steam/carbon ratio dropped below 3.0. Once power had been restored, the space velocity was maintained constant at 600 000 scc·$(g_{cat}·h)^{-1}$ and a linear decline was observed for 15 hours (Figure 5.8). At 25 h on stream the methane conversion stabilized at 65 % for the

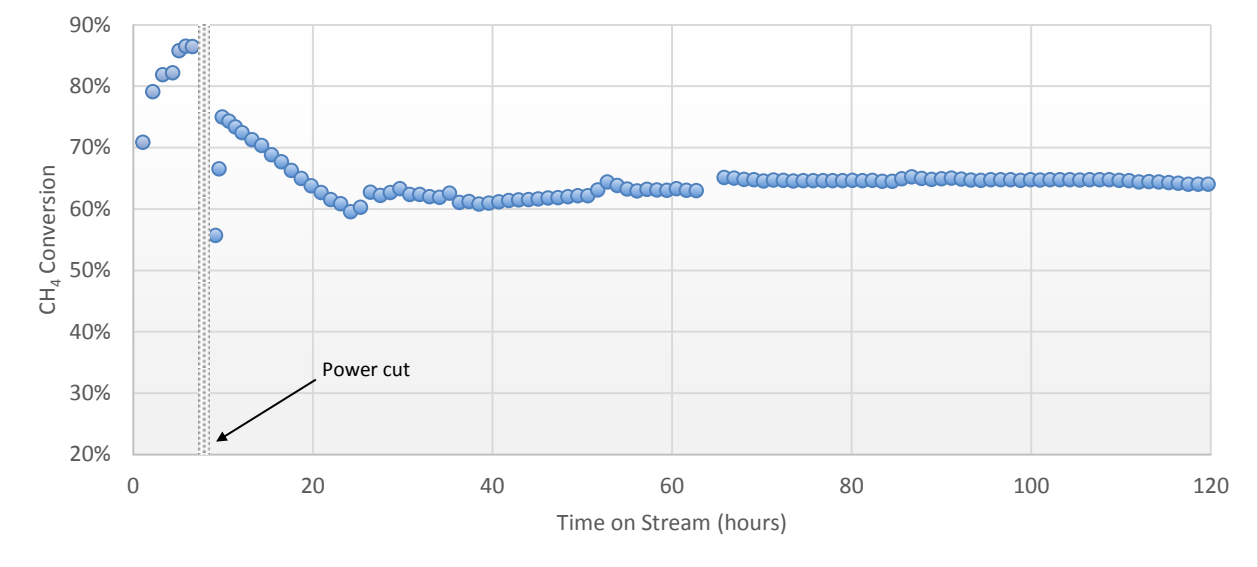

Figure 5.8 – Micro-channel experiment 3 - Stability reproducibility attempt of the in-house prepared and wash-coated Alfa Aesar supported rhodium catalyst in the micro-channel reactor set up at 700 °C, 1 barg and with a steam to carbon ratio of 3 at a space velocity of 600 000 scc·$(g_{cat}·h)^{-1}$

remainder of the experiment, 10 % lower than the same condition in experiment 2 where a small pump malfunction caused the drop in conversion. The difference in the drops in methane conversion would be due to the different types of system malfunctions experienced. The HPLC pump malfunction reduced the water flow in experiment 2, where in experiment 3 there was a complete loss in water flow leaving no steam to enter the reactor while dry gas flowed through the reactor causing perfect conditions for carbon deposition to take place.

After completion of the experiment the micro-channel reactor was cut open and the state of the catalyst was visually observed (Figure 5.9). The catalyst appeared blackened due to the carbon deposition from the pump shutting down during the power outage.

Table 5.11 – Results of the EDS analysis on the spent coated catalyst from experiment 3.

Spectrum	O	Al	Rh	Fe	C
Spectrum 1	43.38	22.02	0.22	22.39	11.98
Spectrum 2	84.25	0.00	0.00	0.00	15.74
Spectrum 3	69.34	14.49	0.08	0.00	16.09

The EDS spectra were conducted on sections of the coated catalyst layer within the micro-channels. Unfortunately, SEM images were not taken in this instance, only EDS analyses were performed.

The EDS (Table 5.11) analysis confirmed that a significant amount of carbon was present on the surface of the catalyst layer in what was assumed to be in the form of coke. Tests weren't conducted to confirm the carbon deposition was in the form of coke. The analysis also detected the presence of rhodium metal with varying percentages. This to a point is consistent with the reactors stable performance (methane conversion) however with the surface depth analysis limitations and variable rhodium percentages one cannot confirm this with no SEM images of the spectral areas.

5.8.3 Experiment 4 – Medium starting space velocity repeat 1

Figure 5.9 – Visual evidence of carbon deposition on the wash-coated catalyst layer

To understand the results from experiment 2 and 3 the experiment was repeated as experiment 4. A new batch of 1.0 wt% Rh/Al_2O_3 (Alfa Aesar alumina) and a new batch of

wash-coating suspension was used (refer to sections 0, 5.2 and 5.3 for summaries of the catalysts and suspensions for each experiment). Preparation procedures were kept identical except for the wash-coating suspension batch size. In this case 1.0 g of catalyst powder was used instead of 2.0 g previously in MC runs 1 and 2. The use of 1.0 g of catalyst powder in the suspension corresponds to a 20-fold reduction from the original wash-coating suspension size used by Zapf et al. (2006).

The experiment was started at a space velocity of 600 000 scc·(g_{cat}·h)$^{-1}$ (similar to experiment 3) and the methane conversion was at equilibrium (see Figure 5.10). After 24 hours on stream the space velocity was increased to 900 000 scc·(g_{cat}·h)$^{-1}$ and a linear decline was observed. At 50 hours on stream the deactivation appeared to slow down, however, shortly after (~65 h) the conversion dropped to the rate of an overall linear decline. To increase the activity after 140 hours, the space velocity was reverted back to 600 000 scc·(g_{cat}·h)$^{-1}$. The catalyst activity had still not stabilized and continued to deactivate but

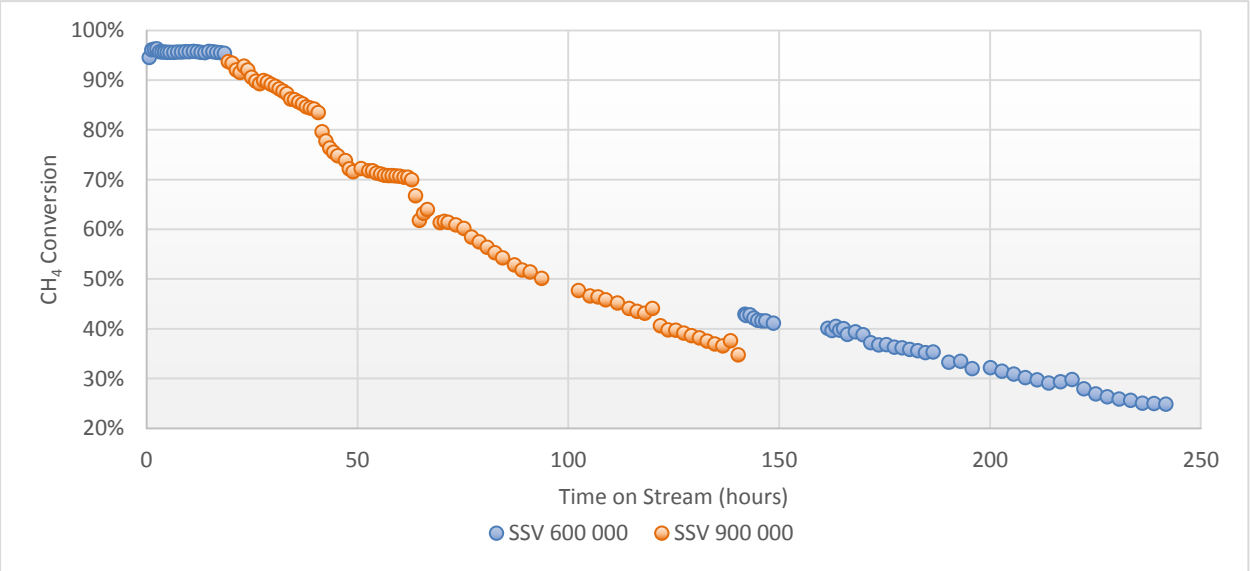

Figure 5.10 – Micro-channel experiment 4 – micro-reactor operating at 700 °C, 1 bar_g and steam to carbon ratio of 3.

at a slower rate.

Figure 5.12 – Imaging of the post-run reactor from experiment 4 with no visible catalyst

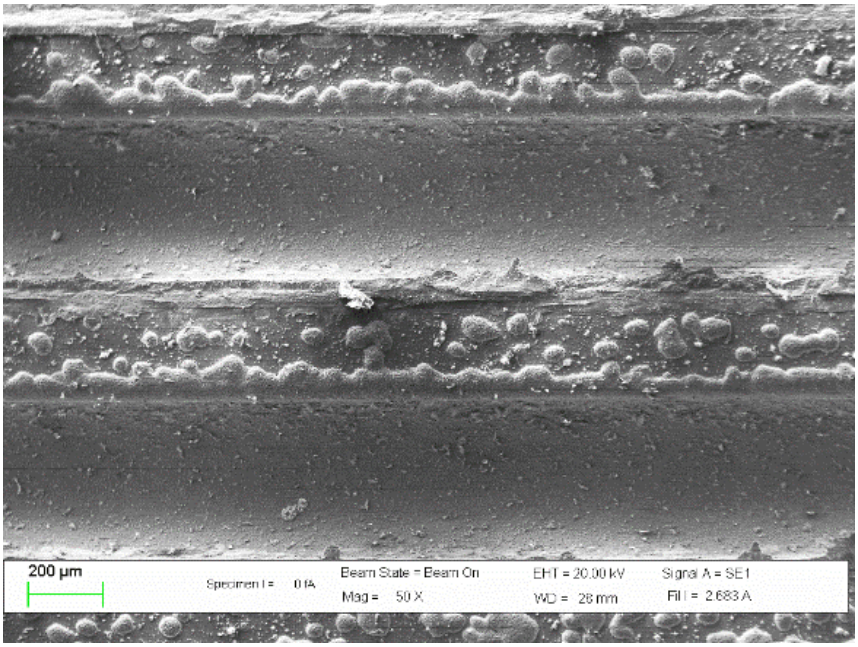

Figure 5.11 – Close up SEM image of two channels without a visible wash-coat

The post-run visual inspection (Figure 5.11) showed no tubular catalyst tubes, as seen in the previous experiments. However, SEM and EDS also found no catalyst material (no Al nor Rh) on the micro-channel reactor walls (Figure 5.12 and Table 5.12).

Table 5.12 – EDS analysis results for experiment 4 indicating no visible catalyst remaining on the reactor plate

Spectrum	O	Al	Rh	Ni	Fe	C
Spectrum 1	61.99	0.07	0	5.09	32.76	0.08
Spectrum 2	63.98	0.57	0	7.52	27.86	0.06
Spectrum 3	61.90	0.14	0	6.84	31.06	0.06

The spectra for the EDS were done on the inside of the micro-channels of the reactor plates. The EDS results show minimal aluminium and carbon present while indicating there is a substantial amount of oxygen and iron with a moderate amount of nickel. This suggests and confirms that the wash-coated catalyst is no longer attached to the walls of the micro-channel reactor plates.

From Experiment 4 through to experiment 7, all the post-run characterisation SEM and EDS tests resulted in the same outcome, whereby the coated catalyst was no longer adhered to the micro-channel reactor wall.

5.8.4 Experiment 5 – Medium starting space velocity repeat 2

Experiment 4 did not yield a stable catalyst and so another reactor from the same catalyst and wash-coating batch was tested in order to match experiment 2. The exact same procedure was followed as in experiment 4. Experiment 5 was started up at a space velocity of 600 000 scc·$(g_{cat}·h)^{-1}$ where after approximately 30 hours the methane conversion seemed to have settled at just over 92 %.

At time on stream of 32 hours or so where the steam to carbon ratio dropped to 2.1 as a result of a pump malfunction (air bubble), this lead to a period with methane conversions of approximately 78 %. Once the correct steam to carbon ratio of 3.0 was re-attained, the methane conversion appeared to have stabilized at 91 %.

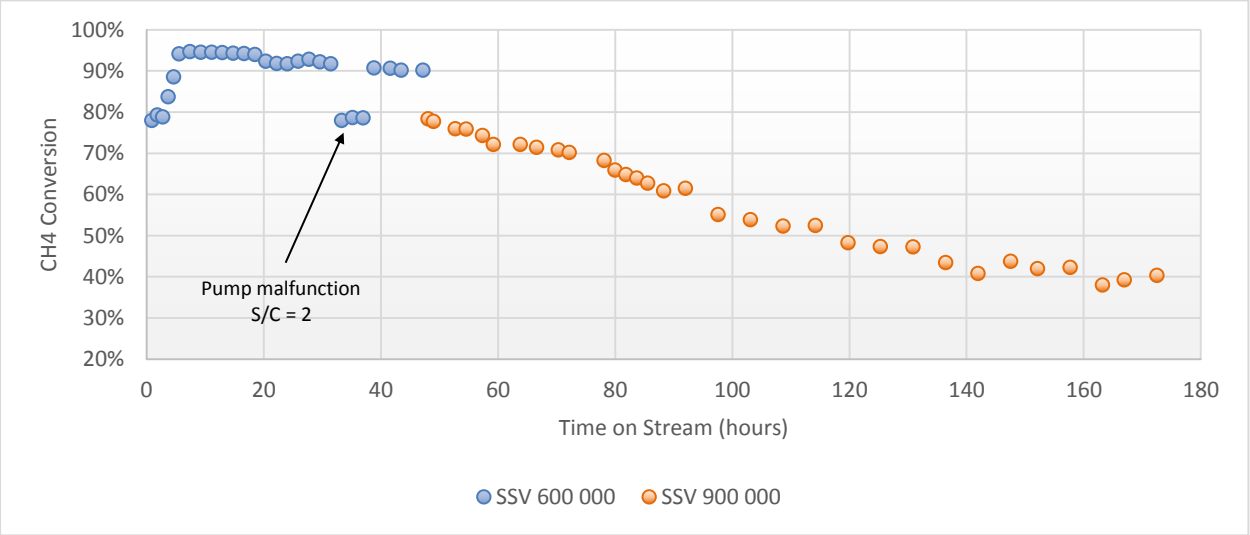

Figure 5.13 – Micro-channel experiment 5 - Stability performance test at at 700 °C, 1 bar_g and with a steam to carbon ratio of 3 showing catalyst instability when starting at a specific space velocity (SSV) of 600 000 scc·$(g_{cat}·h)^{-1}$ before increasing to 900 000 scc·$(g_{cat}·h)^{-1}$.

In order to see the deactivation of the catalyst easier the space velocity was increased to 900 000 scc·$(g_{cat}·h)^{-1}$, however once the increase was implemented the methane conversion began to steadily decrease over time. The EDS results of this experiment yielded the same outcome as experiment 4 where there was no alumina detected on the micro-channel reactor plate.

Figure 5.14 – Post-run imaging after the reactor has been cut open, shows visible similarity to experiment 4

5.8.5 Experiment 6 – Low starting space velocity repeat 1

Due to the deactivation of the catalyst in experiments 4 and 5, it was decided to start the space velocity in the same manner as experiment 2 to determine if this change would aid in stabilizing the catalyst wash-coat. The space velocity was started at 200 000 $scc\cdot(g_{cat}\cdot h)^{-1}$ and increased it to 400 000, 600 000 and 800 000 $scc\cdot(g_{cat}\cdot h)^{-1}$. This was done again to move the conversion away from equilibrium to see the deactivation better.

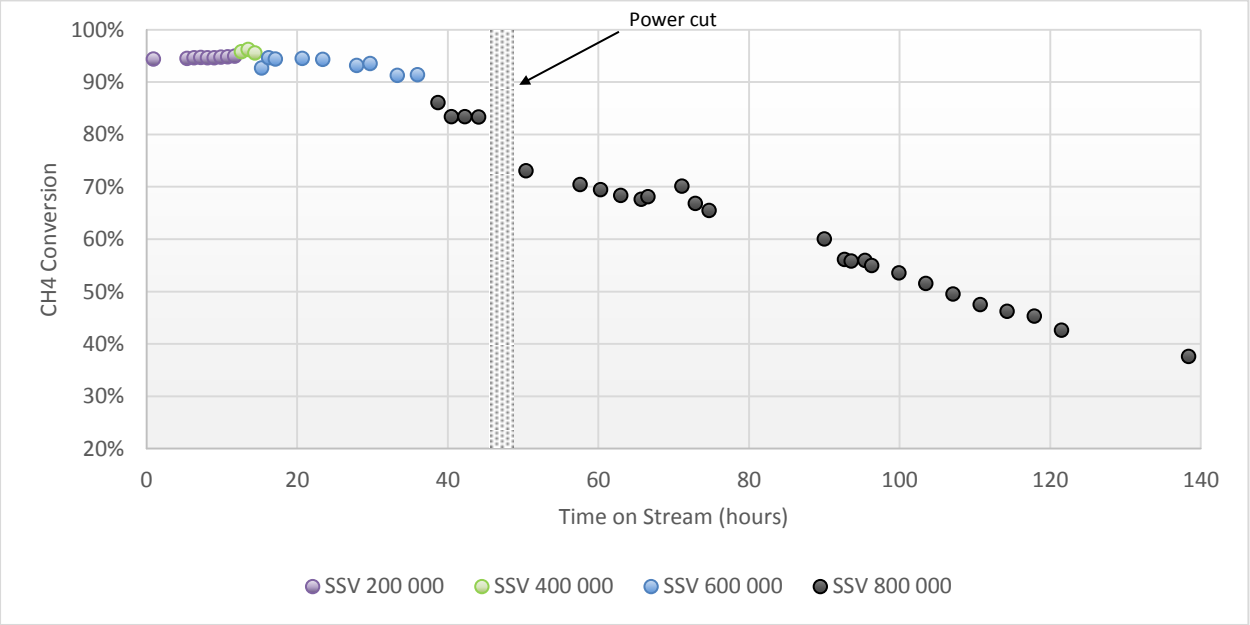

Figure 5.15 – Micro-channel test 6 imitating the low space velocity set point sequence change used in the successful experiment 2 where the SSV started at 200 000 and was slowly increased over time.

The methane conversion was firmly at equilibrium for the space velocities of 200 000 and 400 000 $scc\cdot(g_{cat}\cdot h)^{-1}$, and began drifting slightly away at 600 000 $scc\cdot(g_{cat}\cdot h)^{-1}$ with the methane conversion sitting at 91 %. However as the space velocity was increased to 800 000 $scc\cdot(g_{cat}\cdot h)^{-1}$, the conversion dropped steadily over the next 100 hours.

The conversion had appeared to stabilize at a time on stream of 45 hours but it suddenly dropped and steadily declined after a power outage whereby the pump was offline for approximately 1 minute before the backup power kicked in.

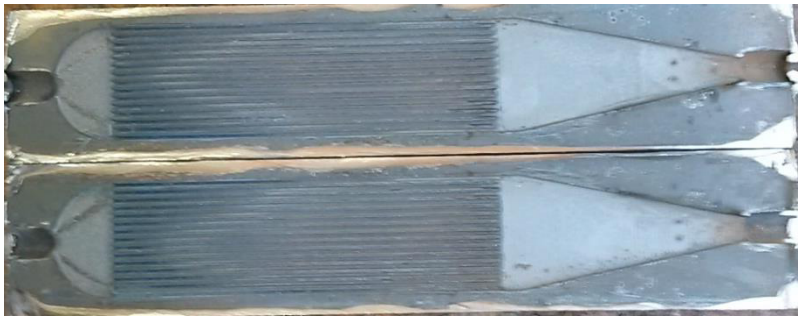

Figure 5.16 – Post-run imaging of experiment 6 whereby the coated catalyst is no longer visibly seen in the micro-channels like in experiments 4 and 5

5.8.6 Experiment 7 – High starting space velocity

Experiment 7 was started at a space velocity of 1.2 million scc·$(g_{cat}·h)^{-1}$ in order to compare starting with a space velocity of 200 000 scc·$(g_{cat}·h)^{-1}$ and see if this has any effect on the stability of the wash-coat. The catalyst wash-coated on this set of reactor plates was prepared in the same suspension batch as experiment 6.

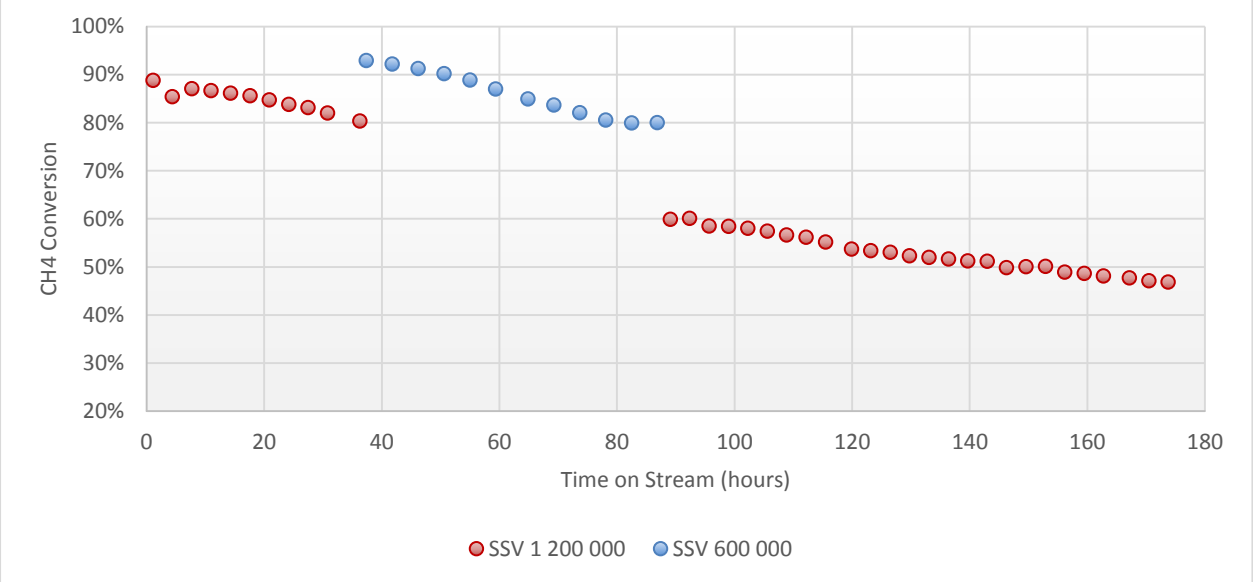

Figure 5.17 – Plot of an Alfa Aesar alumina supported rhodium catalyst in the micro-channel reactor set up at 700 °C, 1 bar_g and with a steam to carbon ratio of 3 with a starting space velocity of 1.2 million scc·$(g_{cat}·h)^{-1}$.

The catalyst activity shown by Figure 5.17 illustrates a steady deactivation from the outset of the experiment at a space velocity of 1.2 million scc·$(g_{cat}·h)^{-1}$. The system never reaches a stable methane conversion even when the space velocity was reduced to 600 000 scc·$(g_{cat}·h)^{-1}$.

5.8.7 Experiment 8 – New reduction procedure with a medium starting space velocity

To resolve the instability of the wash-coated catalyst a new reduction procedure was proposed to see if the standard reduction procedure had any negative effect on the catalyst layer by having an effect on metallic crystallite size. Figure 5.18 illustrates the differences between the two procedures. The standard 1.0 wt % Rh/Al_2O_3 catalyst (Alfa Aesar alumina support) was used in this test; noting the 40.40mg of catalyst was wash-coated onto the pair of reactor plates.

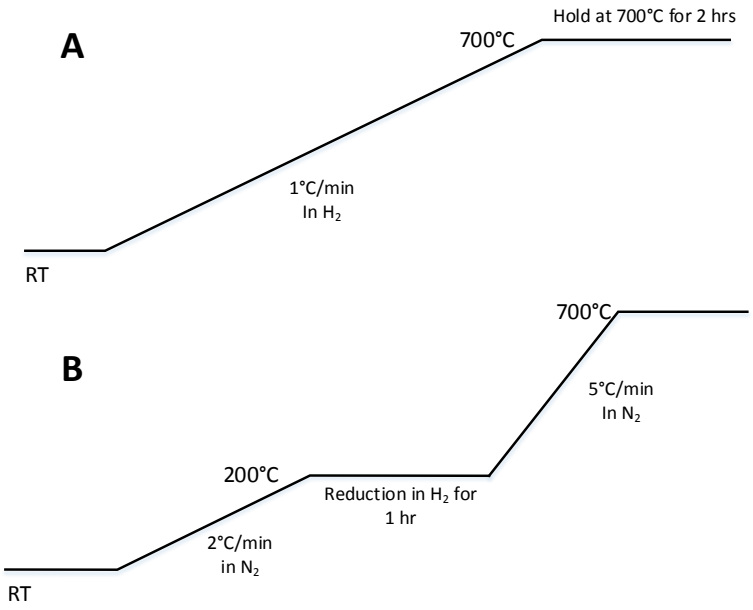

Figure 5.18 – Diagram of the standard reduction procedure (A) and the new proposed reduction procedure (B)

Chemisorption tests were also performed in order to see the differences in metallic crystallite size, metal dispersion and metallic surface area. Table 5.13 below shows these differences between the two reduction procedures and the effect it has on the rhodium crystallites.

Table 5.13 – Chemisorption results showing the comparison between the standard reduction procedure and the new procedure

	Standard reduction procedure at 700 °C	New reduction procedure at 200 °C
Metal Dispersion	68.90 %	53.88 %
Metallic surface area	3.2750 m^2/(g of sample)	2.5613 m^2/(g of sample)
Metallic surface area	303.2416 m^2/(g of metal)	237.1561 m^2/(g of metal)
Crystallite size	1.5944 nm	2.03866 nm

Once the new reduction procedure was followed, time was taken to make sure the system has reached steady state before changing space velocity set points. In doing so the actual changes in set points were not done in a single step-wise change but rather several smaller incremental steps. The order of which when increasing space velocity water increasing

water flow first and allowing to reach steady state before making an equivalent step in dry feed flow.

The test was started at a space velocity of 600 000 scc·$(g_{cat}·h)^{-1}$ however it took a period of 5-6 hours to reach the starting set point with the more frequent but smaller step-wise incremental changes to the flow rates. The methane conversion was sitting at equilibrium at this set point and thus the space velocity was increased to 800 000 scc·$(g_{cat}·h)^{-1}$ and the conversion remained at equilibrium. To move the conversion away from equilibrium enough to see the deactivation better, the space velocity was increased to 900 000, 1.2 million and allowed to settle at 1.5 million scc·$(g_{cat}·h)^{-1}$. The conversion reached steady state at conversion of 81 % at a space velocity of 1.5 million scc·$(g_{cat}·h)^{-1}$. The catalyst activity remained stable at 1.5 million scc·$(g_{cat}·h)^{-1}$ with 100 hours of run time. The space velocity was then increased to 1.8 million scc·$(g_{cat}·h)^{-1}$ and after 10 hours of stable conversion, the conversion began to deteriorate quite rapidly.

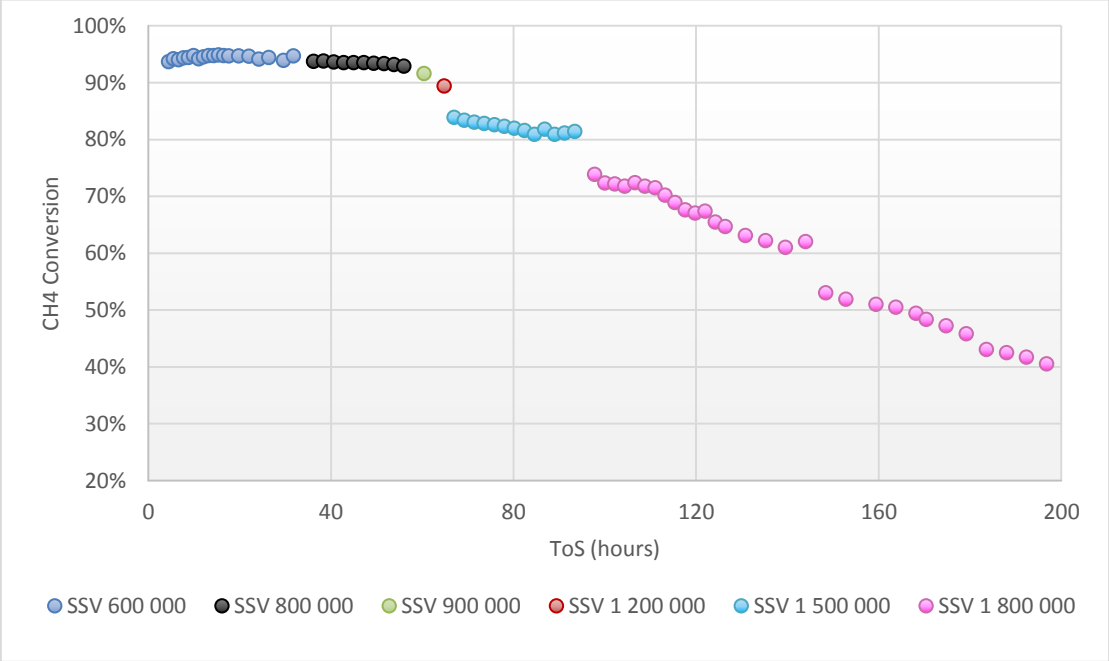

Figure 5.19 - Stability performance plot of the standard 1.0 wt % rhodium catalyst in the micro-channel reactor set up at 700 °C, 1 bar_g and with a steam to carbon ratio of 3 testing the effect of the new reduction procedure

5.8.8 Experiment 9 – Sasol puralox supported catalyst with high starting space velocity

A test was performed using an identical alumina support in the work carried out by Zhou (2014) to find a reason for the instability Zhou (2014) had experienced. The support used was the NWA-155 Puralox alumina manufactured by Sasol. The original size of the alumina was 150 µm and it was milled to a smaller particle size ($d_{0.5}$ - 34 µm) than that in the work of Zhou (2014) and impregnated. This test was to see the effect of using a smaller support particle than Zhou and if the particle size of the support plays a role in the wash-coat stability.

The test was started at a space velocity of 1.2 million $scc\cdot(g_{cat}\cdot h)^{-1}$ and it was left at this space velocity for the duration of the experiment.

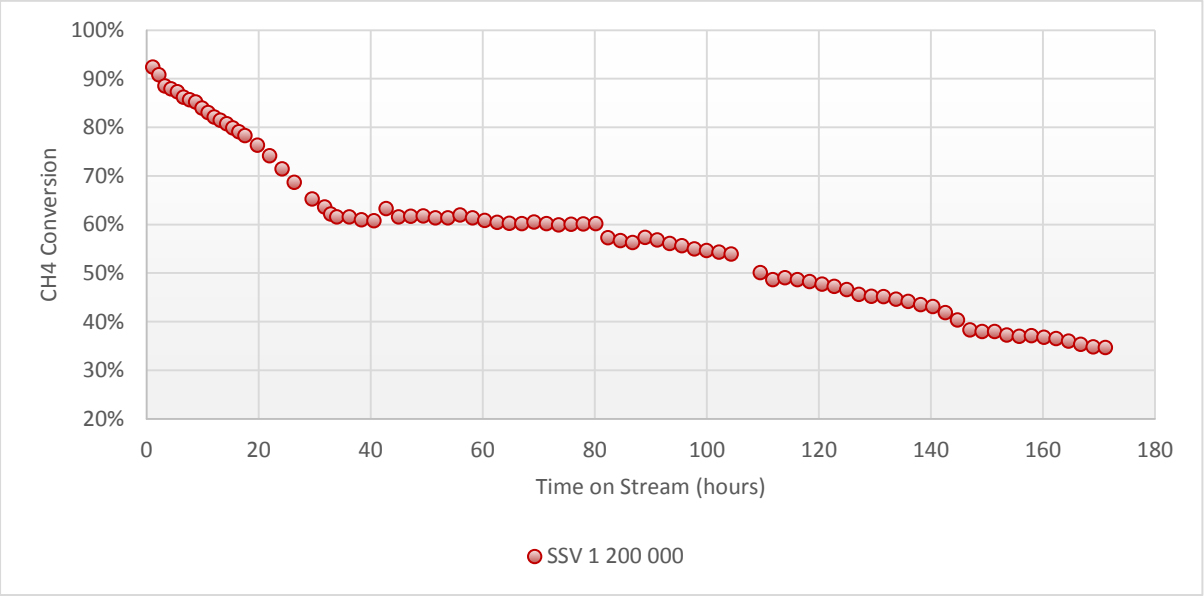

Figure 5.20 - Stability plot of a wash-coated 1.0 wt % rhodium catalyst made using a milled Sasol NWA-155 Puralox alumina support in the micro-channel reactor set up at 700 °C, 1 bar_g and with a steam to carbon ratio of 3

The system only reached a steady state operation after approximately 32 hours after start-up. The CH_4 conversion then stabilized at 60 % for just under 50 hours before steadily decreasing for the rest of the test.

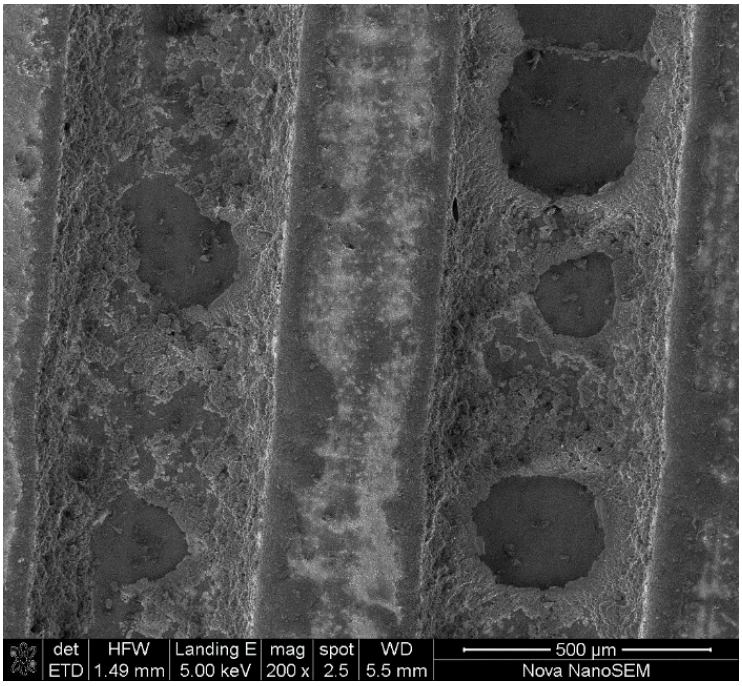

Figure 5.21 – SEM image of the spent micro-channel reactor wash-coated with the Sasol NWA-155 Puralox alumina as the support for the Rh/Al_2O_3 catalyst

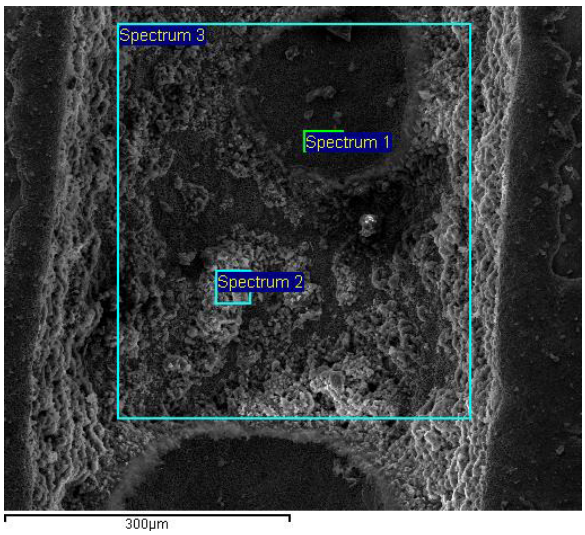

Figure 5.22 – SEM EDS analysis image of the wash-coated with the milled Sasol NWA-155 Puralox supported Rh/Al_2O_3 catalyst showing the different areas (spectra) analysed with EDS

SEM imaging (Figure 5.21) shows the wash-coated catalyst layer as present, but with gaps or holes in the wash-coat also indicating issues with adherence like experiments 4-7 but to a lesser extent.

In spectrum 1, SEM imaging (Figure 5.21 and Figure 5.22) appears to show a gap in the catalyst layer where EDS was carried out. EDS detected no rhodium, but however it did

detect small quantities of aluminium and larger quantities of iron and chromium. These results indicate and confirm that this area analysed is a hole in the coated catalyst layer but with a small quantity of catalyst layer remaining. SEM imaging (Figure 5.22) shows EDS was carried out on the catalyst layer. The EDS results confirmed this was the catalyst layer showing a relatively large presence of rhodium and aluminium while having smaller amounts of iron and chromium.

Table 5.14 – Tabulated EDS results from the Puralox alumina supported, rhodium catalyst

Spectrum	O	Al	Rh	Fe	C
Spectrum 1	39.75	10.09	0.00	28.60	21.57
Spectrum 2	47.49	39.78	0.53	4.62	7.58
Spectrum 3	36.93	24.86	0.09	32.54	5.67

5.9 Adherence tests

Two different adherence tests were performed to gauge the quality of the adhesion of the wash-coated catalyst layer. These were the 'drop test' used by Zapf et al. (2006) and a chemical adherence test used by (Yasaki et al., 1993).

The drop test utilized by Zapf et al. (2006) was performed first but due to the results obtained by the post-run reactor characterization it was decided further testing was required; hence the chemical adherence test was then performed in accordance to the method prescribed by (Yasaki et al., 1993) in the experimental section.

The results from the drop test can be seen below in Table 5.15. Note that the reactor plate numbers do not have any correlation to the experiment numbers, but since they had already been numbered, the choice was completely arbitrary.

Table 5.15 – Tabulated results of the drop test performed on the reactor plates for experiments 2-5

Experiment number	Reactor plate	Catalyst weight before drop (mg)	Catalyst weight after drop (mg)	Weight loss (%)
2	**W01**	22.99	22.71	1.20%
	W02	21.45	21.28	0.80%
3	**W03**	19.77	19.58	0.95%
	W04	18.88	18.54	1.81%
4	**W07**	15.66	15.42	1.55%
	W08	23.03	22.54	2.13%
5	**W09**	20.73	20.48	1.23%
	W10	21.62	21.53	0.42%

The chemical adherence test was performed on unused, heat treated reactor plates and the test yielded the following results:

Table 5.16 - Tabulated results of the chemical adherence test of the wash-coated catalyst layer involving ultrasonication of the micro-channel reactor plates in isopropyl alcohol

Reactor plate	Catalyst weight before (mg)	Catalyst weight after (mg)	Catalyst weight loss (%)
W05	20.16	18.26	9.43%
W11	20.16	13.56	32.74%
W12	20.85	13.83	33.67%

5.9.1 Source of carbon deposition testing

Tests were conducted to ascertain whether the source of carbon deposition during the reforming process is predominantly from the Bouduard reaction or from another reaction pathway. The way in which this was tested was by using a blank micro-channel reactor which had been wash-coated with only the Alfa Aesar support containing no rhodium metal and feeding the normal methane feed in one test and a feed simulating the product composition.

Methane feed

The result of feeding the normal methane feed over the alumina coated micro-channel reactor is shown in Figure 5.23.

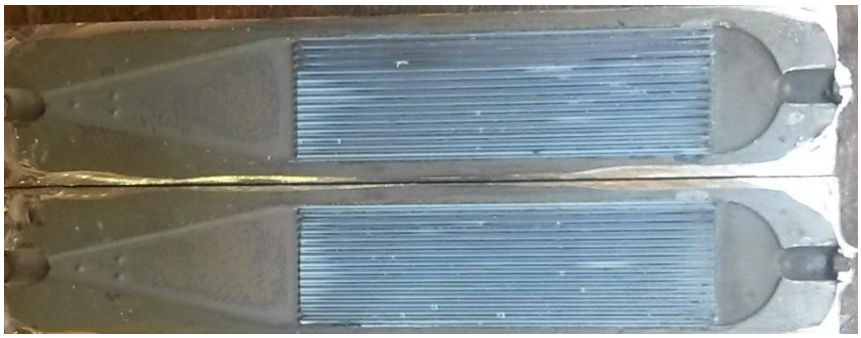

Figure 5.23 – Photographic image of the methane fed, alumina coated micro-channel reactor with visible dark patches from the deposition of carbon

Product feed

The result of feeding the simulation product feed over the alumina coated micro-channel reactor is shown in Figure 5.24.

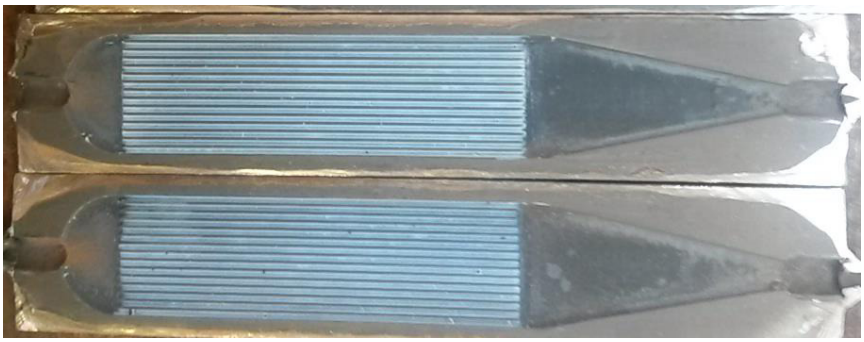

Figure 5.24 – Photographic image of the simulation product fed, alumina coated micro-channel reactor without any visible dark patches from the deposition of carbon

The results indicated that the wet methane feed at reaction conditions had a higher amount of carbon deposition than the product gas simulation feed. This wasn't the expected result as it was thought the Bouduard reaction was the main reaction pathway for coke deposition.

6 Discussion

This study investigates the stability of wash-coating alumina supported rhodium catalysts onto stainless steel micro-channel reactors for the development of intensified methane steam reforming reactors. Micro-channel reactors can help alleviate the heat transfer problems in conventional fixed bed reactors, specifically for highly endothermic reactions. Previous studies by Zhou (2014) showed an unstable catalyst coating during the reforming reaction and a further study into the stability was performed.

The testing procedure involved a proof of concept test in a fixed bed reactor with the same powdered Rh/Al_2O_3 catalyst to set a performance benchmark. Thereafter, several micro-channel tests were performed to determine the behaviour and robustness of the coated catalyst layer. A comparison would then be able to be drawn to compare the micro-channel tests with the powdered catalyst test.

To explain the reason for conducting the fixed bed test, the fixed bed test was performed to test and confirm that the 1.0 wt % rhodium powdered catalyst supported on the 3 µm Alfa Aesar alumina is stable prior to wash-coating it onto the stainless steel micro-channel reactor plates. The activity plot shown in Figure 5.3 showed that the in-house prepared Rh/Al_2O_3 powdered catalyst is stable at several space velocities, during the 150 hours of time on stream. This stability exuded by the catalyst shows that these conditions do not alter the catalyst metal or support. The fact the catalyst metal and support do not change indicates that it is possible for this catalyst to be used in the coating procedure prescribed by Zapf et al. (2006). However, catalyst stability is not a certainty and this needed to be tested at space velocities almost 10 times higher than in the fixed bed.

The results of the first wash-coated micro-channel experiment (Experiment 2 –) showed a stable methane conversion over a 600-hour period on stream. The catalyst experienced some irregularities in terms of variable steam-to-carbon ratio in the first 24 hours due to system power cuts. These power cuts resulted in a 12 % decrease in methane conversion. However, it was observed that the catalyst recovered by 8 % over time at a space velocity of 600 000 $scc\cdot(g_{cat}\cdot h)^{-1}$ from 65 % to 73 % methane conversion; whether the catalyst recovered an activity of fresh catalyst was not able to be determined.

Subsequent micro-channel experiments were performed to reproduce the micro-channel performance, as well as to determine the activity with fresh coated catalyst. During the microchannel experiment 1 (Experiment 2), the space velocity that yielded a stable conversion far enough away from equilibrium was 600 000 $scc\cdot(g_{cat}\cdot h)^{-1}$. Now as a result of this, the second micro-channel experiment was started immediately at a space velocity 600 000 $scc\cdot(g_{cat}\cdot h)^{-1}$. Experiment 3 (micro-channel experiment 2) was performed in order to determine a stable methane conversion far away enough from equilibrium, hence the 600 000 $scc\cdot(g_{cat}\cdot h)^{-1}$, but without any power outage interruptions in order to compare the

methane conversions of the two reactor types. However, experiment 3 also experienced power cuts due to unannounced 'load-shedding', but still showed stable performance. The activity observed was stable but at methane conversion 21 % lower than before the unexpected power outage and thus could not be compared to conversions or activity in experiment 2. These two experiments however both showed catalyst stability. Experiment 2 and 3 were coated with the same catalyst suspension (see sections 5.1, 5.2 and 5.3 for a comprehensive table of experiments, suspensions and catalyst batches used in this study).

Experiment 4 followed a similar starting procedure as experiment 3 at a space velocity of 600 000 $scc\cdot(g_{cat}\cdot h)^{-1}$. The first data points after start-up showed a methane conversion at equilibrium (96%). However, at equilibrium the catalyst deactivation could not be observed and the space velocity had to be increased to lower the conversion. After increasing the space velocity to 900 000 $scc\cdot(g_{cat}\cdot h)^{-1}$, the catalyst performance steadily declined through what was later proved by EDS to be a loss of catalyst. A repeat experiment - experiment 5 – carried out with the exact procedure showed similar results/trend.

To ascertain whether the initial space velocity during the run had any effect on the catalyst's instability, experiment 6 was started identically to experiment 2, with an initial space velocity of 200 000 $scc\cdot(g_{cat}\cdot h)^{-1}$. Initially it was thought that the wash-coated catalyst layer's adhesion could be compromised with the initial high gas velocities before the catalyst surface had acclimatised to the reaction conditions.

The results, however, followed similar trends as experiments 4 and 5 at space velocity of 600 000 $scc\cdot(g_{cat}\cdot h)^{-1}$ and the activity steadily decreased. Experiment 7 studied a start-up space velocity of 1 200 000 $scc\cdot(g_{cat}\cdot h)^{-1}$ to see the effect of starting with a higher specific space velocity and to achieve conversions far away enough from equilibrium to see the change in conversion more prominently. The catalyst was also unstable at the higher space velocity and the methane conversion decreased rapidly over time.

Post-run characterization tests were carried out on certain micro-channel reactors that showed different behaviour - stable performance and rapid decrease in activity. This characterization was done to understand the behaviour observed and ascertain the reasoning for the deactivation of experiments 4-7 and the stability observed in experiments 2 and 3. The reactors from experiments 2 to 7 were opened and SEM-EDS analyses were performed of the catalyst layer.

The EDS characterizations of experiment 2 (stable conversions) confirmed there was still rhodium and alumina present on the walls of the micro-channel plates. EDS also showed the presence of iron and nickel assumed to be in the form of oxides on surface of the catalyst layer. Tests were not performed specifically to determine if these were oxides but as a result of the highly favourable oxidising conditions.

Kamerud et al. (2013) have shown that iron and nickel can leach from the stainless steel in hot conditions and exposed to enough water and thus the nickel and iron are likely to have leached out of the stainless steel reactor pates over the 600 hours of run time in the presence of highly favourable oxidizing conditions (temperature of 700 °C in the presence of steam). The presence of carbon was not indicated by the EDS on the spectra analysed, however with the gradients in reactant and product species it was evident that the coated layer was slightly darkened towards the reactor exit. This is expected with the higher CO and lower steam concentrations at this point along the reactor.

The SEM images and EDS elemental composition analysis for experiment 3 indicated coke deposition occurred as the post-reaction catalyst layer amounted to 13.2 wt % carbon. The activity plots for experiment 3, show that the catalyst was stable, even with the coke deposition - albeit at a lower activity than before the power outage (See Table 5.11 and Figure 5.9). Similar to experiment 2, rhodium was detected by the EDS.

Both, EDS and SEM analyses conducted on experiments 4-8 confirmed a loss of the coated catalyst layer from the walls of micro-channels in all instances. The SEM images show that there is no visible tubular coated catalyst layer and according to the EDS analyses there was no presence of aluminium or rhodium, only iron, nickel and oxygen.

There was a visible flow pattern seen from Figure 6.1 which is characteristic of turbulent flow through a pipe with the paraboloid shape that can clearly be seen. At the reactor exit it is more black in colour due to the higher concentrations of CO and lower steam concentrations making it easier for the carbon deposition to occur. The paraboloid flow pattern shows how more steam flows through the centre channels and thus have a lower

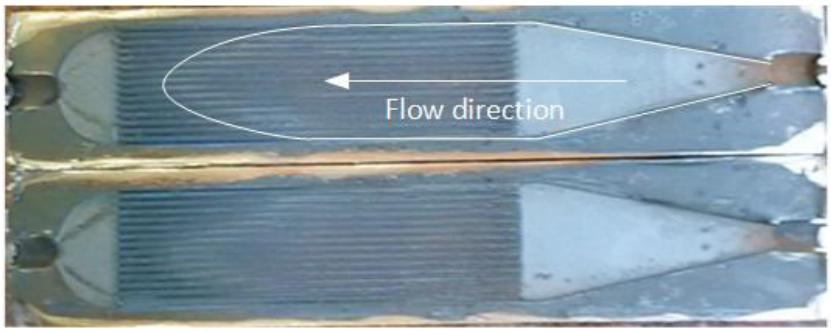

Figure 6.1 – Example of the colour gradient within the reactor from experiment 4, whereby the reactor exit is more visibly blackened due to the concentration gradient and flow patterns within the reactor.

carbon deposition rate than the outer lying channels at the reactor exit.

The drop test showed minimal loss of wash-coated catalyst with a range of 0.5 - 2.1 % loss in adhered catalyst. Germani et al (2007) indicated that a loss of 2 % or less of the wash-coated catalyst layer is deemed to be stable. The deactivation of the wash-coated catalyst through the physical loss of catalyst in experiments 4-7 and the results of the drop test indicating a

good stable adhesion, the drop test in this case was not a good representation of wash-coat adhesion quality. This discrepancy lead to the further investigation into the diminished adhesion quality of the wash-coat and it was later noted that the drop test is generally followed up by another chemical adherence test.

The more vigorous adherence test was conducted through a chemical adherence method patented by Yasaki et al. (1993) and later used by Valentini et al. (2001). This vigorous test involved sonicating the wash-coated catalyst for 30 minutes in an isopropyl alcohol bath at room temperature. Boix et al. (2003) indicated that a 0-10 % loss in the adhered catalyst layer is considered a stable wash-coated catalyst. The results of the chemical adherence test on the reactor plates made in the same suspension batches as the unstable experiments (4-7) gave an average loss of 33.1 % of the catalyst wash-coat after 30 minutes of sonication in isopropyl alcohol. Once this test had been performed, another chemical adherence test was performed on a spare micro-channel reactor plate made in the same suspension batch as experiments 2 and 3. These results gave a loss of 9.4 % after 30 minutes of sonication in the isopropyl alcohol. The chemical adherence test was only conducted for the 30 minutes prescribed by Yasaki et al. (1993).

Peela et al. (2009) attained a loss of only 10% after 1 hour of exposure to ultrasound with a suspension of 20 wt % γ-alumina and 4 wt % PVA binder. It must be noted that Peela et al. (2009) made use of a primer deposition step prior to wash-coating. Such primer deposition was proven to increase the adhesion of the wash-coat to the micro-structured reactor by Agrafiotis and Tsetsekou (2000c), Valentini et al. (2001) and Peela et al. (2009).

In the studies carried out by authors Agrafiotis and Tsetsekou (2000b, 2000c), Valentini et al. (2001) and Peela et al. (2009), the substrates used to be coated were either ceramic monolithic structures, a FeCrAlloy® felt or tubes made up of dense α-Al_2O_3. In this study, stainless steel substrates were used and the work done by Zapf et al. (2006) wash-coated alumina based catalysts onto stainless steel substrates for the reforming of propane. The fact he wash-coated rhodium based catalyst layers onto stainless steel micro-channel substrates is the main reason why the wash-coating procedure created by Zapf et al. (2006) was used. The procedure of Zapf et al. (2006) did not make used of any primer deposition coating prior to wash-coating the catalyst onto the heat treated stainless steel substrates.

Work carried out by Germani et al. (2007), Peela et al. (2009) and Pennemann et al. (2013) utilize small additions of micronized forms of alumina during their primer layer and catalyst coating procedure. These forms of alumina included colloidal alumina, degraded disperal alumina (degraded through nitric acid treatment) or a bohemite sol-gel each with a binder in the wash-coating suspension. The addition of the primer layer prior to the catalyst wash-coating and the addition of either of the micronized forms of alumina can improve the catalyst adhesion.

The wash-coating procedure followed in this study, prescribed by Zapf et al. (2006), was intended for the reforming of propane. The testing done by Zapf et al. (2006) was conducted at equilibrium for a total run time of 200 hours at an undisclosed space velocity. Zapf et al. (2006) had not specified if the coating procedure had any limits in terms of the linear velocities if any. The methods used by Valentini et al (2001), Germani et al. (2007), Peela et al. (2009) and Pennemann et al. (2013) are possible ways to improve upon the procedure designed by Zapf et al. (2006) to improve the wash-coated catalyst layer's adhesion, but this does not explain the reasoning for the stable experiments 2 and 3 and the unstable experiments 4-7.

To draw conclusions as to why the latter experiments (experiments 4-7) were unstable and experiments 2 and 3 were stable a full comparison was needed. The comparison would start from the making of the catalyst and batch size of the wash-coat suspension right through to the start-up procedure and changes between space velocity settings.

The powder catalyst preparation for all catalysts were identical (Table 5.2) with only minor differences in the total rhodium loading. The final metal loading that varied which was due to the hygroscopic nature of the metal precursor salt ($Rh(NO_3)_3$) and the age of the salt used. The age of the salt was unknown and thus introduced the variability in rhodium metal content.

The wash-coat suspensions were all made using the same incipient wetness impregnation procedure prescribed by Zapf et al. (2006), all were dried at 120 °C and heat treated at 600 °C. However, the suspension batch size varied and seemingly changed the suspension characteristics through a change in rheological and surface tension properties. This change in suspension characteristics resulted in a varied mass distribution of the catalyst layer after wash-coating coating onto the micro-channel reactor plates, through the introduction of bubbles into the smaller suspension batches. The varied mass distribution of the catalyst layer's mass is essentially each reactor plate having a large variation in wash-coated catalyst mass due to the presence of bubbles during the wash-coating process. The way in which the suspension characteristics changed with suspension batch size is explained in detail below.

The original suspension size used by Zapf et al. (2006) was based on a solids quantity (catalyst or alumina support) of 20 g per batch. To limit the amount of rhodium salt used, the catalyst quantity was reduced to 0.75 g – 2 g per batch, depending on the number of plates to be coated, keeping all component ratios (on a mass percentage basis) same as Zapf et al. The wash-coating summary has the different catalyst suspension quantities for each batch (Table 5.3). The reduction in wash-coating suspension size visibly altered the characteristics of the suspension with the formation and dissipation of air bubbles when stirring. Such dissolved air might result in gaps/holes/porous/pinholes in the catalyst layers

after coating as the bubbles are difficult to eradicate once the suspension has been applied through the wash-coating procedure into the micro-channels.

The use of 2 g of catalyst in the suspension was a tenfold reduction from the original suspension size while the use of 0.75 g was a 27-fold reduction. The presence of the polyvinyl alcohol (PVA) increased viscosity of the suspension and in turn increased the surface tension of the liquid.

When making the suspension with 2 g of catalyst, the quantity of liquid in the poly-top vial was sufficient to cover the magnetic stirrer completely. This is when the inter-molecular forces exceed the force of the surface tension of the liquid enough to prevent the formation of small bubbles and allow the bubbles formed to dissipate (Tolman, 1949). However, when less than 1 g of catalyst was used in making a wash-coating suspension, the further reduced quantity of liquid resulted in the liquid's surface tension to exceed the intermolecular forces such that the formation of bubbles is favoured (See Figure 6.2 below).

As a result, these bubbles did not dissipate easily when the quantity of liquid was low which made the bubbles move with the suspension when coating the micro-channels. The presence of bubbles in the wash-coat resulted in a large variation in the mass distribution of the wash-coated catalyst which may affect the catalyst adhesion quality as the wash-coat is not uniform. Table 5.2 gives the quantity of solids used in each suspension batch and the resulting range of mass distribution across the different batches of wash-coating suspensions based on the quantity of solids in each suspension.

Figure 6.2 - Image of the presence of bubbles in a suspension prior to wash-coating. The vial on the right with the lighter suspension was made with 0.75 g of catalyst.

The reduction procedure used in experiments 1-7 made use of increasing the reactor temperature from ambient conditions to the reaction temperature of 700 °C at a rate of 1 °C/min while passing hydrogen over the catalyst. To investigate the effect of the start-up reduction procedure, Experiment 8 was conducted using a different reduction procedure. The new procedure involved bringing the reactor up to 200 °C from ambient temperature at 2 °C/min. The feed gas into the reactor was switched from nitrogen to hydrogen and then held for 2 hours at 200 °C. The 200 °C reduction temperature was determined by temperature programmed reduction (TPR). Finally, after the 2 hours of reduction under hydrogen, the gas was switched back to nitrogen and the temperature taken up to 700°C at 5 °C/min before the steam was started.

Experiment 8, while a conducted with a new reduction procedure was used, a special emphasis was placed on allowing a longer period for the reactor to reach a stable, steady state methane conversion. This was done by making much smaller incremental step changes and a longer time between these changes. During experiment 8, the reactor system reached a stable methane conversion at a space velocity of 1 500 000 scc.$(g_{CAT}.h)^{-1}$ at a conversion of 81 %. After increasing the space velocity to 1 800 000 scc.$(g_{CAT}.h)^{-1}$, at 20 hours on stream, a decline in the activity was observed. The post run SEM imaging and EDS analysis showed a loss of catalyst indicating the catalyst adhesion was not sufficient for the linear velocities the reactor experienced. The difference in linear gas velocity between the space velocities of 1 500 000 scc.$(g_{CAT}.h)^{-1}$ and 1 800 000 scc.$(g_{CAT}.h)^{-1}$ is not likely to be the issue causing the decline in methane conversion. The issue causing the drop in methane conversion is more likely to be the time exposed to the higher space velocities. This may indicate that the space velocity condition of 1 500 000 scc.$(g_{CAT}.h)^{-1}$ was not left long enough at the set point to be deemed 'stable'. For future testing, in a single wash-coating batch of catalyst, tests need to be conducted at a single set space velocity starting at 200 000 scc.$(g_{CAT}.h)^{-1}$ up to 1 800 000 scc.$(g_{CAT}.h)^{-1}$. These tests need to be run for an extended period of time at those set points to ascertain that they are in fact truly 'stable' and produce reliable methane conversions in order to compare with fixed-bed tests.

The aim of Experiment 9 was to determine why the work conducted by Zhou (2014) yielded unstable and relatively inactive catalyst wash-coats. The main difference between the procedures Zhou (2014) followed and those conducted in this study was the use of a 3 µm Alfa Aesar alumina instead of a manually milled NWA-155 Sasol Puralox alumina. Experiment 9 was conducted to see if the particle size made the difference in catalyst performance seen in the work of Zhou (2014) and that seen in this study. Zhou (2014) made use of a 50 µm catalyst using the NWA-155 Puralox where in this study, a 34 µm Puralox catalyst was used in Experiment 9.

The use of the 34 µm Puralox catalyst in experiment 9 compared to the 50 µm Puralox catalyst used by Zhou (2014) is inconclusive whether that difference in particle size (16 µm)

is the reason for experiment 9 reaching substantially higher conversions before having the conversions decay. SEM images (Figure 5.21 and Figure 5.22) show that there too was a loss in catalyst during the run but not in the way seen in experiment 4-8 where the entire wash-coat had removed itself from the reactor wall. The Puralox catalyst layer had holes in the wash-coat where the wash-coat had separated from the wall of the micro-channel.

Looking at experiments 2, 3 and 6 where there was a loss in power and subsequently a loss in pump operation which had a detrimental effect on the methane conversion achieved by the catalyst. The conversion achieved after the loss in pump operation was lower than before, and the amount the conversion had dropped by was proportional to the time the pump was offline. This indicates how sensitive this micro-structured reactor system is to the concentration of water and the subsequent coking after the lower steam concentrations.

The pathway through which carbon deposition takes place in the steam reforming of methane was initially thought to follow the Bouduard reaction pathway. The results, however, proved that the Bouduard reaction was not the predominant pathway for coke

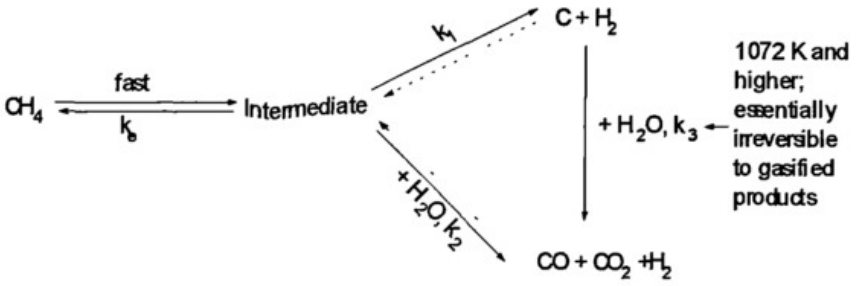

formation. The test feeding a gas mixture mimicking the product gas did not deposit any noticeable amounts of carbon on the reactor plates. The test feeding the methane feed did deposit noticeable quantities of carbon on the alumina. The coke formation found on the alumina wash-coat after feeding methane and steam (Figure 5.23), indicates the direct formation of coke from methane degradation through a side reaction proposed by Fujimoto (1933). The mechanism proposed by Fujimoto (1933) is shown in Figure 6.3 below.

Figure 6.3 – Illustration of the two possible reaction pathways during steam methane reforming, the reforming reaction and the methane degradation side reaction proposed by Fujimoto (1933)

Simsek et al. (2011) mentions that the higher steam/carbon ratio in the feed reduces the quantity of coking by favouring the reforming reaction and not methane degradation or Bouduard reaction. In hindsight, the introduction of an external water vapouriser was a crucial one in helping reduce the amount of coking on the catalyst layer on the micro-channels in this study, despite the fact coking still occurred. The vapouriser continuously provides super-heated steam into the reactor which allows the correct steam/carbon ratio to be maintained by not allowing any condensed water vapour into the micro-reactor system. However, another viable way of combatting the presence of coking is to allow a small fraction of air or oxygen into the system to burn of the carbon deposited on the catalyst layer.

From the numerous tests, the deviation in results from the two successful runs and the other unstable catalyst adherence; is likely to be due to the change in the wash-coat's physico-chemical characteristics when the batch size was reduced too much. The over-reduction of the wash-coating suspension size changed the surface tension properties; making the presence of bubbles during the wash-coating procedure more prominent, which may have adversely affect the adhesion quality of the catalyst layer. This may explain the difference in stability seen in the experiments conducted.

The carbon deposition occurring in the experiments occurred during periods where the pump was not able to maintain a high enough steam to carbon ratio. Simsek et al. (2011) mentions that the carbon deposition seen in the case of the steam reforming of methane is generally coke. Thus, the deposition of coke did affect the performance of the wash-coated catalyst negatively by reducing the methane conversion once the pump operation had been rectified. The presence of coke may have introduced a ‘brittleness’ into the catalyst layer allowing the layer to break away easier than if there was no coke deposition. However, considering the variability introduced by power outages, the amount of information is insufficient to draw conclusions whether coking influences the robustness and stability of the wash-coat.

Another possibility, and the most probable cause, is the effect of thermal expansion of the stainless steel micro-channel reactor itself that may add to and amplify the insufficient adhesion of the wash-coated catalyst. In line with the use of the wash-coating procedure for the reforming of propane which occurs at a lower temperature of around 300 °C (Kolb, 2009), the effect of thermal expansion is far less pronounced than at the 700 °C required for steam methane reforming (Steele and Heinzel, 2001). The expansion of the micro-channel along with an insufficient wash-coat adhesion will make it far easier for the catalyst to break away from the reactor wall. In the case of the successful experiments the catalyst layer, despite exuding stable behavior had also broken away from the micro-channel wall. However, it broke away in a single complete tubular catalyst layer which would not have been able to pass through the reactor causing a loss of catalyst. In the case of the latter

experiments where air bubbles were present in the wash-coat, these bubbles may have caused the catalyst layer to break apart easier by creating weak points in the wash-coat. This would allow the broken pieces of the catalyst layer to pass through the reactor like that seen in the SEM images of experiment 9.

Future testing needs to focus on many aspects. The first aspect is to focus on the wash-coating procedure and testing the wash-coating of the micro-channels with suspension batch sizes with a smaller reduction in the original size. An example is to make a suspension with 3 g of catalyst solids and prepare enough micro-channel reactors to coat all of them.

The second aspect to consider in the future testing is the use of a thin alumina primer layer to coat the heat treated micro-channel before wash-coating the catalyst layer. This should be able to increase the adhesion quality of the subsequent wash-coat by adding more possible oxide bonds for the wash-coat to adhere and bond to (Peela et al., 2009). As a result of the increased number of oxide bonds, the stability of the catalyst layer is said to increase.

Thirdly the use of a stainless-steel alloy that handles the heat better and does not allow for as much heat expansion. Thus, when used in combination with the increased stability of an alumina primer layer a far more stable wash-coated catalyst layer will result.

Another final aspect to consider is that of coke suppression. The instances where coking had occurred had been directly linked to the outages of power. To avoid this the system needs to be placed on a UPS or at very least the HPLC pump. This will then only leave malfunctions in the pumps operation responsible for these cases. Another option to suppress coke formation is to get rid of the coke by adding a minute fraction of air or oxygen to the dry feed. This will allow partial oxidation to occur and burn off some of the carbon deposited on the catalyst layer (Holladay et al., 2009).

7 Conclusions and recommendations

A wash-coating method developed by Zapf et al. (2006) was used for applying a rhodium based catalyst layer, supported on 3 µm alumina, onto heat treated stainless steel micro-channel plates in the hope of obtaining a stable, active and uniform catalyst layer.

The in-house produced Rh/Al_2O_3 catalyst performed well in the case of the benchmark fixed bed test. The fixed bed catalyst proved to be stable for at least 140 hours of time on stream. However, the results of the in-house catalyst when wash-coated onto the micro-channel reactor plates showed a few conflicting results.

The first two micro-channel tests (experiments 2 and 3) proved to be stable with the first test being stable for a time on stream for 600 hours, despite both tests experiencing power cuts and consequently a loss in pump operation. Post-run characterisation of these stable runs showed a slightly coked but with the catalyst layer still adhered to the micro-channel wall.

Subsequent micro-channel tests (experiment 4 – experiment 8) proved to be unstable. Post-run characterisation proved that there was no catalyst layer adhered to the micro-channel plates.

A change to the reduction procedure in experiment 8 saw the increase in the specific space velocity at which the catalyst began to lose activity due to a loss of catalyst. The new reduction procedure, with a faster temperature ramp, was used to see if the shorter exposure to heat during the exposure to hydrogen would affect the catalyst layer. A specific space velocity (SSV) of 1 500 000 $scc\cdot(g_{cat}\cdot h)^{-1}$ was achieved before losing activity at 1 800 000 $scc\cdot(g_{cat}\cdot h)^{-1}$. The reason for this was the new reduction procedure gave rise to slightly larger rhodium crystallites which make the metal particle slightly more difficult to sinter. As only test with this reduction procedure was carried out, further testing on this new procedure is required to make a decisive conclusion as to whether this reduction procedure allows a higher SSV to be reached.

The latter test instability and lack of the catalyst layer's adherence was initially unexpected. The drop test, used by Zapf et al (2006), was performed on each batch of reactors that were coated before the reactor were welded and tested. The results showed that the adherence of each batch tested was sufficient with a maximum of 2.0 % loss of the adhered catalyst layer.

Due to the instability seen during the micro-channel tests and 'stable' wash-coat results from the drop tests, a more vigorous, patented method to test adherence was used. This method was a chemical adherence test patented by Yasaki et al. (1993), where the coated micro-channel is sonicated in isopropyl alcohol for 30 min.

The results of the chemical adherence test showed that plates made in the same batch as those used in experiments 2 and 3 had a 9.4 % loss in the catalyst layer. Boix et al. (2003) performed these tests in their study and indicated that a 0-10 % loss in the adhered catalyst layer is considered a stable wash-coated catalyst. The results of the chemical adherence test on the reactor plates made in the same suspension batches as the unstable experiments (4-8) gave an average loss of 33.1 % of the catalyst wash-coat after 30 minutes of sonication in isopropyl alcohol. Another paper by Peela et al. (2009) attained a loss of only 10% after 1 hour of exposure to ultrasound with a suspension of 20 wt % γ-alumina and 4 wt % PVA binder. It must be noted that Peela et al. (2009) made use of an alumina primer deposition step prior to wash-coating.

These results then conclude that the adhesion of the catalyst layer in experiments 2 and 3 was good but close to being over the threshold value of 10 % which would classify the adhesion as being insufficient. While, the adhesion of the catalyst layer in experiments 4-8 were not sufficient as they were way over the threshold value.

The reasoning for the difference in the quality of the catalyst layer adhesion was speculated to be the result of reducing the original wash-coating suspension batch size too much in the attempt to minimise wastage. The original suspension size used 20 g of catalyst and 75 ml of de-ionised water along with a binder (polyvinyl alcohol – PVA) and peptising agent (acetic acid). For the ease of following, only the water and solids are referred to in the following explanation.

In the case of experiments 2 and 3 this was reduced tenfold to the use of 2 g of catalyst and 7.5 ml of water. In these cases, no bubbles were formed during the aging of the suspension or during the wash-coating procedure itself.

The wash-coating suspensions for experiments 4-7 were made with 0.75 g of catalyst and 3.75 ml of water. During the aging of the suspensions, where the suspension is stirred continuously for a few days, bubbles began forming and were not able to be dispersed prior to wash-coating. It's speculated that the presence of the bubbles during wash-coating and the subsequent calcination results in a non-uniform catalyst layer and negatively affecting the quality of the adhesion the catalyst layer has with the metal micro-channel substrate.

As for the bubble formation, its believed to be due to the change in surface tension and intermolecular forces between the particles in suspension. In the case of the successful experiments (2 and 3), the intermolecular forces are stronger than the surface tension causing no bubble formation, while in the unsuccessful experiments it's the converse. The surface tension of the liquid near the surface is stronger than the intermolecular forces and when sufficiently far away from the sheer forces of the stirrer, bubbles can form; and with the increased viscosity of the liquid the bubbles can remain for a longer time without popping. From these results, it can be concluded that the adhesion of the catalyst layer was insufficient and methods to improve the adhesion need to be tested.

The coating procedure that Zapf et al. (2006) developed was used in the reforming of propane which occurs a temperature far lower than that of methane steam reforming. In the work of Zapf et al. (2006), the operating space velocity is not disclosed and is operated at or close to equilibrium. This may indicate that this method needs to be modified to withstand the higher temperatures and harsher reaction conditions. Reasons for using the procedure was due to Truter (2011) successfully coated stainless steel micro-channels with micronized Zeolite to produce Thymol; while Maduna (2011) successfully creating a wash-coated catalyst for the water gas shift (WGS) reaction in micro-channels, both studies done at UCT.

As mentioned before Peela et al. (2009) had a 10 % loss of catalyst after 1 hour of sonication in isopropyl ether, which is double the time prescribed by Yasaki et al. (1993). Peela et al. (2009) along with Valentini et al (2001), Germani et al. (2007), and Pennemann et al. (2013) utilised an alumina primer coating prior to the actual wash-coating step which is proven to improve the quality of adhesion of the wash-coat. The way these studies differed was the type of micronized alumina used in the primer deposition step. These forms of alumina included colloidal alumina, degraded disperal alumina (degraded through nitric acid treatment) or a bohemite sol-gel each with a binder in the wash-coating suspension. Currently, no type of micronized alumina has been proven to perform better than another. Note once the primer is applied it undergoes a calcination step before another wash-coat is applied.

In line with the use of the wash-coating procedure for the reforming of propane which occurs at a lower temperature of around 300 °C (Kolb, 2009), the effect of thermal expansion is far less pronounced than at the 700 °C required for steam methane reforming (Steele and Heinzel, 2001). The thermal expansion of the micro-channel reactor plate could possibly exacerbate the low adhesion quality of the catalyst layer. In all the experiments, the catalyst layer had removed itself from the micro-channel wall, but in the case of the successful experiments it broke away in a single complete tubular catalyst layer which would not have been able to pass through the reactor causing a loss of catalyst. This would have shown a stable performance or activity profile as the catalyst layer was still in the reactor channels. In the case of the latter experiments where air bubbles were present in the wash-coat, these bubbles may have caused the catalyst layer to break apart easier by creating weak points in the wash-coat. This would allow the broken pieces of the catalyst layer to pass through the reactor like that seen in the SEM images of experiment 9. However, further testing is required to confirm the effect of the thermal expansion.

Thus, it is possible to get a stable catalyst layer for the steam reforming of methane, however reproducibility is an issue. Its recommended that the coating procedure pioneered by Zapf et al. (2006) be altered to improve the adhesion of the alumina supported catalyst layer on the stainless steel micro-channel reactor plates. With the procedure developed by Zapf et al. (2006), the harsher conditions involved with methane steam reforming are unsuited to standard coating methods and small changes should be made to increase wash-

coat adhesion. It is also unknown whether the thermal expansion of the microchannel reactor or coking that takes place during the tests negatively affects the catalyst layer by making the wash-coat more brittle and more susceptible to breaking away from the micro-channel wall.

The following changes are recommended for future projects:

- Place the reactor set up on a UPS if possible, particularly the pump due to the sensitivity of the system to steam concentration

- Implementation of a two-step coating procedure. After the heat treatment of micro-channels, a preliminary alumina primer wash-coat should be added before wash-coating the rhodium containing catalyst layer.

- More reactors need to be made and subsequently wash-coated at once (after primer application). This will require making a bigger batch of the rhodium containing wash-coating suspension so as not to allow the formation of bubbles and not transferring the bubbles to the micro-channels during wash-coating.

- The use of a micro-channel reactor with a high heat tolerance that will be less susceptible to the effects of thermal expansion.

- Possible test schedule would include the following:

    - Coat and test a batch of micro-channel reactors with the original coating method but with a wash-coating suspension batch with 3 or more grams of catalyst powder and note the quality of the wash-coat. Test this with the chemical adherence test from Yasaki et al. (1993) and note results.

    - Add the alumina primer coating step before wash-coating the metal containing catalyst layer using the original wash-coating procedure by Zapf et al. (2006) (3 or more grams of catalyst powder or the identical quantity used in tests recommended above) and again note the quality of the wash-coat. Test the micro-channel adhesion with the chemical adhesion test by Yasaki et al (1993).

    - These tests can also be performed using the stainless steel micro-channel reactor plates with a higher tolerance to heat and reduced thermal expansion.

8 References

- Aartun, I. et al., 2005. Hydrogen production from propane in Rh-impregnated metallic microchannel reactors and alumina foams. *Catalysis Today*, 105(3–4), pp.469–478.

- Agrafiotis, C. & Tsetsekou, A., 2000a. The effect of powder characteristics on washcoat quality. Part II: Zirconia, titania washcoats—multilayered structures. *Journal of the European Ceramic Society*, 20, pp.825–834.

- Agrafiotis, C. & Tsetsekou, A., 2000b. The effect of powder characteristics on washcoat quality . Part I : Alumina washcoats. *Journal of the European Ceramic Society*, 20, pp.815–824.

- Agrafiotis, C. & Tsetsekou, A., 2000c. The effect of processing parameters on the properties of γ -alumina washcoats. *Journal of Materials Science*, 35(4), pp.951–960.

- Barbero, B.P. Costa-Almeida, L., Sanz, O., Morales, M., Cadus, L., Montes, M., 2008. Washcoating of metallic monoliths with a MnCu catalyst for catalytic combustion of volatile organic compounds. *Chemical Engineering Journal*, 139(2), pp.430–435.

- Barbir F., 2005. PEM fuel cells: theory and practice. New York: Elsevier/Academic Press.

- Boix, A. V., Zamaro, J. M., Lombardo, E. A., Miro, E., 2003. The beneficial effect of silica on the activity and thermal stability of PtCoFerrierite-washcoated cordierite monoliths for the SCR of NOx with CH4. *Applied Catalysis B: Environmental*, 46(1), pp.121–132.

- Carrette, L., Friedrich, K. A., & Stimming, U. (2000). Fuel Cells: Principles, Types, Fuels, and Applications. ChemPhysChem, 1(4), 162–193.

- Cao, C., Wang, Y. & Rozmiarek, R.T., 2005. Heterogeneous reactor model for steam reforming of methane in a microchannel reactor with microstructured catalysts. *Catalysis Today*, 110(1–2), pp.92–97.

- Dagle, R.A., Wang, Y., Xia, G., Strohm, J., Holladay, J., Palo, D., 2007. Selective CO methanation catalysts for fuel processing applications. *Applied Catalysis A: General*, 326(2), pp.213–218.

- Dautzenberg, F.M. & Mukherjee, M., 2001. Process intensification using multifunctional reactors. *Chemical Engineering Science*, 56(2), pp.251–267.

- Ehrfeld, W., Hessel, V. & Haverkamp, V., 2012. Microreactors. *Ullmann's Encyclopedia of Industrial Chemistry*, pp.173–198.

- Farrauto, R., Hwang, S., Shore, L., Ruettinger, W., Lampert, J., Giroux, T., Liu, Y., Illnich, O., 2003. New Material Needs For Hydrocarbon Fuel Processing : Generating Hydrogen for the PEM Fuel Cell. *Annual Review of Materials Research*, 33(1), pp.1–27.

- Farrauto, R. J., Liu, Y., Ruettinger, W., Illnich, O., Shore, L., Giroux, T., 2007. Precious Metal Catalysts Supported on Ceramic and Metal Monolithic Structures for the Hydrogen Economy. *Catalysis Reviews*, 49 (December 2006), pp.141–196.

- Germani, G., Stefanescu, A., Schuurman, Y., van Veen, A. C., 2007. Preparation and characterization of porous alumina-based catalyst coatings in microchannels. *Chemical Engineering Science*, 62(18–20), pp.5084–5091.

- Holladay, J.D., Hu, J., King, D. L., Wang, Y., 2009. An overview of hydrogen production technologies. *Catalysis Today*, 139(4), pp.244–260.

- Hou, K., 1998. *EXPERIMENTAL STUDIES OF INTRINSIC KINETICS AND DIFFUSION DURING METHANE STEAM REFORMING*. Ph.D. at the University of Salford.

- Hwang, S.-M., Kwon, O.J. & Kim, J.J., 2007. Method of catalyst coating in micro-reactors for methanol steam reforming. *Applied Catalysis A: General*, 316(1), pp.83–89.

- Ihara, K., Ohkuba, K., Yasaki, S., Yoshino, Y., 1993. Method of manufacturing an exhaust gas purifying catalyst. *US Patent 5, 208, 206*.

- Jensen, K., 1999. Microchemical systems: Status, Challenges and opportunities. AiChE Journal, 45(10), pp.2051-2054.

- Joensen, F. & Rostrup-Nielsen, J.R., 2002. Conversion of hydrocarbons and alcohols for fuel cells. *Journal of Power Sources*, 105(2), pp.195–201.

- Johnson, B.R., Canfield,N. L., Tran, D. N., Dagle, R. A., Li, X. S., Holladay, J. D., Wang, Y., 2007. Engineered SMR catalysts based on hydrothermally stable, porous, ceramic supports for microchannel reactors. *Catalysis Today*, 120(1), pp.54–62.

- Kamerud, K.L., Hobbie, K.A. & Anderson, K.A., 2013. Stainless steel leaches nickel and chromium into foods during cooking. *Journal of Agricultural and Food Chemistry*, 61(39), pp.9495–9501.

- Kiwi-Minsker, L. & Renken, A., 2005. Microstructured reactors for catalytic reactions. *Catalysis Today*, 110(1–2), pp.2–14.

- Kolb, G., Hoffman, C., O' Connell, M., Schurer, J., 2009. Microstructured reactors for diesel steam reforming, water-gas shift and preferential oxidation in the kiloWatt power range. *Catalysis Today*, 147, pp.S176–S184.

- Kolb, G., 2013. Review: Microstructured reactors for distributed and renewable production of fuels and electrical energy. *Chemical Engineering and Processing: Process Intensification*, 65, pp.1–44.

- Kolb, G. & Hessel, V., 2004. Micro-structured reactors for gas phase reactions. *Chemical Engineering Journal*, 98(1–2), pp.1–38.

- Koryabkina N, Ribeiro F, Ruettinger W. 2002. Fuel cell technology: opportunities and challenges. *New York: Am. Inst. Chem. Eng. Presented at AICHE Spring Meet. New Orleans*. pp. 92–97.

- Kuznetsov, V. V., Vitovsky, O. V. & Gasenko, O. a., 2009. Methane steam reforming in an annular microchannel with Rh/Al2O3 catalyst. *Journal of Engineering Thermophysics*, 18(3), pp.187–196.

- Liu, J.A., 2006 (M. Sc.). *Kinetics , catalysis and mechanism of methane steam reforming*. Worcester Polytechnic Institute.

- Maciver, D. S., Tobin, H. H., Barth, R.T., 1963. Catalytic Aluminas I. Surface Chemistry of Eta and Gamma Alumina. *Journal of Catalysis 2,* pp. 485-497.

- Matsumura, Y. & Nakamori, T., 2004. Steam reforming of methane over nickel catalysts at low reaction temperature. *Applied Catalysis A: General*, 258(1), pp.107–114.

- Meille, V., 2006. Review on methods to deposit catalysts on structured surfaces. *Applied Catalysis A: General*, 315, pp.1–17.

- Mehta, V., & Cooper, J. S. (2003). Review and analysis of PEM fuel cell design and manufacturing. Journal of Power Sources, 114(1), 32–53.

- Mitra, B. & Kunzru, D., 2008. Washcoating of Different Zeolites on Cordierite Monoliths. *Journal of the American Ceramic Society*, 91(1), pp.64–70.

- O'Connell, M., Kolb, G., Schelhaas, K., Wichert, M., Tiemann, D., Penneman, H., Zapf, R., 2012. Towards mass production of microstructured fuel processors for application in future distributed energy generation systems: A review of recent progress at IMM. *Chemical Engineering Research and Design*, 90(1), pp.11–18.

- Peela, N.R., Mubayi, A. & Kunzru, D., 2009. Washcoating of γ-alumina on stainless steel microchannels. *Catalysis Today*, 147, pp.S17–S23.

- Pennemann, H., Dobra, M., Wichert, M., Kolb, G., 2013. Optimization of Wash-Coating Slurries as Catalyst Carrier for Screen Printing into Microstructured Reactors.

Chemical Engineering & Technology, 36(6), pp.1033–1041.

- Provendier, H., Petit, C. & Estournes, C., 1999. Stabilisation of active nickel catalysts in partial oxidation of methane to synthesis gas by iron addition. *Applied Catalysis A:*, 180, pp.163–173.

- Quiram, D.J., Jensen, K., Schmidt, M., Mills, P., Ryley, J., Wetzel, M., Kraus, D., 2007. Integrated Microreactor System for Gas-Phase Catalytic Reactions. 1. Scale-up Microreactor Design and Fabrication. *Industrial & Engineering Chemistry Research*, 46(25), pp.8292–8305.

- Reuse, P., Renken, A., Haas-Santo, K., Gorke, O., Schubert, K., 2004. Hydrogen production for fuel cell application in an autothermal micro-channel reactor. *Chemical Engineering Journal*, 101(1–3), pp.133–141.

- Rostrup-Nielsen, J.R., 1993. Production of synthesis gas. *Catalysis Today*, 18(4), pp.305–324.

- Rostrup-Nielsen, J.R., 1984. Sulfur-passivated nickel catalysts for carbon-free steam reforming of methane. *Journal of Catalysis*, 85(1), pp.31–43.

- Santanach Carreras, E., Chabert, F., Dunstan, D., Franks, G., 2007. Avoiding "mud" cracks during drying of thin films from aqueous colloidal suspensions. *Journal of Colloid and Interface Science*, 313(1), pp.160–168.

- Schaper, H., Doesburg, E.B.M. & Van Reijen, L.L., 1983. The influence of lanthanum oxide on the thermal stability of gamma alumina catalyst supports. *Applied Catalysis*, 7(2), pp.211–220.

- Sebastián, V., de la Iglesia, O., Mallada, R., Casada, L., Kolb, G., Hessel, V., Santamaria, J., 2008. Preparation of zeolite films as catalytic coatings on microreactor channels. *Microporous and Mesoporous Materials*, 115(1–2), pp.147–155.

- Steele, B. & Heinzel, A., 2001. Materials for fuel-cell technologies. *Nature*, 414(1), pp.345-352.

- Sen, I. & Avci, A.K., 2014. Exhaust Gas Reforming of Methane in a Catalytic Microchannel Reactor. *Industrial & Engineering Chemistry Research*, 53(5), pp.1760–1767.

- Simsek, E., Avci, A.K. & Önsan, Z.I., 2011. Investigation of catalyst performance and microstructured reactor configuration for syngas production by methane steam reforming. *Catalysis Today*, 178(1), pp.157–163.

- Stefanescu, A., van Veen, A. C., Mirodatos, C., Beziat, J., Duval-Brunel, E., 2007. Wall coating optimization for microchannel reactors. *Catalysis Today*, 125(1–2), pp.16–23.

- Taylor, S., Fabbri, E., Leveque, P., Schmidt, T. J., Conrad, O., 2015. The effect of platinum loading and surface morphology on oxygen reduction activity. *Electrocatalysis*, 7, pp.287-296.

- Tolman, R. C., (1949). The effect of droplet size on surface tension. *Journal of Chemical Physics,* 17(3), pp.333.

- Tonkovich, A.Y., Perry, S., Wang, Y., Qiu, D., La Plante, T., Rogers, W., 2007. From seconds to milliseconds to microseconds through tailored microchannel reactor design of a steam methane reformer. *Catalysis Today*, 120(1), pp.21–29.

- Tonkovich, A. Y., Yang, B., Perry, S., Fitzgerald, S., Wang, Y., 2004. Microchannel process technology for compact methane steam reforming. *Chemical Engineering Science*, 59(22–23), pp.4819–4824.

- Trimm, D., 1999. Catalysts for the control of coking during steam reforming. *Catalysis Today*, 49(1–3), pp.3–10.

- Trimm, D.L. & Önsan, Z.I., 2001. Onboard Fuel Conversion for Hydrogen-Fuel-Cell-Driven Vehicles. *Catalysis Reviews*, 43(1–2), pp.31–84.

- Truter, L., 2012 (M. Sc.). *Development of a zeolite washcoating technique for micro-channel reactors*. University of Cape Town.

- Valentini, M., Groppi, G., Cristiani, C., Levi, M., Tronconi, E., Forzatti, P., 2001. The deposition of γ-Al_2O_3 layers on ceramic and metallic supports for the preparation of structured catalysts. *Catalysis Today*, 69(1–4), pp.307–314.

- Vallar, S., Houivet, D., El Fallah, J., Kervadec, D., Hausonne, J., 1999. Oxide slurries stability and powders dispersion: optimization with zeta potential and rheological measurements. *Journal of the European Ceramic Society*, 19(6–7), pp.1017–1021.

- Van Hook, J., 1980. Methane-Steam Reforming. *Catalysis Reviews - Science and Engineering*, 21(1), pp. 1-54.

- Viswanathan, B. & Aulice Scibioh, M., 2006. Fuel Cells Principles and Applications. India: University Press.

- Wang, S. & Lu, G., 1998a. Catalytic activities and coking characteristics of oxides-supported Ni catalysts for CH4 reforming with carbon dioxide. *Energy & fuels*, 624(13), pp.248–256.

- Wang, S. & Lu, G., 1998b. Reforming of methane with carbon dioxide over Ni/Al_2O_3 catalysts: Effect of nickel precursor. *Applied Catalysis A: General*, 169, pp.271–280.

- Wang, Y., Chin, Y., Rozmiarek, R. T., Johnson, B., Gao, Y., Watson, J., Tonkovich, A. L., Vander Wiel, D., 2004. Highly active and stable Rh/MgO-Al_2O_3 catalysts for methane steam reforming. *Catalysis Today*, 98(4), pp.575–581.

- Wang, Y., Chen, K. S., Mishler, J., Cho, S. C., & Adroher, X. C. (2011). A review of polymer electrolyte membrane fuel cells: Technology, applications, and needs on fundamental research. Applied Energy, 88(4), 981–1007.

- Xu, J. & Froment, G.F., 1989. Methane steam reforming, methanation and water-gas shift: I. Intrinsic kinetics. *AIChE Journal*, 35(1), pp.88–96.

- Xu, J. & Froment, G., 1989. Methane steam reforming: II. Diffusional limitations and reactor simulation. *AIChE Journal*, 35(1), pp.97–103.

- Yasaki, S., Yoshino, Y., Ihara, K., Ohkubo, K., 1993. Method of manufacturing an exhaust gas purifying catalyst.

- Zamaro, J., Ulla, M. & Miro, E., 2005. Zeolite washcoating onto cordierite honeycomb reactors for environmental applications. *Chemical Engineering Journal*, 106(1), pp.25–33.

- Zapf, R., Kolb, G., Penneman, H., Hessel, V., 2003. Alumina-based catalyst coatings within microchannels and their testing. *Institute of Chemical Engineers*, 81 (August).

- Zapf, R., Berresheim, K., Bolz, H., Gnaser, H., Hessel, V., Kolb, G., Pannwitt, A. K., Ziogas, A., 2006. Basic Study of Adhesion of Several Alumina-based Washcoats Deposited on Stainless Steel Microchannels. *Chemical Engineering & Technology*, 29(12), pp.1509–1512.

- Zhai, X., Cheng, Y., Zhang, Z., Jin, Y., Cheng, Y., 2011. Steam reforming of methane over Ni catalyst in micro-channel reactor. *International Journal of Hydrogen Energy*, 36(12), pp.7105–7113.

- Zhou, Y., 2014 (M. Sc.). *Platinum Group Metals Catalyzed Steam Methane Reforming via Micro-channel Reactor*. University of Cape Town.

9 Appendices

9.1 Mass flow controller calibration

The mass flow controller (MFC) calibration was conducted with the MFC in the percentage output mode whereby the display is set to show 0-100 % of the MFC's output. The actual flow rate will depend on the MFC range. For example, a MFC with a range 0-500 ml/min range, should ideally have a 500 ml flow of nitrogen per minute at a setting of 100 % and 250 ml/min at 50 %.

For each component, an MFC was allocated. In the case of each component's MFC calibration the MFC was set at a minimum of 5 set points between 0-100 % including 100 % and averaged. The actual flow rate of gas was measured using a bubble flow meter, where the time taken for a bubble to move through a standard 50 ml measuring cylinder was measured. From the measured time and set volume, the flow rate was calculated and plotted against the set point of the MFC. The plots below are the results of these MFC calibrations. Note the reactor MFC was calibrated with nitrogen and adjusted using calibration constant to account for the mixture of gas to flow through.

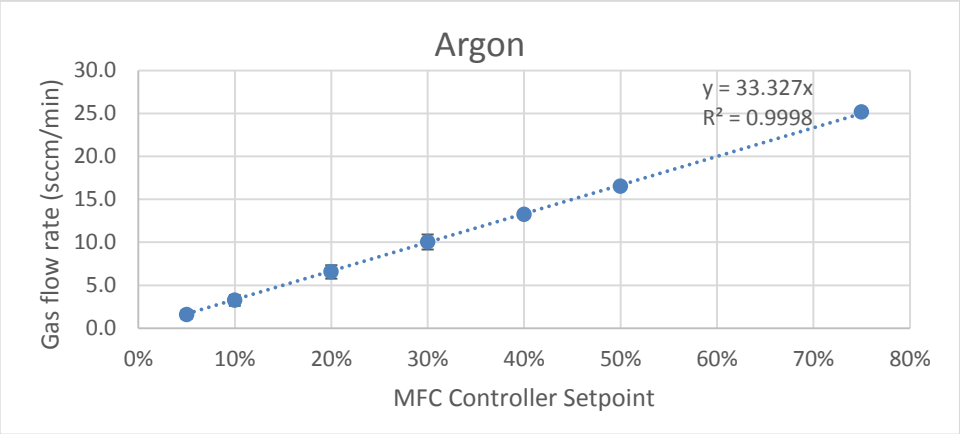

Figure 9.1 – MFC calibration of the 0-50 ml Argon MFC

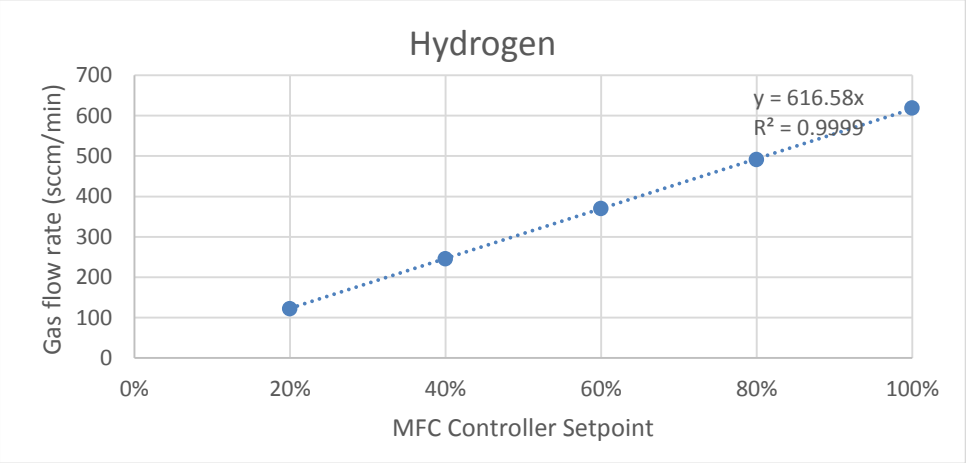

Figure 9.2 – MFC calibration of the 0-500 ml hydrogen MFC

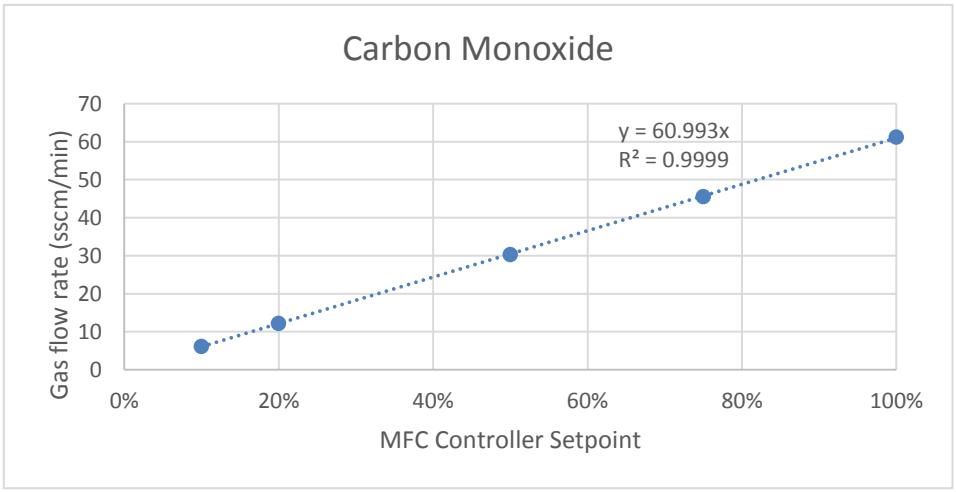

Figure 9.4 – Carbon monoxide, 0-50 ml MFC calibration

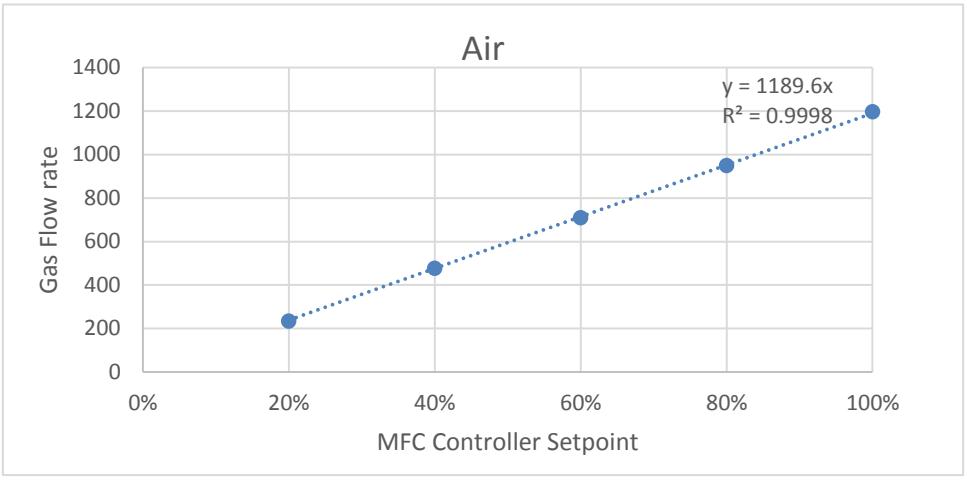

Figure 9.5 – 0-1000 ml, Air MFC calibration plot

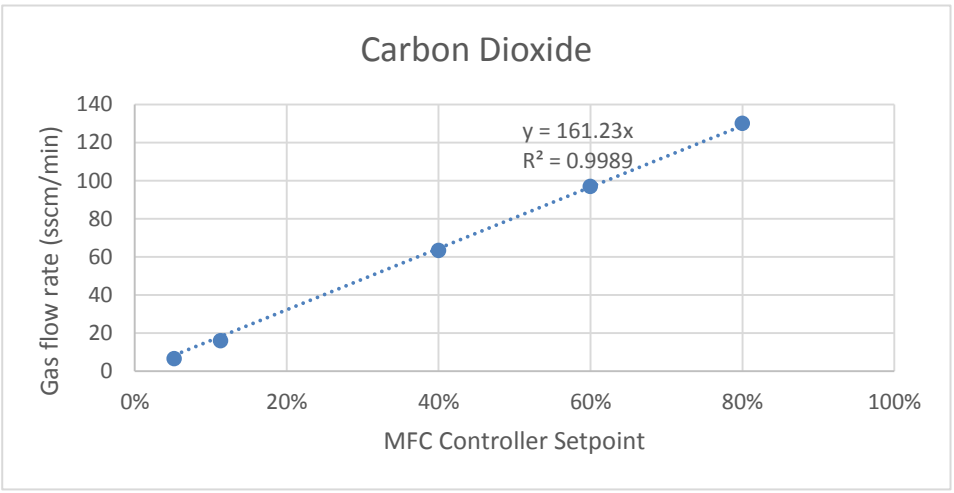

Figure 9.3 – Carbon dioxide, 0-200 ml, MFC calibration plot

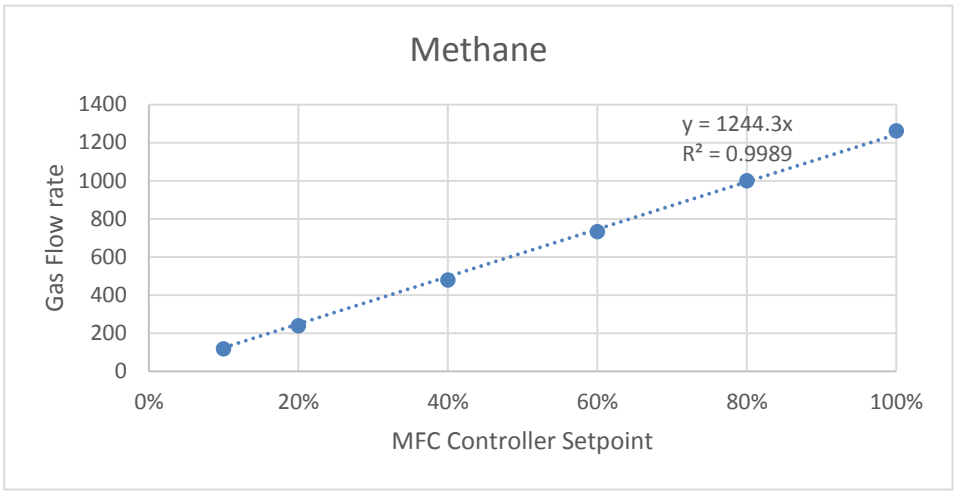

Figure 9.7 – Methane MFC calibration with a 0-1000 ml range

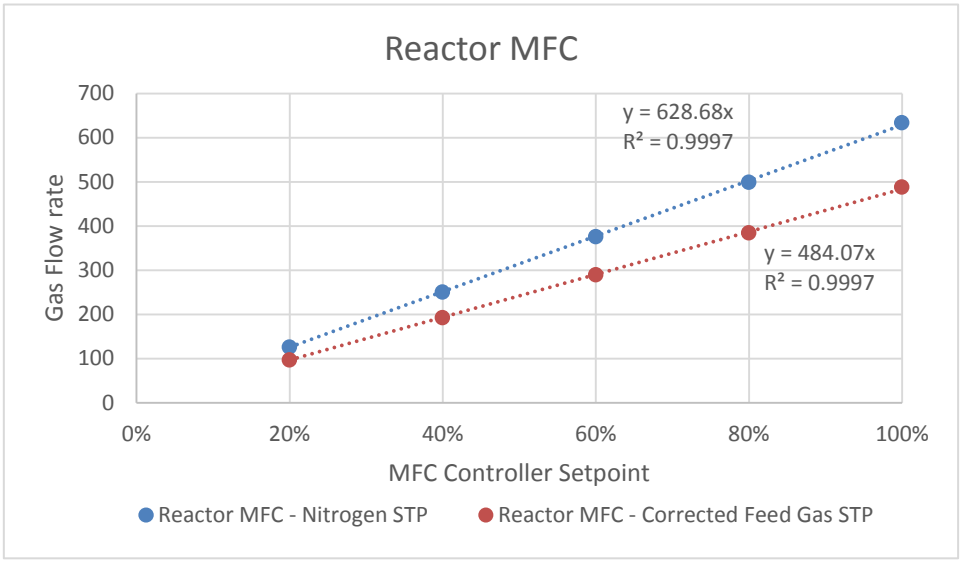

Figure 9.6 – Reactor MFC calibration with Nitrogen and then corrected using standard calibration constants

9.2 Gas chromatography response factor calculation

The internal standard used in this study was argon gas. The internal standard is used to quantify the amount of each species in a given injection sample of gas. In the GC, each component has a 'response factor' relative to the internal standard and is calculated using equation 26.

$$\left(\frac{Moles_i}{Moles_{Ar}}\right) RRF_i = \left(\frac{Peak\ Area_i}{Peak\ Area_{Ar}}\right) \tag{32}$$

$$RRF_i = \frac{\left(\frac{Peak\ Area_i}{Peak\ Area_{Ar}}\right)}{\left(\frac{Moles_i}{Moles_{Ar}}\right)} \tag{34}$$

The RRF or relative response factor for each species was determined by passing a mixture of known composition through the through GC sample loop. The area response for each component was put relative to the area response of the argon internal standard. This was done numerous times for several gas mixtures which resembled different methane conversions. The relationship of the molar ratios (between the component and the internal standard) and the area ratios was then plotted. A linear relationship was seen and a linear trend line was plotted through the origin to fit the data correctly. The graphs below show that the relative response factors were valid over quite a wide range of concentrations which covered all those applicable to the experiments of this study.

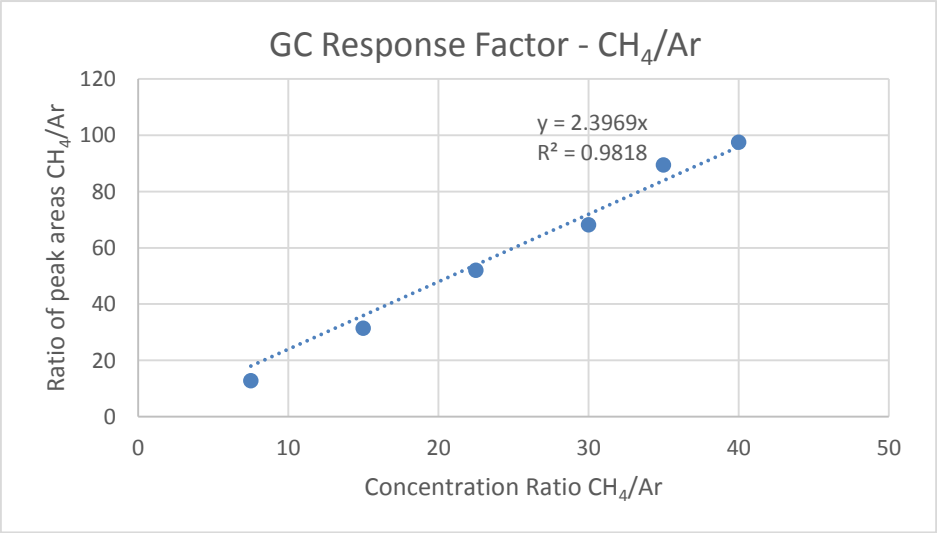

Figure 9.8 – Methane GC response factor

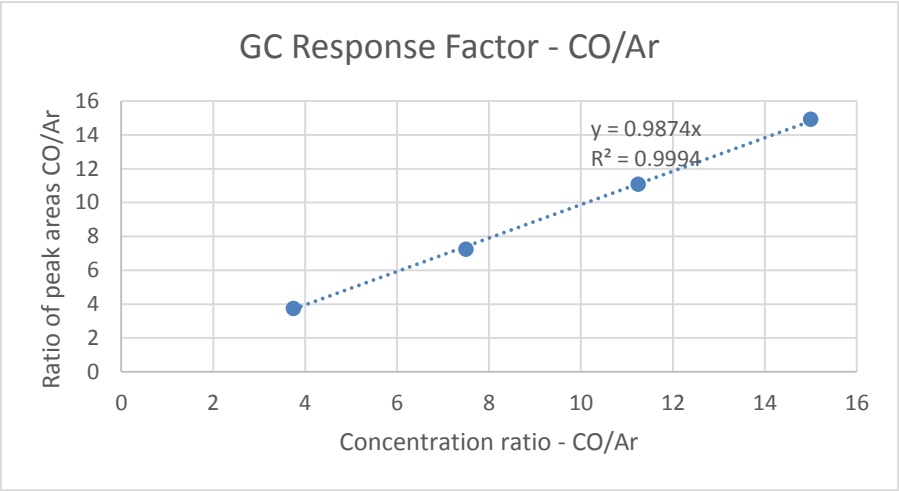

Figure 9.9 – Carbon monoxide GC response factor calculation

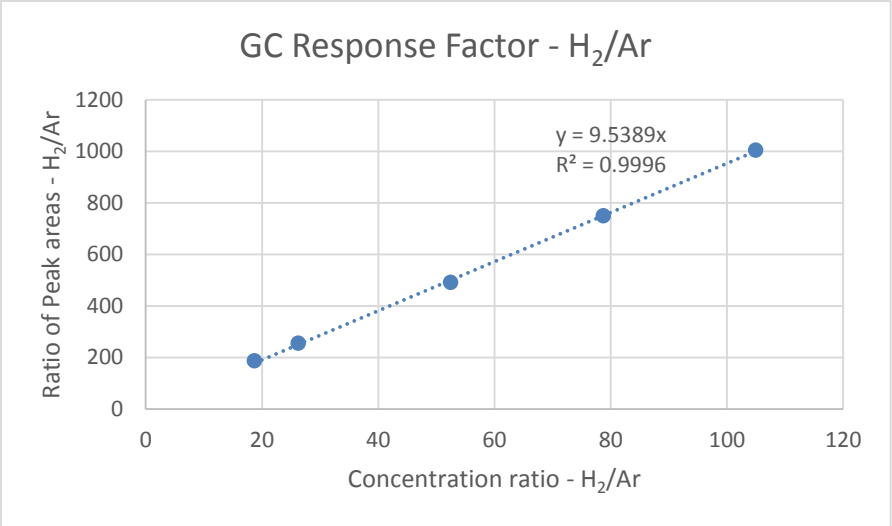

Figure 9.10 – Carbon dioxide GC response factor determination

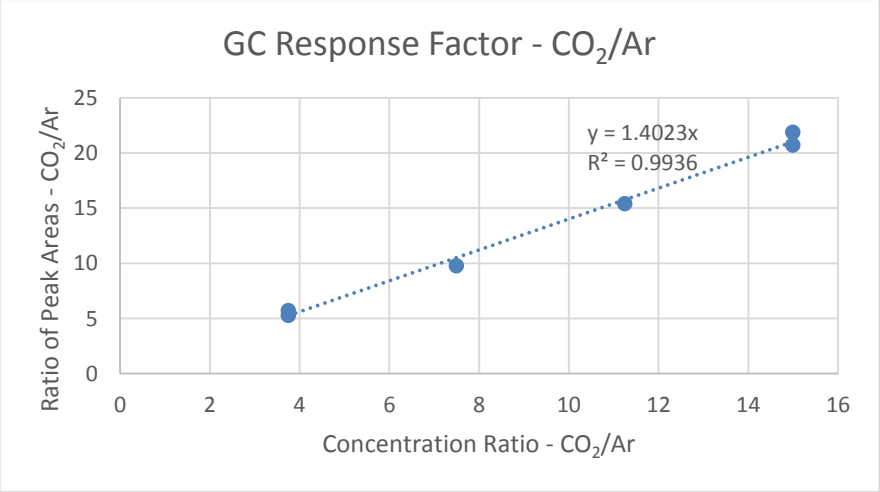

Figure 9.11 – Hydrogen GC response factor

9.3 Reactor temperature profile

To determine the isothermal zone for placement of the catalyst bed in the case of the fixed bed and the micro-channel reactor itself, a temperature profile along the three heating bands of the furnace is required. It was conducted at the required 700 °C using a fixed bed reactor filled with inert silicon carbide. The thermowell in the centre was where readings were taken and the length of reactor refers to the distance from the bottom of the reactors

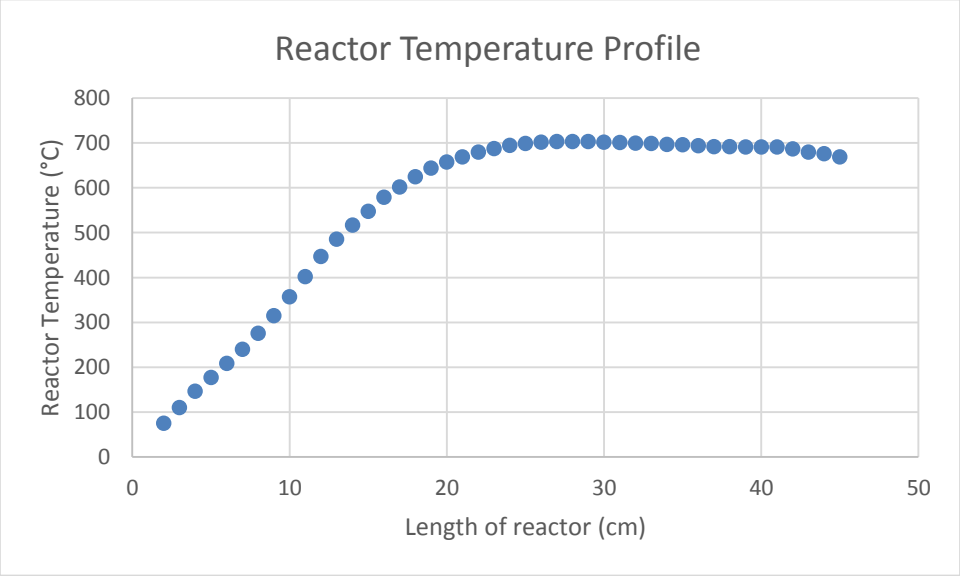

Figure 9.12 - Isothermal zone determination through a temperature profile across the electrical furnace

thermowell.

9.4 HPLC pump calibration

The HPLC pump was calibrated by blocking the outlet and subsequently viewing and noting the build-up of pressure at 5 second intervals. The relationship between pressure build-up is expected to be a linear one and the results below illustrates and confirms that.

9.5 Specific space velocity calculation

For the calculation of the wet mass specific space velocity ($scc \cdot (g_{cat} \cdot h)^{-1}$) the following method was used:

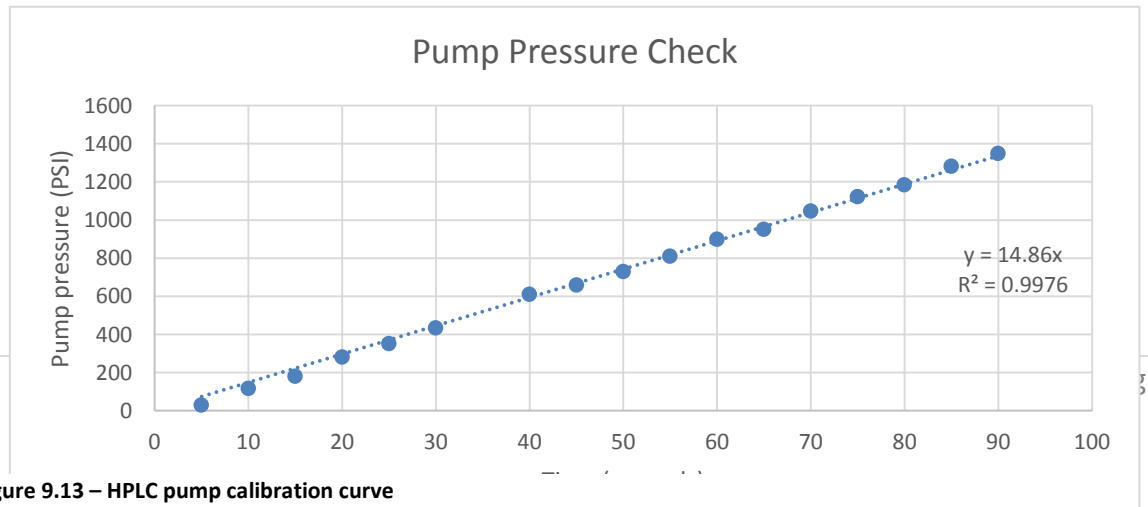

Figure 9.13 – HPLC pump calibration curve

From the target wet specific space velocity and the mass of the two catalyst layers a total wet volumetric flow rate can be determined. A set methane to argon ratio for the dry feed is chosen with a steam to carbon ratio and a catalyst density of 1 g/cm^3. From these a methane flow rate is first estimated and using the dry feed composition the argon flow rate can be determined at STP. From the flow rate of methane and a steam to carbon molar ratio of 3, the moles of water can be determined and converted to a mass and volumetric flow rate. Using the combined volumetric flow rate of the dry feed and steam from the initially estimated methane flow can be compared to what the total flow rate should be by creating a differential. Excel solver can then be used to set the differential to zero by changing the estimated methane feed and subsequently changing the required water flow. The set of tables below in Figure 9.14

shows the method used to determine the required dry feed and water flow rates and MFC set points.

Target $SGHSV_{WET}$	**600000**	**sml.(g.hr)$^{-1}$**
$M_{catalyst}$	0.0404	g
$\rho_{Catalyst}$	1	g/cm^3
$V_{total\ WET\ feed,\ Reactor}$	404	cm^3/min
$V_{CH4\ feed,\ Reactor}$	100.487	cm^3/min
$V_{Ar\ feed,\ Reactor}$	2.05	cm^3/min
$V_{water\ feed,\ Reactor}$	301.46	cm^3/min
$V_{total\ DRY\ feed,\ Reactor}$	102.54	cm^3/min
S/C	3	
Sum	**404**	
Difference	**0**	
Mol % Methane	0.98	
Mol % Argon	0.02	
$n_{H2O\ feed,\ corrected}$	13.59125897	mmol/min
$m_{H2O\ feed,\ corrected}$	0.245	g/min
$V_{H2O\ liquid\ feed,\ corrected}$	0.245	cm^3/min
Scale Factor	1.5	
$V_{CH4\ feed,\ corrected}$	150.7309645	cm^3/min
$V_{Ar\ feed,\ corrected}$	3.076142132	cm^3/min
CH_4 MFC Set point	12.1%	
Ar MFC Set point	9.2%	
Feed Gas MFC Setpoint	21.2%	

$$SGHSV = \frac{feed,dry}{catalyst}$$
$$2$$

Reactor Plates	Mass Catalyst	
W58	0.01989	0.0404
W59	0.02051	

Gas Factors	
Nitrogen	1.000
Argon	1.395
Methane	0.763
Feed Gas	0.770

$$Sensor\ Conversion\ Factor\ for\ a\ Gas\ Mixture = \frac{100}{\frac{P_1}{F_1} + \frac{P_2}{GF_2} + \frac{P_n}{GF_n}}$$

	MFC Calibration gradients	
Ar	33.327	0
CH_4	1244.3	0
Feed Gas	484.07	0

$$PV = nRT$$

$$n = \frac{PV}{RT}$$

Pressure	1.01	atm
Temperature	273	K
Gas Constant	0.08206	L.atm.mol^{-1}.K^{-1}
Molar mass H_2O	18	g/mol
Density of H_2O	1	g/cm^3

Figure 9.14 – Methodology used to determine the flow rates of methane, argon and water from a chosen specific space velocity

9.6 TGA results for PVA coating suspension

A thermogravimetric analysis was conducted on a sample of the binder used in the wash-coating suspension, polyvinyl alcohol (PVA), to confirm that the PVA is completely removed at the arbitrary temperature of 460 °C. The temperature program used in this analysis is as follows:

- Heat to 460 °C at a rate of 10 °C/min
- Hold at 460 °C for an hour
- Cool to ambient temperature

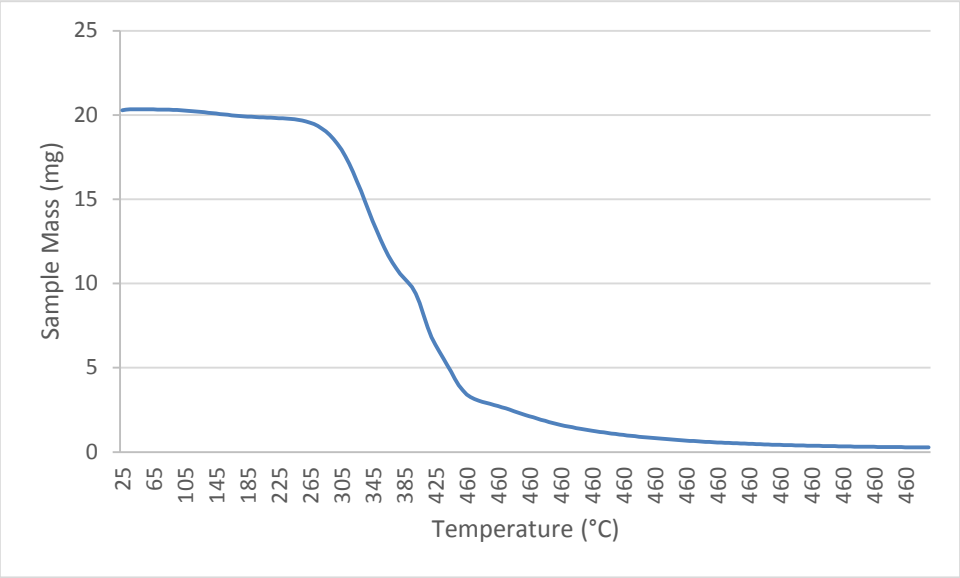

Figure 9.15 – Thermo-gravimetric analysis of a sample of PVA in air whereby the temperature was increased at a rate of 10 °C/min to 460 °C and held there for 1 hour

From the plot above, the initial sample mass dropped from 20.29 mg to 3.65 mg by the time 460 °C was reached. Over the hour at 460 °C the sample dropped to 0.27 mg and remained at that weight. This proves that the PVA is completely removed after an hour at 460 °C and thus 2 hours of calcination at 600 °C used in the method is more than sufficient.

9.7 Temperature programmed reduction

A temperature programmed reduction procedure was carried out on the powdered catalyst to confirm the temperature at which the fresh catalyst with the rhodium nitrate precursor being supported on the Alfa Aesar alumina becomes metallic rhodium.

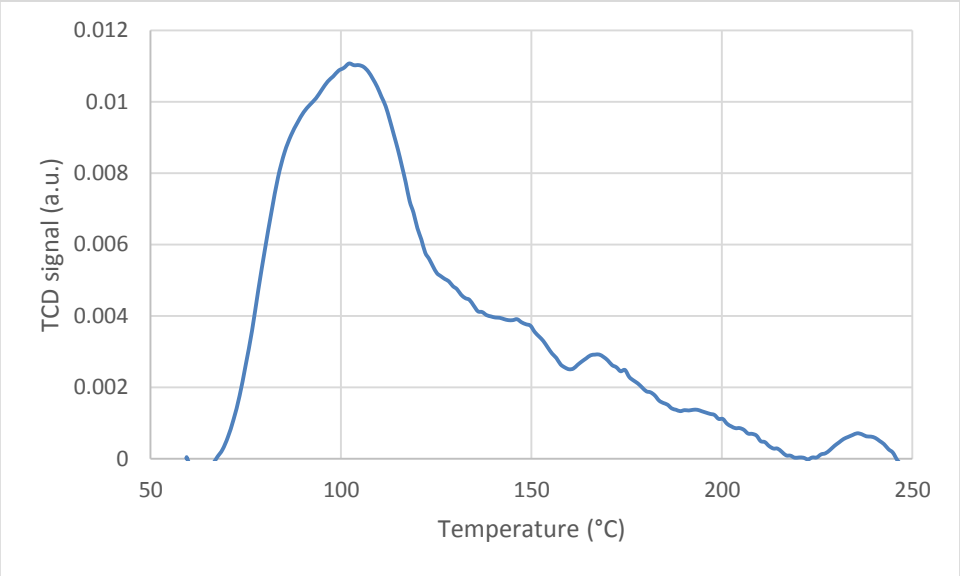

Figure 9.16 - Plot of the temperature programmed reduction of the powdered Rh/Al_2O_3 catalyst with the temperature versus TCD signal

Figure 9.16 shows that the temperature at which the reduction of rhodium takes place is at its peak at 105 °C and it almost completely reduced at 200 °C. Thus, the reduction temperature for the new reduction procedure that was conducted at 200 °C for 2 hours was more than sufficient to reduce all of the rhodium to its metallic state.

9.8 Ethics Acknowledgement

EBE Faculty: Assessment of Ethics in Research Projects

Any person planning to undertake research in the Faculty of Engineering and the Built Environment at the University of Cape Town is required to complete this form before collecting or analysing data. When completed it should be submitted to the supervisor (where applicable) and from there to the Head of Department. If any of the questions below have been answered YES, and the applicant is NOT a fourth year student, the Head should forward this form for approval by the Faculty EIR committee: submit to Ms Zakiya Chikte (Zakiya.chikte@uct.ac.za); New EBE Building, Ph 021 650 5739). Students must include a copy of the completed form with the dissertation/thesis when it is submitted for examination.

Name of Principal Researcher/Student: Wesley van Niekerk Department: Chemical Engineering

If a Student: Degree: MSc Eng (Chemical Engineering) Supervisor: Jack Fletcher

If a Research Contract indicate source of funding/sponsorship:

Research Project Title: Investigation into the behaviour of a wash-coated PGM-based catalyst layer in micro-channel reactors for the steam reforming of methane.

Overview of ethics issues in your research project:

Question 1: Is there a possibility that your research could cause harm to a third party (i.e. a person not involved in your project)?	YES	NO X
Question 2: Is your research making use of human subjects as sources of data? If your answer is YES, please complete Addendum 2.	YES	NO X
Question 3: Does your research involve the participation of or provision of services to communities? If your answer is YES, please complete Addendum 3.	YES	NO X
Question 4: If your research is sponsored, is there any potential for conflicts of interest? If your answer is YES, please complete Addendum 4.	YES	NO X

If you have answered YES to any of the above questions, please append a copy of your research proposal, as well as any interview schedules or questionnaires (Addendum 1) and please complete further addenda as appropriate.

I hereby undertake to carry out my research in such a way that

- there is no apparent legal objection to the nature or the method of research; and
- the research will not compromise staff or students or the other responsibilities of the University;
- the stated objective will be achieved, and the findings will have a high degree of validity;
- limitations and alternative interpretations will be considered;
- the findings could be subject to peer review and publicly available; and
- I will comply with the conventions of copyright and avoid any practice that would constitute plagiarism.

Signed by:

	Full name and signature	Date
Principal Researcher/Student: Wesley van Niekerk	Signed	03/02/2015

This application is approved by:

Supervisor (if applicable):	Signed	11 JAN 2016
HOD (or delegated nominee): Final authority for all assessments with NO to all questions and for all undergraduate research.	Signed	11/01/2016
Chair : Faculty EIR Committee For applicants other than undergraduate students who have answered YES to any of the above questions.		